ASCERTAINING A HANDS-ON APPROACH TO ESTIMATE DEBRIS FLOW VELOCITIES FOR RATIONAL DEBRIS HAZARD MITIGATION

（土石流被害軽減のための実践的な土石流速推定手法の探求）

A dissertation submitted in partial fulfillment of the requirements for the degree of

DOCTOR OF PHILOSOPHY (in ENGINEERING)

By

MD. AFTABUR RAHMAN

Examination Committee

Prof. Kazuo Konagai (Chair)

Dr. Hiroshi Ikeya

Prof. Kimitoshi Hayano

Prof. Takashi Matsushima

Assoc. Prof. Mamoru Kikumoto

Department of Civil Engineering

Graduate School of Urban Innovation

Yokohama National University, Japan

September 2016

Published and distributed by:

Graduate School of Urban Innovation
Yokohama National University, Japan

Printed in Japan

ABSTRACT

Debris flow is one of the shattering natural disasters, mostly ensuing in mountainous areas. Rational estimation of debris flow velocity is one of the key issues in debris hazard mitigation. Among the various procedures, back-calculation of debris flow velocity is a widely used approach. Back-calculation procedure includes determinations of super-elevation and channel properties, and velocities are calculated using the forced-vortex equation ($v = \sqrt{\frac{gR\Delta h}{kb}}$). A debris mass, when travels through a curved flume, leaves the highest flow mark on the outer bend, and the difference between the flow depths of outer and inner bends is referred to as 'super-elevation'. However, in a post-flow field investigation, only the highest flow marks on both inner and outer bends are visible, which does not portray the actual maximum super-elevation that must have been reached in the unsteady flow event, and eventually leads to a misjudgment of the real velocity. Another important parameter of forced vortex equation is the channel radius of curvature. Any natural channel has hardly been a circle, rather it has varying curvature. How the curve is approximated can affect velocity estimation. Considering the unsteady nature of debris flows, this research work aims to figure out a coherent way of estimating debris flow velocities. Therefore, a series of numerical curved flume tests using Smoothed Particle Hydrodynamics (SPH) are carried out to check the aptness of the mud-marks derived velocities. Estimated velocities from flow marks underestimate the actual velocities near the source, while they converge on the actual velocities as the distance to source increases. Based on the simulations, a best fit curve is proposed to adjust the mud-marks derived velocities. Law of similarity allows to apply the findings from these small scale simulations to the real debris flow problems. Three debris flow events in Japan are taken for the validation of the proposed procedure and adjusted velocities are proven to be consistent with verbal evidences and previous analyses.

Key words: Debris flow, velocity, super-elevation, SPH, mud-marks

(Dedicated to my parents)

ACKNOWLEDGEMENT

Alhamdulillah (all praise belongs to Allah Subhanahu O Ta'ala)

The author owes his heartfelt gratitude to ***Prof. Kazuo Konagai***, for everything he has done for the author over the last three years. ***Prof. Konagai's*** guidance, positive attitude, continuous encouragement worked as a stimulant to overcome the hurdles during the PhD study.

The author greatly acknowledged to his external committee members, ***Dr. Hiroshi Ikeya***, ***Prof. Kimitoshi Hayano***, ***Prof. Takashi Matsushima*** and ***Assoc. Prof. Mamoru Kikumoto*** for their constructive comments and reviews. Specially, **Dr. Ikeya's** decisive comments and recommendations helped the author in a great deal to improve the dissertation.

The author also thankful to his former master's supervisor ***Assoc. Prof. Hisashi Taniyama*** at Saitama University, who's motivation had a great influence at the very early stage of the author's research career.

The author would like to acknowledge the ***Ministry of Education, Culture, Sports, Science and Technology, Japan (MEXT)*** for providing financial support to carry out his research study.

The ***Chittagong University of Engineering & Technology (CUET)***, Bangladesh are gratefully acknowledged for giving the author study leave to pursue his PhD study at Yokohama National University, Japan.

All the members of Geotechnical Engineering Laboratory of Yokohama National University are acknowledged owing to their support in preceding three years. Specially, ***Mr. Kazuhiro Kajihara, Mr. Shiga Masataka, Mr. Hiroki Okuda, Mr. Keigo Fukuda*** and ***Mr. Yohei Koike*** deserve special thanks from the author for their support not only in the academic affairs, but also in daily activities. Without their assistance, it would not be so smooth journey.

The author would also like to thank ***Dr. Md. Naimul Haque,*** who helped him from the very start of the admission procedure at Yokohama National University.

Most significantly, the author would like to pay innermost homage ***to his parents and all other family members*** for their undivided love, divine guidance and continuous reinforcement. It would not be possible to write any line of the dissertation without affection, encouragement and moral support provided by the parents since his childhood.

At last but certainly not the least, the author would wish to offer special acknowledgement to his wife, beloved ***Hasina Iasmin*** for her love, patience and understanding to him. Her staying in Japan has breathed in a lot for overcoming many obscure circumstances, having come out while getting along this research study.

LIST OF PUBLICATIONS

Peer-reviewed Journals

[1] ***Rahman MA***, Konagai K (2016) Substantiation of debris flow velocity from super-elevation: a numerical approach. Landslides, doi: 10.1007/s10346-016-0725-3

[2] ***Rahman MA***, Hashimoto T, Konagai K (2015) An attempt for velocity estimation of Nebukawa debris flow triggered by the Great Kanto earthquake, 1923. Structural Engineering & Earthquake Engineering (SE/EE), Journal of JSCE, 71(4): 387-394

Peer-reviewed Proceedings

[3] ***Rahman MA***, Konagai K (2017) Rational way to estimate velocities of earthquake-induced debris flow from super-elevations. Submitted to the 16th World Conference on Earthquake Engineering, Chile.

Non-reviewed Proceedings

[4] ***Rahman MA***, Konagai K (2016) A Numerical curved flume test for debris flow velocity estimation: justification of using super-elevation. Proceedings of the 18th International Summer Symposium, JSCE

[5] ***Rahman MA***, Hashimoto T, Konagai K (2014) An attempt for velocity estimation of Nebukawa debris flow triggered by the Great Kanto earthquake. Proceedings of the 34th Earthquake Engineering Workshop

TABLE OF CONTENTS

LIST OF FIGURES

LIST OF TABLES

Chapter-1

INTRODUCTION

1.1 Background

With the increasing population, people have been expanding their sphere of life into mountainous regions, and so have been industrial and commercial areas. For example, about 75% of Japan is mountainous (Ikeya 1989). Earthen masses on steep slopes of these mountains immediately behind urbanized areas can be detached at any time due to intense rainfalls and/or intense ground shakes, which phenomenon is, in a broader sense, known as a slope failure. Among them, those moving fast and long distances are referred to as debris flows. Tragedies caused by landslides have been handed down orally and/or in writings over centuries (Takahashi 2000). The May 8, 1847 Zenkoji earthquake triggered about 44000 landslides in the earthquake-hit areas (Kazmi 2013).

Inaccessibility and adverse conditions of the source areas were the primary constraint to set out the meticulous idea of the dynamics of debris flow. However, researches on modeling the dynamics of landslide masses were dramatically accelerated particularly in the 1950s in Japan. Since then, theoretical framework as well as experimental and observational investigations have keenly fascinated researchers. Moreover, governments stepped forward to estimate the risk of long travelling slope failure disasters. Eventually, this kind of disaster has started to be frequently covered by TV and newspapers.

Moreover, debris flow disaster causes both social and economic losses. Social loss includes numerous death toll owing to the sudden triggering of the detached mass movement. As well, fast moving debris materials destroy houses, lifeline facilities such as roads, bridges, rail tracks, etc. In addition, debris flows damage agricultural lands, livestock, and fisheries, which events have a highly negative impact on the economy of the affected country. For example, a disruption of transportation system in North American transcontinental rail lines costed approximately 10 million US dollars for only one day (Jakob and Hungr 2005). Alleviation of damage by implementing proper hazard mitigation strategy can reduce both social and economic losses.

Realizing the impact of debris flow disaster, this research carries out a series of three dimensional numerical flume tests using the Smoothed Particle Hydrodynamics (SPH) (Lucy 1977), with special focus on the velocity of flowing mass. Similarity law allows to apply these small scale numerical outcomes to real debris flow events. The numerical scheme accounts the viscous nature of debris flows for a wide range of viscosities compatible with the in-situ scenario. Navier-Stokes equations are solved at each time step for both Newtonian and non-Newtonian models so that model responses can be substantiated from a broader view of debris flow dynamics (Takahashi 2000). Moreover, recent advance of remote sensing and GIS tools allows to use the numerical results for real debris disasters (Berti et al. 1999; Malet et al. 2005; Nomura et al. 2010; Chen et al. 2014).

1.2 Motivation and objectives of this research

Development of an early warning system for hazard mitigation is the ultimate goal of the debris flow study. For this, extensive research works have been started both experimentally and numerically since 1950s. Both laboratory investigations and numerical analyses have provided crucial acumens into hazard mitigations. However, these analyses are based on small scale model tests which is outlying the reality. To address the said glitches, scaling law is a way to draw the small scale model as the real debris flow event. But, unavailability of scaled debris material properties restricts the experimental investigation in many events. Instead, a scaled numerical analysis is a plausible approach to study the dynamics of debris flows.

In reality, debris is a complex mixture of many things and substantially vary its nature both in time and space. Therefore appropriate modeling of debris flow dynamics is always a challenging task for the researchers (Iverson 2003). So far, a plenty of rheological formulations have been evolved from very elementary to the complicated mixture model to rationally describe the flowing nature of debris materials. In addition, determination of dynamic parameters of the moving mass is an important key for mapping out a strategic plan for quick evacuations.

Peak discharge, volume, impact force, run-out length, velocity are the featuring factors for debris flow analysis. Among them, velocity is one of the important parameters as it

affects the impact force, travel distance and erosion rate. Several ways of velocity estimation procedure are described in technical writings. However, field investigated back-calculation of velocity is the most pragmatic and widely applied method to real debris events (Pierson 1985; Prochaska et al. 2008). All the same, this widely used approach has some inappropriate measurement of input parameters and misjudge the actual velocities of flowing mass. Research on this topic is seldom found whatever the means are.

Summing up the above discussion and seeing the real world problem, this PhD dissertation is solely founded on noticing out the rational approach of estimating debris flow velocities. To be more specific, improvement of current back-calculation procedure of velocity determination approach is the primary objective of this research study. The explicit aims of this study are written below:

(a) Development of a numerical tool for the adjustment of velocities derived from back-calculated procedure.
(b) Validation of developed procedure with real debris flow events.

1.3 Contribution of current research

Among the several approaches of velocity estimation procedure, back calculated velocity estimation is a rational approach. Back-calculation principally relies on field investigated channel properties at particular cross-sections of the flow trace. These include flow depth at both inner and outer bend, channel width, bend radius and channel gradient. However, remnant flow marks and variation of bend radius is the biasing parameters of velocity estimation. Thus, improving the existing path is much required for rational hazard mitigation. The followings are the major contribution to the area of debris hazard mitigation

(a) Numerical analysis reveals that back calculated velocities converge on real velocities with the increasing distance from the initial source and a cumulative form of negative exponential function ($1 - e^{-\alpha x}$) is proposed to adjust back calculated velocities to real velocities.
(b) Flowing features of both Newtonian and non-Newtonian Bingham fluids are simulated to cover both forefront and tale of debris flow.

(c) In debris hazard mitigation policy, estimation of time for any susceptible debris mass to reach the distal end is a crucial part. This research describes the relation between estimated time from back-calculated velocities and estimated time for the front to reach the distal end.

(d) Sloshing period of debris mass along the curved section of a flume is determined by using simple 2D numerical simulation and is correlated with the time for the debris mass to attain the maximum super-elevation along the curved section.

(e) Three well known debris flow disasters in Japan, namely, Shiraito River debris flow in 1923, Ontake avalanche in 1984, and Komano-yu debris flow in 2008 are chosen to validate the numerical findings for determining the velocities along their flow paths. These velocities are found consistent with previous numerical simulations by other researchers, and portray scenarios close to the verbal evidences. Estimated times are also consistent with verbal evidences, which fact implicitly justifies the aptness of the numerical results.

1.4 Dissertation outline

Chapter 2 describes the fundamentals of debris flow and its kinetics. Triggering condition of debris disaster and size classifications are discussed. Background of velocity estimation of debris flow is described in detail. Existing models and procedures are reviewed and problems in the real field are identified critically. How this problem will be improved to get the comprehensive velocity of flowing mass is also outlined briefly.

Chapter 3 outlines the in detail features of numerical tool that has been used to verify the existing velocity estimation procedure. Mathematical formulation as well as verification of the 3D model is also included in this chapter.

Chapter 4 describes the 3D modeling of flume test for the debris flow analysis. Data extraction, detail descriptions on constitutive modeling, sensitivity of different parameters to the simulated flows are given in this chapter. Results of numerical simulation and discussion are also added.

Outcomes of the numerical study of debris flow velocities are verified in ***Chapter 5***. Three well known debris flow disasters in Japan are chosen for validation of the proposed procedure and detail discussion is included in this chapter.

Chapter 6 concludes and highlights the most important aspects of this dissertation. Possible future extension of this study is also discussed briefly.

References

Berti M, Genevois R, Simoni A, Tecca PR (1999) Field observations of a debris flow event in the Dolomites. Geomorphology 29:265–274. doi: 10.1016/S0169-555X(99)00018-5

Chen HX, Zhang LM, Zhang S (2014) Evolution of debris flow properties and physical interactions in debris-flow mixtures in the Wenchuan earthquake zone. Engineering Geology 182:136–147. doi: 10.1016/j.enggeo.2014.08.004

Ikeya H (1989) Debris flow and its countermeasures in Japan. Bulletin of the International Association of Engineering Geology-Bulletin de l'Association Internationale de G{é}ologie de l'Ing{é}nieur 40:15–33.

Iverson R (2003) The debris-flow rheology myth. 3rd International Conference on Debris-Flow Hazards Mitigation: Mechanics, Prediction, and Assessment 303–314.

Jakob M, Hungr O (2005) Debris-flow Hazards and Related Phenomena. Praxis Publishing , UK

Kazmi ZA (2013) Extraction of Lagrangian ground displacements and subsurface seismic stress changes for rational earthquake disaster mitigation. University of Tokyo

Lucy LB (1977) A numerical approach to the testing of the fission hypothesis. Astronomical Journal 82:1013–1024.

Malet J-P, Laigle D, Remaître A, Maquaire O (2005) Triggering conditions and mobility of debris flows associated to complex earthflows. Geomorphology 66:215–235. doi: 10.1016/j.geomorph.2004.09.014

Nomura F, Konagai K, Tajima Y (2010) EXTRACTION OF GEOTECHNICAL PARAMETERS FROM TRACES LEFT IN THE JUNE 14 th 2008 , IWATE-MIYAGI INLAND EARTHQUAKE. Bulletin of ERS, University of Tokyo 43:13–24.

Pierson TC (1985) Initiation and flow behavior of the 1980 Pine Creek and Muddy River lahars, Mount St. Helens, Washington (USA). Geological Society of America Bulletin 96:1056–1069. doi: 10.1130/0016-7606(1985)96<1056:IAFBOT>2.0.CO;2

Prochaska AB, Santi PM, Higgins JD, Cannon SH (2008) A study of methods to estimate debris flow velocity. Landslides 5:431–444. doi: 10.1007/s10346-008-0137-0

Takahashi T (2000) Debris flow Mechanics, Prediction and Countermeasures. Taylor & Francis

Chapter-2

LITERATURE REVIEW

2.1 Fundamentals of debris flow

Translation of any pile of earth materials by gravity is defined as a slope failure in a broader sense. This is a geological phenomenon, including a wide range of earth movements, such as rock falls, topples, debris slides, avalanche etc. Usually, a detached mass contains sand, silt, clay, snow, wood, water i.e. a complex variety of fabrics. Variation of water content determines the triggering condition in most cases. With high water content, the moving mass follows the hydrodynamic laws, while low water content governs the granular dynamics.

A Debris flow is a dangerous and destructive phenomenon in the mountainous region, usually consists of a complex mixture of fine and coarse materials with variable water quantity and long run-out behavior. Defining debris flow in a quantitative manner is a difficult task, though (Hungr et al. 2001) defined debris flow as a very rapid to the extremely rapid flow of saturated non-plastic debris in a steep channel. Generally, it has three distinctive segments: source region, transport channel and depositional area (Fig 2.1). Source region is defined as the site of the detached mass and needs to have an abundant supply of loose debris. Most of the debris flows are channelized and each flow trace is known as a transport channel. Maximum velocities are customarily seen along its transport channel and mass entrainment also occurs in this zone. Finally, flowing mass deposits in the alluvial fan and spreads over a larger area.

Failure of an earth mass and subsequent conversion of gravitational potential energy to kinetic energy initiates a debris flow, mainly on a steep channel gradient. Instability of the slope caused by the reduction of effective stress during an intense rainfall in a short timescale mainly triggers the mass flow. Besides, an intense shake of a mega-earthquake triggers a large number of landslides, leaving a huge amount of loose materials on the steep slopes. These loose materials turn down into debris flow during torrential rains. Aftershocks of any strong shake can also be responsible for the initiation of debris flows. Moreover, repetitive debris flow was also observed after any mega-quake. The swath of

mountainous land affected by the 2008 Wenchuan earthquake for example is a good example of repetitive debris flow occurrence (Chen et al. 2014; Zhang et al. 2014). Total 800 debris flow events had been recorded near the epicenter of the Wenchuan earthquake over the time period of 4 years since the earthquake (Liu et al. 2014). Volcanic eruptions, failures of weakly jointed exposed rocks, sparse vegetation on steep slopes, and breaches of landslide dams can also spark off debris flows.

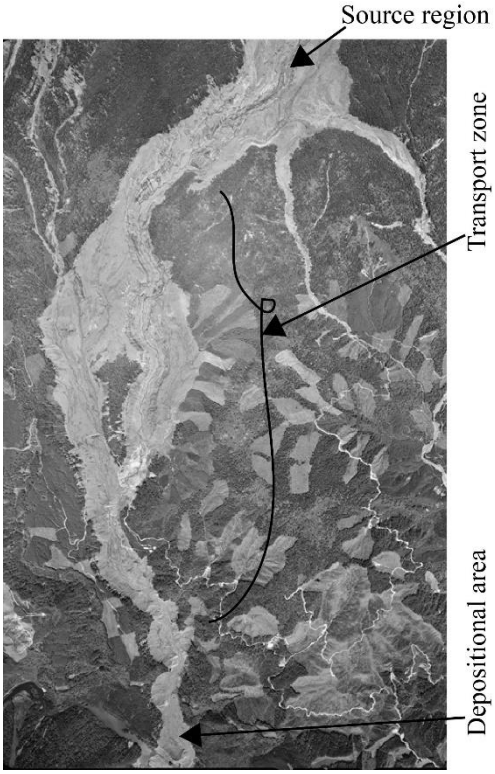

Fig 2.1 Debris flow trace, Satellite imagery showing the entire area of Ontake avalanche which was triggered immediately after the earthquake on September, 1984. (Source: GSI, Japan)

Lack of early warning system, high impact force and entrainment of materials with large inundated area make the debris flow more hazardous and accountable for severe damage all over the world particularly in mountainous areas. 118 people were killed and 4000 became homeless due to Buffalo Creek disaster in USA in 1972 and it costed about 50 million US dollar properties (Vick 1990). Flow slides at Aberfan in 1966 killed 144 people, among them 116 were children (Qiao and Clayton 2013). There was a death toll of about 210 people by a debris flow that occurred on September 9, 1987 in Venezuela which flow was triggered by an intense rainfall in a very short period (Wieczorek et al.

2001). One person was killed and thirteen others injured by the Sham Tseng San Tsuen debris flow in 1999 (Maunsell et al. 2005). In general, at least a median of 165 people have been killed by debris flows worldwide annually (Dowling and Santi 2014).

2.1.1 Classification of debris flow

To describe the debris flow in a subjective manner, debris flow size classification is necessary. (Jakob 2005) proposed a classification considering debris volume, peak discharge and inundated area and a description of the consequences are also given rather qualitative expressions. Using only one parameter for classifying debris flow may not be an ingenious way; thus (Jakob 2005) used several key parameters for his classification. Typically, debris flow volume, run out distance and peak flow rate are needed in designing protective structures. Moreover, the inundated area implicitly determines the flow mobility of the debris mass. Size classification for debris flow is given in Table 2.1.

Table 2.1 Debris flow size classification (Jakob 2005)

Size class	V (m^3)	Q_b (m^3/s)	Q_v (m^3/s)	B_b (m^2)	B_v (m^2)	Potential consequences
1	$<10^2$	<5	<1	$<4x10^2$	$<4x10^3$	Very localized damage, known to have killed forestry workers in small gullies, damage small buildings
2	10^2-10^3	5-30	1-3	$4x10^2$-$2x10^3$	$4x10^3$-$2x10^4$	Could bury cars, destroy a small wooden building, break trees, block culverts, derail trains
3	10^3-10^4	30-200	3-30	$2x10^3$-$9x10^3$	$2x10^4$-$9x10^4$	Could destroy larger buildings, damage concrete bridge piers, block or damage highways and pipelines
4	10^4-10^5	200-1500	30-300	$9x10^3$-$4x10^4$	$9x10^4$-$4x10^5$	Could destroy parts of villages, destroy sections of infrastructure corridors, bridges, could block creeks
5	10^5-10^6	1500-12000	300-$3x10^3$	$4x10^4$-$2x10^5$	$4x10^5$-$2x10^6$	Could destroy parts of towns, destroy forests of 2 sq km in area, block creeks and small rivers
6	10^5-10^6	N/A	$3x10^3$-$3x10^4$	$>2x10^5$	$2x10^6$-$3x10^7$	Could destroy towns, obliterate valleys or fans up to several tens of sqkm in size, dam rivers
7	10^6-10^7	N/A	$3x10^4$-$3x10^5$	N/A	$3x10^7$-$3x10^8$	Could destroy parts of cities, obliterate valleys or fans up to several tens of sqkm in size, dam large rivers
8	10^7-10^8	N/A	$3x10^5$-$3x10^6$	N/A	$3x10^8$-$3x10^9$	Could destroy cities, inundate larg valleys up to 100 sqkm in size, dam large rivers
9	10^8-10^9	N/A	$3x10^6$-$3x10^7$	N/A	$3x10^9$-$3x10^{10}$	Vast and complete destruction over hundreds of sqkm
10	$>10^9$	N/A	$3x10^7$-$3x10^8$	N/A	$>3x10^{10}$	Vast and complete destruction over hundreds of sqkm.

(Here, Q_b and Q_v are the peak discharge for boulder and volcanic debris flows, respectively, B_b and B_v are the area inundated by boulder and volcanic debris flows, and V is the total volume. N/A signifies that boulder debris flows of this magnitude have not been observed)

2.2 Debris flow velocity

A debris flow is characterized by its long run-out, high impact force, large velocity and deposition of its huge debris mass in the alluvial fan. Studies of the dynamic features of debris flow have been an attractive concern for researchers in the field of Geo-hazards. Recognition of key elements which regulate the run-out and physical characteristics of debris slurry are an important issue in the debris flow analysis. Peak discharge, volume, impact force, velocity and material properties are some of the substantial parameters. Among them, velocity is of critical interest in hazard mitigation as velocity affects the run-out length, impact force and time taken for the debris mass to reach the alluvial fan. Any debris mitigation structure requires velocity of the flowing mass either explicitly or implicitly. Therefore, the rational estimation of velocity is prerequisite for this kind of natural hazard prevention.

There are various ways of estimating velocities in hydrodynamics. Nevertheless, highly uncertain and complex nature of debris flow restrict the use of conventional velocity estimation procedures. Merely, a few ways have been used in determining velocity of flowing mass. Broadly, the debris flow velocity estimation procedures are classified into two categories: (1) Analytical solution of velocity approximation, (2) Field investigation, which includes real time monitoring and/or back calculation from super-elevations.

Since 1950s, researchers have devoted much of their energy in modeling debris flow dynamics. Keeping the different features of debris materials on the spotlight, several models have been developed till date. Using these models, analytical solutions of the velocity of flowing mass were developed and reported in technical papers (Takahashi 1987; Takahashi 1991; Coussot et al. 1998; Pudasaini 2011). In recent years, two-phase fluid model gets attraction, and analytical solution for velocity estimation is now available in debris flow dynamics (Pudasaini 2012; Guo et al. 2015). Most of the analytical solutions determine the average flow velocity at a particular section. However, distribution of velocities along the flow depth at a certain section is important to get an insight of the flow dynamics. Recently, several analytical models have been developed to determine the cross-sectional velocity distribution and tested with some real debris events (Han et al. 2014; Han et al. 2015).

Besides, advancement of technology now-a-days allows to use different types of sensors and video cameras for monitoring debris flows (Arattano and Moia 1999; Uddin et al.

1999; Berti et al. 2000; Hürlimann et al. 2003; Galgaro et al. 2005; Takeshi 2011). Sensors have been placed in several positions along natural channels which channels are highly susceptible to debris flow occurrence. Once the mass starts flowing, time taken by the debris front to travel from one position to another is used to estimate the velocity of the flowing mass. Video cameras have also been used to determine velocities using frame by frame analysis (Fig 2.2). Recently, cross-correlation technique has been developed which can be used to estimate flow velocities without distinctive front bores (Arattano and Marchi 2005). Though these approaches of velocity estimation are quite comprehensive, they can't be applied to all debris flow events. Only the highly susceptible areas can be monitored remotely in most countries.

Fig 2.2 Video installation at Kamikami horizawa creek (source: DPRI, Kyoto University, Japan)

However, back calculation of velocity from a measured super-elevation at a curved portion of flow trace is another way to get velocity and is a widely used approach for many practical debris flow analyses (Watanabe and Ikeya 1981; Pierson 1985; Ikeya 1989; Malet et al. 2005; Munoz-Salinas et al. 2007; Prochaska et al. 2008; Chen et al. 2014). Fundamentals of velocity estimation from super-elevations is discussed in detail in the subsequent section.

2.3 Estimation of velocity from super-elevation

Super-elevations and channel geometries that are observed in post-event field surveys have been widely used to estimate flow velocities by practicing engineers. Prior to detail discussion, super-elevation needs to be clearly defined. Super-elevation or banking refers to the difference between flow depths of outer and inner bends of a flow through a curved section. The curved section accelerates any entering flow due to the centrifugal action which results in a higher banking on the outer curve. Schematic outline of super-elevation is illustrated in Fig 2.3.

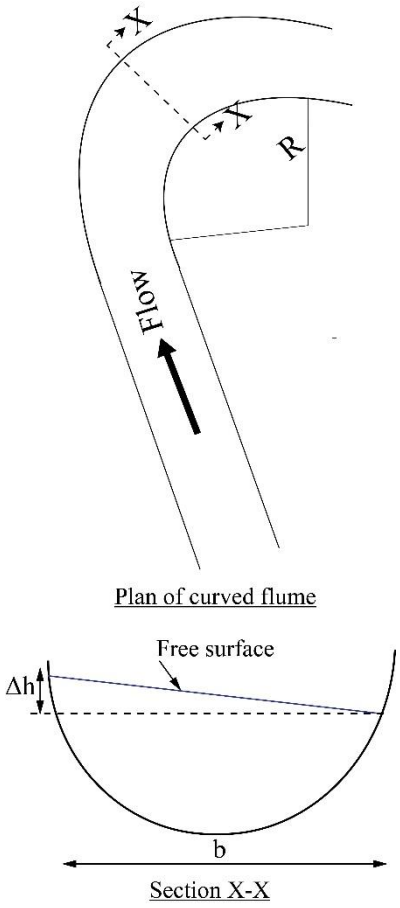

Fig. 2.3 Conceptual illustration of super-elevation

A detached mass usually travels through a channelized gulley and super-elevation appears when the debris mass flows along a curved section of the gulley (Fig. 2.4). By means of the measured super-elevation and other geometrical properties, velocity at a particular section along the bend is approximated using the forced vortex equation (Chow

1959; Apmann 1973) which equates fluid pressure to centrifugal force (McClung 2001) and is given in Eq. 2.1.

$$v = \sqrt{gR_L \frac{\Delta h}{b}} \tag{2.1}$$

where, R_L= radius of curvature of selected flume stretch, Δh= super-elevation, b= width of channel, g= acceleration due to gravity, and v= velocity of debris flow.

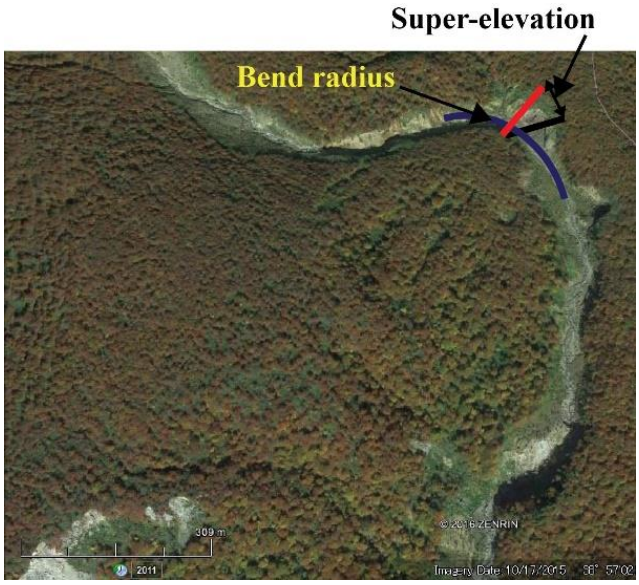

Fig 2.4 Super-elevation along the natural debris channel (source: Google Earth)

The above forced vortex equation is based on the assumption that the flow is subcritical, equal radius of curvature for all the streamlines, and every stream line's velocity is equal to the mean flow velocity. Channel gradient is considered replacing g with$g' = g\cos\alpha$; where α is longitudinal channel inclination. However, this equation, which has been originally derived for a steady pure water flow, does not always yield a good estimate of velocity for a real unsteady debris flow, and to adjust it, a controversial correction factor k has been used for long.

$$\mathrm{v} = \sqrt{g'R \frac{\Delta h}{kb}} \tag{2.2}$$

2.3.1 Discussion on correction factor 'k'

The vortex equation was earlier derived for steady pure water flows; hence it has been considered to be necessary to add a correction factor to the forced vortex equation as

shown in Eq. (2.2) for debris flow analysis. The implementation of the correction factor has been justified as it is linked to the velocity distribution within the flow regime and thus reflecting the viscous nature of the flowing debris mass.

Yet, there are discrepancies in choosing this value and, no significant conclusion was reached to deal with the complicated debris flows. Researchers assume different values depending on the flow condition and material properties. (Hungr et al. 1984) suggested to use k as 2.5 in estimating velocities based on the previous works of (Mizuyama and Uehara 1981; Ikeya and Uehara 1982), which showed that actual super-elevation might be 2.5~5 times larger than that predicted by the vortex equation, $\Delta h = \frac{bv^2}{g/R_L}$. Later (Hungr 2007) revised his statement and now believes that k value is 1.0 for debris flow analysis (Prochaska et al. 2008). (Suwa and Yamakoshi 2000) said that k should be greater or equal to 1.0 for debris flow velocity estimation. (VanDine 1996) stated that k may vary from 1 to 5, while (Chen 1987) reported that k may be as high as 10. (Costa 1984) suggested to use k as 1.0 in the vortex equation. On the contrary, (Bulmer 2002) used k values less than 1.0 to estimate velocities of General's slide, a debris flow in Madison County Virginia, USA. In recent times, (Proctor 2012) related k to the Reynolds number and momentum correction co-efficient. Momentum correction co-efficient value is unity when velocity distribution is uniform over the entire depth alike turbulent flow, while it has values greater than 1.0 for non-uniform velocity distribution. From this aspect, k value is preferred to be 1.0 or greater than 1.0. A bar chart shown in Fig. 2.5 outlined the extent of k values given by the various researchers.

Given a large variation of debris mass features, and lacking rational grounds to use a particular value of k, k value is tentatively set at 1.0 for all the simulations in this dissertation.

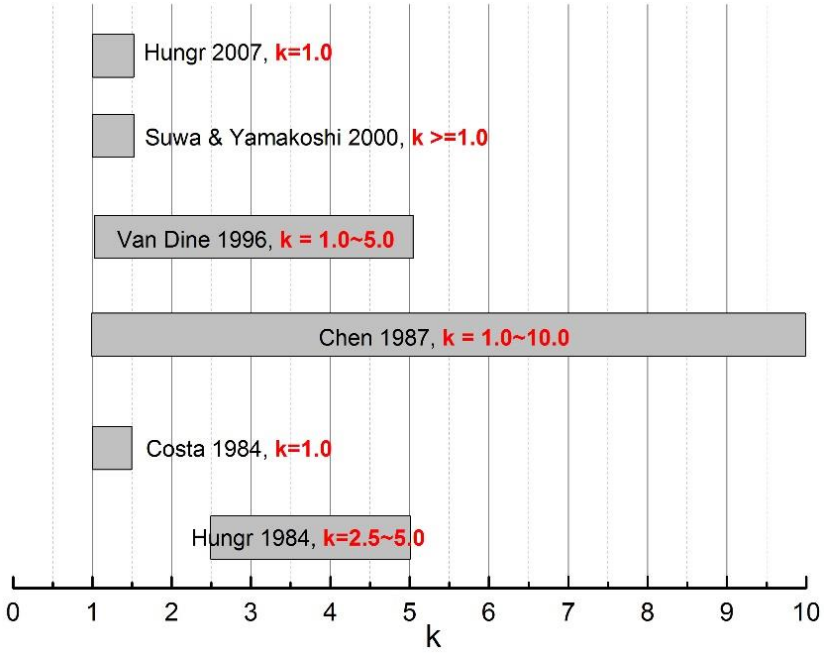

Fig. 2.5 Different *k* values used in vortex equation

2.4 Problems in reality

A post-event field investigation requires measurement of super-elevations and other geometrical properties at selected cross-sections. Even so, extracting these parameters from the field in a quantitative manner is indeed a challenging job. Particularly, determination of bend radius and super-elevation is affected by the flow traces and terrain morphology.

2.4.1 Measurement of radius of curvature

Selection of an appropriate radius for a chosen curved section of natural flow channel is mandatory in estimating the debris flow velocity from the vortex equation. However, one of the problems that comes up in a field survey is that any natural channel is hardly a perfect circle, rather has a varying curvature. The value of *R* depends on how the curve of natural channel with abrupt changes is approximated. Detail discussion on how bend radius is to be estimated is seldom found in any technical writings except (Prochaska et al. 2008) who described difficulties associated with determining the radius. Fig 2.6 depicts the glitches associated with radius approximation. Selection of spacing for a particular section of flow trace (point A in Fig 2.6) changes the approximated radius in a great deal. To address this shortcomings, an iterative approach has been developed in the

earlier stage of this research study, which avoids the subjective way of determining the radius of curvature and will be discussed in detail in later sections.

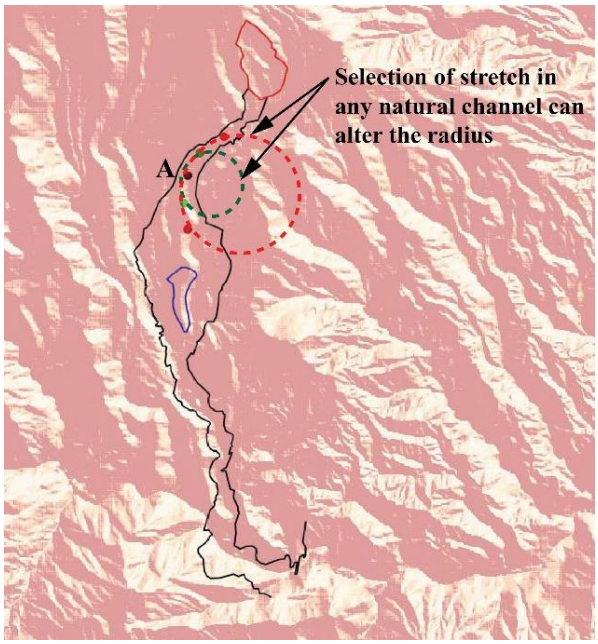

Fig 2.6 Problems in reality in approximating radius of curvature

2.4.2 Measurement of super-elevation

One more critical issue in a field investigation is that only highest flow marks are visible after the disaster which is smaller than actual maximum super-elevation that a particular cross-section experienced during the flow. Fig. 2.7 illustrates the scenario that actually happens in-situ. Therefore, measurement of super-elevation from the mud marks inaccurately predicts the speed of flowing slurry. In some cases, splashing can also lead to an erroneous measurement of super-elevation. Flow, which may strike the outer bend and splashes back to the inner bend, attributes to the higher elevation on the inner side which eventually decrease the actual super-elevation. To account for this problem, a series of numerical analyses are run and is the core part of this dissertation.

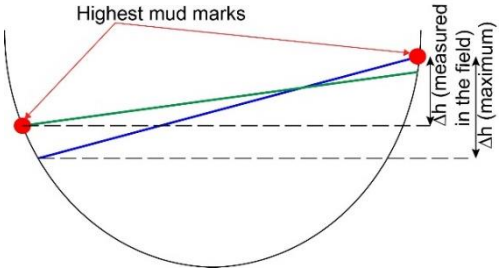

Fig. 2.7 Problems in reality in estimating super-elevation

2.5 Earlier studies on velocity estimation

2.5.1 Previous experimental investigations

Research to check out the suitability of using super-elevation to estimate debris flow velocity has started in 1980s. (Ikeya and Uehara 1982), firstly conducted a curved flume test to justify the application of super-elevation. Their s-shaped curved flume is shown in Fig. 2.8.

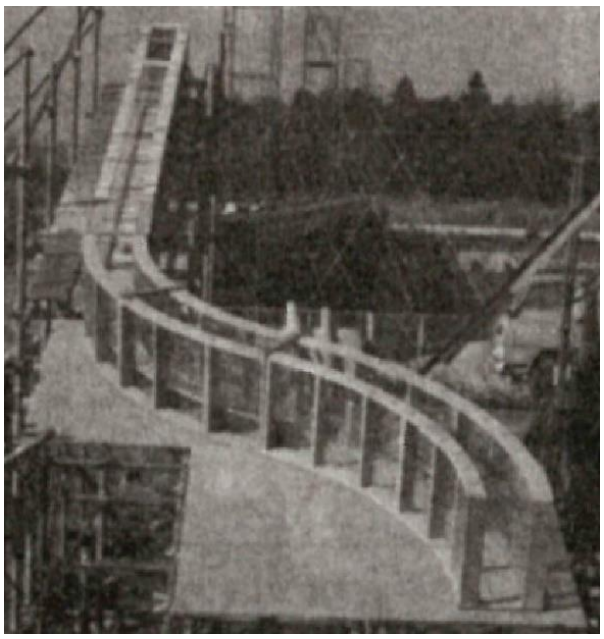

Fig 2.8 An s-shaped flume for debris flow analysis (Ikeya and Uehara 1982)

Afterward, (Iverson et al. 1994) performed a flume test in USGS laboratory. They concluded that super-elevation derived velocity underestimates actual velocity by about 30%, and also examined the selection criteria of channel width. Effective channel width that follows the examined criteria yielded velocities closer to real velocities than those obtained from the entire flume width. (Mizuno 2004) published experimental results of small scale s-curved channel to estimate the velocity of flowing mass.

In recent years, (Proctor 2012) did an experimental investigation using an 8m long flume to find the effects of different parameters on velocity estimation. He also performed straight channel experiments to compare his curved flume test with the ones through the straight flume. Different material properties were taken into consideration. His experimental results revealed the significant effect of channel gradient on velocity estimation. He also found that super-elevation increases in a power law relationship with

increasing velocity, which was the largest for tighter bend geometry. A non-linear increase in super-elevation with decreasing velocity was also seen in his experimental findings. Moreover, he tried to determine *k* value, which was not always constant and was less than 1.0 on contrary to the widely used theories. Layout of his curved flume is shown in Fig. 2.9.

Furthermore, the latest research on this topic was published in 2015 by (Scheidl et al. 2014) which describes the insights into super-elevation derived velocity estimation procedure. A series of flume tests were run for different channel inclinations, radius and material properties so that the effects can be described in a quantitative manner. They found that channel gradient as well as centerline radius has large effects on velocity estimation. Variation of *k* values depending on other parameters was also examined and their results revealed a statistically significant relation between *k* and Froude number. Techniques to extract necessary parameters along the curved section were also described in detail in this research work.

Fig 2.9 A curved flume for debris flow analysis (Source: Durham University)

The research works mentioned above are found in technical writings. Flume tests in previous experimental works were mainly focusing on the effects of different parameters in velocity estimation. However, in reality, these parameters are determined from field investigations and arbitrary extraction of these parameters can prejudice velocities in a great deal; more specifically measuring super-elevation and equivalent radius of curvature needs a second thought before using them in the vortex equation to estimate

the flow velocity. Next section describes an attempt to rationally estimate the radius of curvature of a natural flow channel.

2.5.2 Iterative approach of velocity estimation

Flow surface of debris slurry tilts once it gets into the curved section and at a certain point reaches its maximum tilting surface and gradually lessens to the flat surface again with the decreasing curvature. Hence, the time taken for the slurry to reach the maximum tilting position is considered to be a function of the sloshing period of the selected cross-section. Subsequently, estimated time of sloshing period is employed to set the length of the curved section of the natural flume for rationally estimate the equivalent radius of curvature and a repetitive procedure is formulated, which procedure avoids the subjective means of determining curve radius (Rahman Md. et al. 2015). This iterative process is based on some simplified assumptions and given as follows:

(a) The plan of the flume is approximated by an arc of radius R_L connecting two straight channels at its both ends (Fig 2.10). This assumption indicates that a single square time history of centrifugal force is applied to the debris slurry through the arc section.

(b) The transverse cross-section of the flume is assumed to be a constant arc with radius R_c over its entire stretch.

(c) Viscous feature of the debris slurry is ignored.

(d) Steady state flow is discussed. Other than this,

(e) All Lagrangian particles of the debris slurry that exist on a particular transverse cross-section of the flume at a certain time remain plane throughout the entire flowing process.

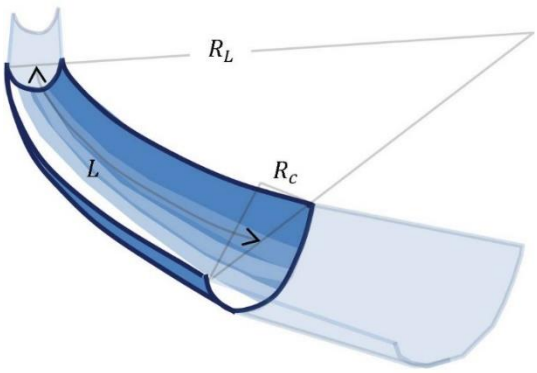

Fig 2.10 Curved stretch of a flume connecting two straight channel

2.5.2.1 Principles of sloshing

Sloshing is defined as the motion of fluid within a particular cross-section by the external excitation (Wu et al. 1998). Fig 2.11 gives the conceptual outline of one sloshing period.

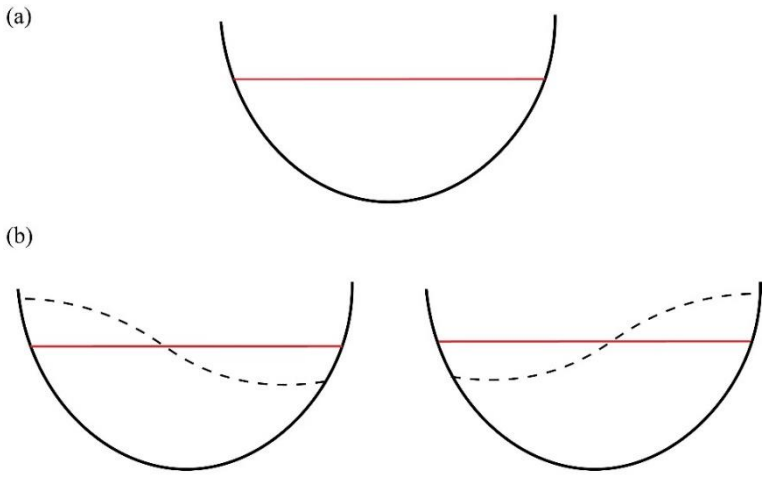

Fig 2.11 Fundamentals of sloshing; (a) initial static channel section, (b) one complete cycle of sloshing

In Fig 2.11 (a), the red solid line represents the static flow surface of a cross-section. With external excitation, the free surface moves back and forth in the transverse direction. The time taken from the free surface to complete one cycle of periodic movement is referred as sloshing period.

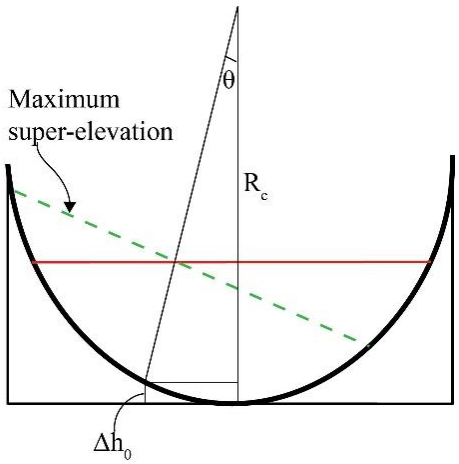

Fig 2.12 Determination of sloshing period

Fig 2.12 portrays the basic idea of determining sloshing period. Consider a typical cross-section having a constant arc of radiusR_c. Red solid line represents the initial free surface of the flowing mass. Finally, the flow surface is elevated and the maximum super-

elevation is reached as illustrated with the green dotted line in Fig.2.12. It is assumed through this process that all the initial kinetic energy in the transverse direction can be converted to potential energy. Thus equating these energies, one obtains:

$$\frac{1}{2}mv_{max}^2 = mg\Delta h_0 \tag{2.3}$$

$$v_{max}^2 = \sqrt{2g\Delta h_0} \tag{2.4}$$

From Fig 2.12,

$$\Delta h_0 = R_c(1 - \cos\theta) \tag{2.5}$$

Substituting Δh_0 in Eq 2.4,

$$v_{max} = \sqrt{2gR_c(1 - \cos\theta)} \cong \sqrt{gR_c\theta^2} \tag{2.6}$$

Assuming the principle of harmonic motion,

$$v = R_c \sin\theta \sin\frac{2\pi t}{T} \tag{2.7}$$

Applying the condition of maximum value,

$$v_{max} = \frac{2\pi}{T}R_c \sin\theta \cong \frac{2\pi}{T}R_c\theta \tag{2.8}$$

Equating Eq. (2.6) and (2.8), gives the sloshing period and written below:

$$T = 2\pi\sqrt{\frac{R_c}{g}} \tag{2.9}$$

2.5.2.2 Step wise procedure of velocity estimation

Rahman et al (2005) developed the following iterative procedure to determine objectively the velocity along the bend section:

(a) First, specify the target curved channel of length L_1

(b) For this specified stretch of the channel, obtain the average radius of curvature $R_{L,1}$, and the average transverse cross-section with radius $R_{c,1}$ (Assumption 2)

(c) Given the observed super-elevation Δh across the flow width b, and ignoring viscous features of the debris slurry (Assumption 3), obtain the initial estimate of flow velocity $v_{0,1}$ using Eq. 2.2

(d) For the average transverse cross-section with radius$R_{c,1}$, obtain the time for the maximum super elevation to be reached, $T_{0,1}$, which time is tentatively set at a quarter the sloshing period $T_{s,1}$ given by Eq. 2.9

(e) Multiplying initial constant (steady state) flow velocity $v_{0,1}$ by $T_{0,1}$, the entire stretch of the flume was updated to be L_2.

(f) For this updated stretch, the above mentioned procedures (i) through (v) were repeated until sufficient and necessary convergence is reached.

The above procedure allows us to avoid any arbitrariness in estimating the equivalent radius of curvature to be sure, but the adopted assumptions (a) through (e) on page 20 may not be always appropriate. Moreover, the time $T_{0,i}$ for the slurry to reach its maximum super elevation may not be equal to a quarter the sloshing period $T_{s,i}$ depending on the initial condition, rather closer to halt of it. This problem will be further discussed in detail through numerical simulations in this dissertation.

2.6 Significance of the study

Setting up video cameras at different points of susceptible area could make a reasonable estimate of debris flow velocity. But, this technique is expensive and requires continuous monitoring, and we cannot monitor every suspicious natural channel. Thus far, readily available and plausible information to estimate velocity is the mud prints that left after the disaster. Accordingly, extensive study is required to develop or modify the strategy for plausible estimation of debris flow velocity. Only few experimental works (Mizuno 2004; Proctor 2012; Scheidl et al. 2014) were conducted so far to check the suitability of using forced vortex equation and no numerical study is reported.

Addressing all the shortcomings is impossible in any case. Small scale laboratory flume test can surely provide rational ideas about debris flow velocity. However the law of similarity will not be well satisfied in a small scale model test. At the other extreme, a model test of a full scale debris flow is cumbersome and very difficult to realize. With the progress of computer facilities, these large scale events are now-a-days modelled numerically and provide better agreement with the actual state of event. Thus, keeping all the issues in mind, this research develops a numerical tool for the adjustment of debris flow velocity, and findings from numerical simulations are validated with three devastating debris flow events in Japan. The research procedures and results are described in the succeeding chapters.

References

Apmann RP (1973) Estimating discharge from superelevation in bends. Journal of the Hydraulics Division 99:65–79.

Arattano M, Marchi L (2005) Measurements of debris flow velocity through cross-correlation of instrumentation data. Natural Hazards and Earth System Sciences 5:137–142. doi: 10.5194/nhess-5-137-2005

Arattano M, Moia F (1999) Monitoring the propagation of a debris flow along a torrent. Hydrological Sciences Journal 44:811–823. doi: 10.1080/02626669909492275

Berti M, Genevois R, LaHusen R, et al (2000) Debris Flow Monitoring in the Acquabona Watershed on the Dolomites (Italian Alps). Physics and Chemistry of the Earth, Part B: Hydrology, Oceans and Atmosphere 25:707–715. doi: doi: DOI: 10.1016/S1464-1909(00)00090-3

Bulmer MH (2002) An empirical approach to studying debris flows: Implications for planetary modeling studies. Journal of Geophysical Research 107:5033. doi: 10.1029/2001JE001531

Chen CL (1987) Comprehensive review of debris flow modeling concepts in Japan. Reviews in Engineering Geology 7:13–30.

Chen HX, Zhang LM, Zhang S (2014) Evolution of debris flow properties and physical interactions in debris-flow mixtures in the Wenchuan earthquake zone. Engineering Geology 182:136–147. doi: 10.1016/j.enggeo.2014.08.004

Chow VT (1959) Open-Channel Hydraulics.

Costa JE (1984) Physical geomorphology of debris flows. In: Developments; and applications of geomorphology. Springer-Verlag; New York, pp 268–317

Coussot BP, Laigle D, Arattano M, et al (1998) Direct determination of rheological characteristics of debris flow. Journal of hydraulic engineering 865–868.

Dowling CA, Santi PM (2014) Debris flows and their toll on human life: A global analysis of debris-flow fatalities from 1950 to 2011. Natural Hazards 71:203–227. doi: 10.1007/s11069-013-0907-4

Galgaro a., Tecca PR, Genevois R, Deganutti a. M (2005) Acoustic module of the Acquabona (Italy) debris flow monitoring system. Natural Hazards and Earth System Science 5:211–215. doi: 10.5194/nhess-5-211-2005

Guo S, Xu P, Zheng Z, Gao Y (2015) Estimation of flow velocity for a debris flow via the two-phase fluid model. Nonlinear Processes in Geophysics 22:109–116. doi: 10.5194/npg-22-109-2015

Han Z, Chen G, Li Y, et al (2014) A new approach for analyzing the velocity distribution of debris flows at typical cross-sections. Natural Hazards 74:2053–2070. doi: 10.1007/s11069-014-1276-3

Han Z, Chen G, Li Y, et al (2015) Exploring the velocity distribution of debris flows: An iteration algorithm based approach for complex cross-sections. Geomorphology 241:72–

82. doi: 10.1016/j.geomorph.2015.03.043

Hungr O, Evans SG, Bovis MJ, Hutchinson JN (2001) A review of the classification of landslides of the flow type. Environmental & Engineering Geoscience VII:221–238. doi: 10.2113/gseegeosci.7.3.221

Hungr O, Morgan GC, Kellerhals R (1984) Quantitative analysis of debris torrent hazards for design of remedial measures. Canadian Geotechnical Journal 21:663–677. doi: 10.1139/t84-073

Hürlimann M, Rickenmann D, Graf C (2003) Field and monitoring data of debris-flow events in the Swiss Alps. Canadian Geotechnical Journal 40:161–175. doi: 10.1139/t02-087

Ikeya H (1989) Debris flow and its countermeasures in Japan. Bulletin of the International Association of Engineering Geology-Bulletin de l'Association Internationale de G{é}ologie de l'Ing{é}nieur 40:15–33.

Ikeya H, Uehara S (1982) Debris flow in S-shaped channel curves. Civil Engineering Journal, PWRI 24:645–650.

Iverson RM, LaHusen RG, Major JJ, Zimmerman CL (1994) Debris flow against obstacles and bends; dynamics and deposits. Eos, Transactions, American Geophysical Union 274.

Jakob M (2005) A size classification for debris flows. Engineering Geology 79:151–161. doi: 10.1016/j.enggeo.2005.01.006

Liu J, You Y, Chen X, et al (2014) Characteristics and hazard prediction of large-scale debris flow of Xiaojia Gully in Yingxiu Town, Sichuan Province, China. Engineering Geology 180:55–67. doi: 10.1016/j.enggeo.2014.03.017

Malet J-P, Laigle D, Remaître A, Maquaire O (2005) Triggering conditions and mobility of debris flows associated to complex earthflows. Geomorphology 66:215–235. doi: 10.1016/j.geomorph.2004.09.014

Maunsell F, Wilson S, Venture J (2005) Debris flow at Sham Tseng San Tsuen of 23 August 1999.

McClung DM (2001) Superelevation of flowing avalanches around curved channel bends. Journal of Geophysical Research 106:16489. doi: 10.1029/2001JB000266

Mizuno H (2004) Experimental study on a estimating method for velocity of debris flow in bending curves. Journal of Erosion Control Engineering 57:56–59.

Mizuyama T, Uehara S (1981) Debris flow in steep slope channel curves. Civil Engineering Journal, PWRI 23:243–248.

Munoz-Salinas E, Manea VC, Palacios D, Castillo-Rodriguez M (2007) Estimation of lahar flow velocity on Popocat??petl volcano (Mexico). Geomorphology 92:91–99. doi: 10.1016/j.geomorph.2007.02.011

Pierson TC (1985) Initiation and flow behavior of the 1980 Pine Creek and Muddy River lahars, Mount St. Helens, Washington (USA). Geological Society of America Bulletin

96:1056–1069. doi: 10.1130/0016-7606(1985)96<1056:IAFBOT>2.0.CO;2

Prochaska AB, Santi PM, Higgins JD, Cannon SH (2008) A study of methods to estimate debris flow velocity. Landslides 5:431–444. doi: 10.1007/s10346-008-0137-0

Proctor CM (2012) Debris flow dynamics: A flume study of velocity and superelevation. Durham University

Pudasaini SP (2011) Some exact solutions for debris and avalanche flows. Physics of Fluids. doi: 10.1063/1.3570532

Pudasaini SP (2012) A general two-phase debris flow model. Journal of Geophysical Research: Earth Surface 117:1–28. doi: 10.1029/2011JF002186

Qiao SF, Clayton CRI (2013) Flow slides run-out prediction using a sliding-consolidation model. Landslides 10:831–842. doi: 10.1007/s10346-013-0426-0

Rahman Md. A, Hashimoto T, Konagai K (2015) An attempt for velocity estimation of Nebukawa debris flow triggered by the Great Kanto Earthquake, 1923. Journal of Japan Society of Civil Engineers, Ser A1 (SE/EE) 71:I_387–I_394. doi: doi.org/10.2208/jscejseee.71.I_387

Scheidl C, Mcardell BW, Rickenmann D (2014) Debris-flow velocities and superelevation in a curved laboratory channel. 20:1–20. doi: 10.1139/cgj-2014-0081

Suwa H, Yamakoshi T (2000) Estimation of debris-flow motion by field surveys. In: Proceedings of The Second International Conference on Debris-Flow Hazards Mitigation.

Takahashi T (1987) High velocity flow in steep erodible channels. In: Proc. IAHR Congress. pp 42–53

Takahashi T (1991) Debris flow: Monograph of IAHR. Rotterdam:1–165.

Takeshi T (2011) Evolution of Debris-flow Monitoring Methods on Sakurajima. International Journal of Erosion Control Engineering 4:21–31.

Uddin MS, Inaba H, Itakura Y, et al (1999) Adaptive computer-based spatial-filtering method for more accurate estimation of the surface velocity of debris flow. Applied optics 38:6714–21. doi: 10.1364/AO.38.006714

VanDine DF (1996) Debris Flow Control Structures for Forest Engineering.

Vick SG (1990) Planning, Design, and Analysis of Tailings Dams. BiTech Publishers Limited

Watanabe M, Ikeya H (1981) Investigation and analysis of volcanic mud flows on Mt Sakurajima, Japan. Proceedings of Symposium on Erosion and Sediment Transport Measurement 245–256.

Wieczorek GF, Larsen MC, Eaton LS, et al (2001) Debris-flow and flooding hazards associated with the December 1999 storm in coastal Venezuela and strategies for mitigation.

Wu GX, Ma QW, Eatock Taylor R (1998) Numerical simulation of sloshing waves in a

3D tank based on a finite element method. Applied Ocean Research 20:337–355. doi: 10.1016/S0141-1187(98)00030-3

Zhang Y, Cheng Y, Yin Y, et al (2014) High-position debris flow: A long-term active geohazard after the Wenchuan earthquake. Engineering Geology 180:45–54. doi: 10.1016/j.enggeo.2014.05.014

Chapter-3

SMOOTHED PARTICLE HYDRODYNAMICS

3.1 Introduction to numerical modeling

Debris flow analysis is one of the primary topics of natural hazard mitigation. Now-a-days, advancement of high computing tools makes numerical analysis a feasible and reliable option to identify the key factors that govern the dynamic features of debris flow. Over recent decades, several numerical simulations based on Eulerian description have been used in analyses of debris flows (O'Brien et al. 1993; Troncone 2005; Jakob et al. 2013). However, large deformation characteristics of debris flow materials restrict the use of conventional mesh-based method. Recently, several mesh free methods (Hungr 1995; Abe et al. 2007; Abe et al. 2013; Kazmi et al. 2014; Manzanal et al. 2016) have been applied for studying debris flows. Among several mesh-free methods, Smoothed Particle Hydrodynamics (SPH) is a promising numerical tool described in Lagrangian description and used in the current research studies.

3.2 Background of SPH

SPH was initially formulated to use in astrophysical problems (Lucy 1977) and later expanded into diverse fields including viscous flows (Fang et al. 2006), hydrodynamics problems (Gomez-Gesteria, M. 2004; Crespo et al. 2008; Zheng and Duan 2010; Chang et al. 2011; Jian et al. 2015) , free surface flows (Ferrari et al. 2009; Ferrari 2010; Ozbulut et al. 2014), seepage studies (Maeda et al. 2006; Zhang and Maeda 2014; Zhang and Maeda 2015), liquefaction studies (Naili et al. 2005; Huang et al. 2011b) ,slope stability studies (Bui et al. 2008; Bui et al. 2011; Bui and Fukagawa 2013), long-lasting geotechnical hazard issues (Huang et al. 2011a; Dai et al. 2014; Hu et al. 2014; Huang et al. 2014; Wang et al. 2016) and many other fields. It can track the motion of each particle, accurately predict the velocity and naturally handle the free surface flows, hence make it purely Lagrangian in nature. Complex geometrical modelling can also be done easily as there is no mesh connectivity in the SPH method.

In recent years, run-out analysis of real scale flow-like landslides and debris flows were simulated using SPH both in 2D and 3D space (Huang et al. 2011a; Minatti and Pasculli 2011; Viccione and Bovolin 2011; Dai et al. 2014; Hu et al. 2014; Wang et al. 2016). Furthermore, depth integrated SPH techniques has also been formulated and used in landslide and debris-flow modeling (Pastor et al. 2009; Calvo et al. 2014; Pastor et al. 2014; Manzanal et al. 2016). Accumulating all the affirmative features, SPH is a doable approach for debris flow velocity analysis. This research developed a 3D numerical model based on weakly compressible SPH with two validation examples. Afterward numerical simulations of curved flumes were performed and super-elevations at different cross sections were taken to estimate the speed of flowing debris. Detail features of SPH are described in the subsequent sections of this chapter.

3.3 Fundamentals of SPH

In SPH, the continuum is described by a set of arbitrary points without any connectivity which makes this method mesh free. Each point has a prescribed area/domain, referred to as a particle and contemplates as an integration point in the calculation scheme. Particles update their properties from neighboring particles using a smoothing kernel function and mass and momentum equations are solved. Afterward, their positions are updated using numerical integration over the entire domain. As there is no mesh connectivity among particles over the entire problem domain, it can easily simulate free surface flow and large deformation in hydrodynamics as well as solid mechanic's problems. Fig 3.1 illustrates the fundamentals of SPH formulation.

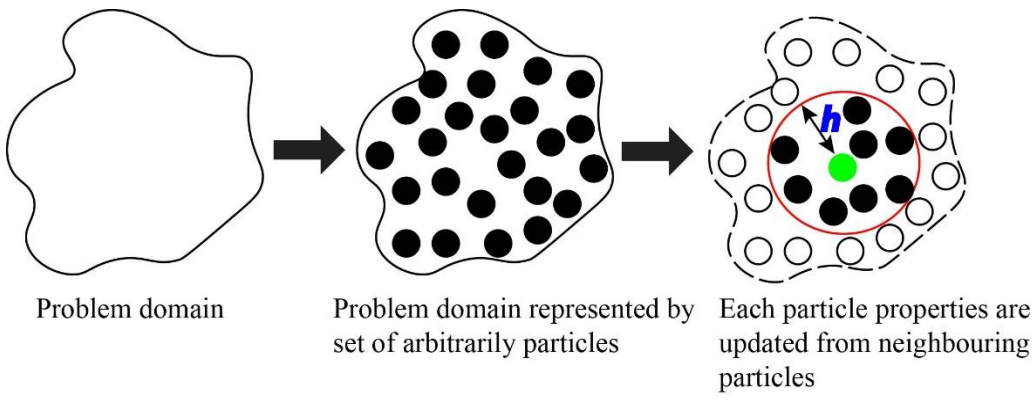

Fig 3.1 Basic idea of SPH formulation

The basic formulation of SPH is divided into two steps: kernel approximation and particle approximation. The integration of the multiplication of an arbitrary function and a smoothing kernel function gives the kernel approximation in the form of integral representation of the function. Using the kernel approximation, the integral representation can be formulated as

$$f(x) = \int_{\Omega} f(x')W(x - x', h)dx' \tag{3.1}$$

Where, f is a function of the three-dimensional position vector x, W is the smoothing kernel and Ω is the volume of integral that contains x. The continuous kernel approximation can be summed up over all the particles within the support domain, which is known as particle approximation. After some trivial transformations, Eq. 3.1 can be written as

$$f(x_i) = \sum_{j=1}^{N} \frac{m_j}{\rho_j} f(x_j) W_{ij} \tag{3.2}$$

where, m_j is the mass of particle 'j', ρ_j is the density of particle 'j', N is the total number of particles within the influence domain of particle 'i' . Particle 'j' refers to the particles of interest within the support domain of particle 'i'. Support domain of any particles is determined by the influence length 'h'.

3.3.1 Smoothing function

Several smoothing functions are used in SPH scheme which meets the basic properties of smoothing kernel function (Liu and Liu 2010). Yet, the most commonly used smoothing function is cubic spline or B-spline (Monaghan and Lattanzio 1985) and applied in many practical SPH analyses (Maeda et al. 2006; Bui et al. 2008; Crespo et al. 2008; Huang et al. 2014). The main advantage of using cubic spline is that it resembles a Gaussian function while having a narrower compact support. Therefore, the cubic spline smoothing function was used in current SPH formulation which is written in Eq. 3. 3

$$\mathrm{W}(R, h) = \frac{3}{2\pi h^3} \begin{cases} \frac{2}{3} - R^2 + \frac{1}{2}R^3 & 0 \le R < 1 \\ \frac{1}{6}(2 - R)^3 & 1 \le R < 2 \\ 0 & R \ge 2 \end{cases} \tag{3.3}$$

3.4 Governing equations

The Navier-Stokes equations are introduced as governing equations in SPH framework. Based on the previous description of fundamentals of SPH, the SPH formulation of Navier-Stokes equation i.e. mass and momentum equations can be written as:

$$\frac{d\rho_i}{dt} = \sum_{j=1}^{N} m_j \left(v_i^\beta - v_j^\beta\right) \nabla_i W_{ij} \tag{3.4}$$

$$\frac{dv_i^\beta}{dt} = \sum_{j=1}^{N} m_j \frac{\sigma_i^{\alpha\beta} + \sigma_j^{\alpha\beta}}{\rho_i \rho_j} \nabla_i W_{ij} \tag{3.5}$$

where, $\sigma_i^{\alpha\beta}$ is the stress tensor which has pressure part and viscous part, $\nabla_i W_{ij}$ is the derivative of kernel function calculated using Eq. 3.6

$$\nabla_i W_{ij} = \frac{X_{ij}}{r_{ij}} \frac{\partial W_{ij}}{\partial r_{ij}} \tag{3.6}$$

Following Eq. 3.6, derivative of cubic spline kernel function is written as,

$$\nabla_i W_{ij} = \frac{3}{2\pi h^3} \begin{cases} \frac{X_{ij}}{r_{ij} h_{ij}} \left(-2R + \frac{3}{2} R^2\right) & 0 \le R < 1 \\ \frac{-X_{ij}}{2 h_{ij} r_{ij}} (2 - R)^2 & 1 \le R < 2 \\ 0 & R \ge 2 \end{cases} \tag{3.7}$$

Total stress tensor can be represented as,

$$\sigma^{\alpha\beta} = -pI + \tau^{\alpha\beta} \tag{3.8}$$

where, p is the pressure term, I is identity matrix and $\tau^{\alpha\beta}$ is the viscous stress tensor determined by the appropriate constitutive law. In-depth discussion about constitutive law for debris flow analysis is given in Chapter-4.

3.5 Evolution of pressure

Pressure in SPH is usually computed in two ways: either using equation of state (EOS) or solving the pressure Poisson equation (PPE). Incompressible SPH (ISPH) approximates pressure by solving PPE and has the advantage of smoothing pressure distribution especially near the boundary (Shao and Lo 2003; Khayyer et al. 2008; Khayyer et al. 2009; Ran et al. 2015), while using an EOS sometimes makes the entire solution unstable. However, recently (Shadloo et al. 2012) made a comparison between traditional SPH & ISPH and found compatible results for some benchmark tests. Hence,

in the current research, pressure was approximated using the widely used EOS (Liu and Liu 2003), which is given in the following form:

$$p = B\left[\left(\frac{\rho}{\rho_0}\right)^{\gamma} - 1\right] \tag{3.9}$$

where, ρ_0 is the initial density, ρ is the density at current time step, γ is a dimensionless parameter taken as 7.0 based on literatures, B is the problem dependent parameter and calculated using the following equation.

$$B = \frac{c^2\rho_0}{\gamma} \tag{3.10}$$

where, c is the speed of sound. In SPH calculation, speed of sound needs careful observation. If the actual velocity of sound is used, the real fluid is as assumed to be the artificial fluid, which is ideally incompressible. According to (Monaghan 1994), the density variation is

$$\delta = \frac{\Delta\rho}{\rho_0} = \frac{v_b^2}{c^2} = M^2 \tag{3.11}$$

Here, v_b is the fluid bulk velocity and M is the Mach number and preferable value of M is 0.1. Sometimes c is set at ten times the maximum velocity (Liu and Liu 2003).

3.6 Incorporation of artificial viscosity

Unphysical oscillation and particle penetration can lead to blow up of particles in SPH simulations. To dissipate this kind of oscillation, an artificial viscosity term is added to the pressure term of the momentum equation (Monaghan and Gingold 1983; Monaghan and Pongracic 1985; Monaghan 1989). This Monaghan type artificial viscosity (Π_{ij}) not only provides the necessary dissipation but also prevents unphysical penetration of particles approaching each other. Its mathematical expression is given below:

$$\Pi_{ij} = \begin{cases} \dfrac{-\alpha_\Pi c_{ij}\phi_{ij} + \beta_\Pi \phi_{ij}^2}{\rho_{ij}} & v_{ij}x_{ij} < 0 \\ 0 & v_{ij}x_{ij} > 0 \end{cases} \tag{3.12}$$

where,

$$\phi_{ij} = \frac{h_{ij}v_{ij}x_{ij}}{\left|x_{ij}\right|^2 + \left(0.1h_{ij}\right)^2} \tag{3.13}$$

$$h_{ij} = \frac{h_i + h_j}{2} \tag{3.14}$$

$$\rho_{ij} = \frac{\rho_i + \rho_j}{2} \tag{3.15}$$

$$c_{ij} = \frac{c_i + c_j}{2} \tag{3.16}$$

3.7 Boundary condition

Traditional grid based method can easily handle the boundary condition, whereas boundary is an immense problem in particle method. Furthermore, complex geometrical shape makes it more complicated to deal with. SPH suffers much from its beginning to accurately model the boundary condition. Properties of each particle in the problem domain are updated by taking summation over the supporting domain in SPH. However, near the boundary region, the deficiency of particles may lead to unrealistic results in many cases. Researches to overcome this boundary deficiency has been studied widely and several techniques are now-a-days adopted to elucidate this issue. Common approaches are solid boundary treatment, symmetrical particles, fixed virtual particles and wall boundary treatment (Adami et al. 2012; Liu et al. 2012; Shao et al. 2012). Typically used boundary treatments are described in the following sub-sections.

3.7.1 Fixed boundary particles

Single layer of fixed particles is placed along the boundaries of the problem domain to generate the boundary condition and its conceptual scheme is illustrated in Fig 3.2. Any real particles approaches within the support area of boundary particles feel a repulsive force which prevents penetration of real particles beyond the boundary. Lennard-Jones type repulsive force is the initial formulation of repulsive force that added to the existing SPH method (Liu and Liu 2003). Nevertheless, this force is highly sensitive and leads to a sudden blowup of particles, especially for 3D simulations and several trial simulations with this sort of repulsive force reveals the above assertion.

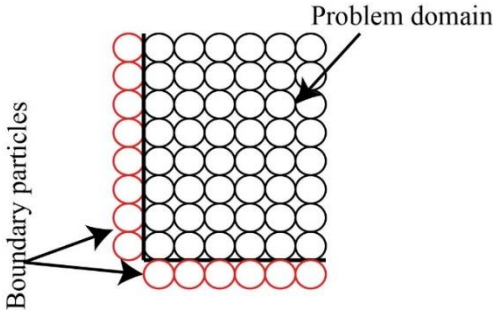

Fig 3.2 Fixed boundary particles

Recently, a novel type of repulsive force (f_{ij}) formulation has been developed and checked with several benchmark tests (Liu et al. 2012; Shao et al. 2012). This repulsive force quite satisfactorily prevents particle penetration and provide smooth flow condition. Detail formulations are depicted below:

$$\mathrm{f}_{ij} = 0.01\, c^2 \chi f(\eta) \frac{X_{ij}}{r_{ij}^2} \tag{3.17}$$

where,

$$\chi = \begin{cases} 1 - \dfrac{r_{ij}}{1.5\Delta d} & 0 < r_{ij} < 1.5\Delta d \\ 0 & otherwise \end{cases} \tag{3.18}$$

$$\eta = \frac{r_{ij}}{0.75 h_{ij}} \tag{3.19}$$

$$f(\eta) = \begin{cases} 2/3 & 0 < \eta < 2/3 \\ 2\eta - 1.5\eta^2 & 2/3 < \eta < 1 \\ 0.5(2-\eta)^2 & 1 < \eta < 2 \\ 0 & otherwise \end{cases} \tag{3.20}$$

Here, Δd is initial particle spacing, r_{ij} is the distance between particle i and particle$j$, and h_{ij} is the smoothing length.

3.7.2 Mirroring boundary particles

When any real particle approaches close to the boundary region, i.e. within the support domain from the boundary, a mirror particle is placed beyond the boundary to prevent penetration of real particle (Liu and Liu 2003; Liu et al. 2012). These mirror particles are produced at every time step based on the position of real particles. The idea of mirror particle can be best understood from the following schematic Fig. 3.3.

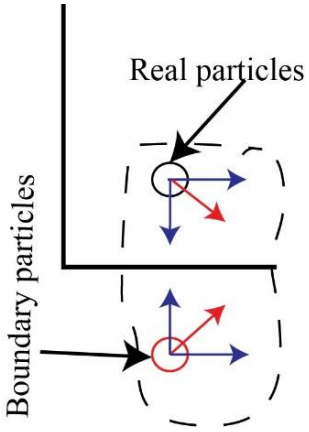

Fig 3.3 Mirror boundary particles in SPH

3.7.3 No slip boundary condition

Another method to describe a solid boundary is to place several layers of boundary particles. These boundary particles have density and mass of the initial values. Boundary particles contribute to the usual SPH approximation of mass and momentum equations. For any interacting real and boundary particles, normal distance from the boundary line are calculated and an artificial velocity is applied to exert no-slip condition (Morris et al. 1997; Bui et al. 2008). For a regular problem domain, this approach performs quite satisfactorily and portrays smoothed flow conditions. However, in dealing with a curved surface, this type of particle may not be so appropriate because of the complicated calculations which eventually increase the computational time.

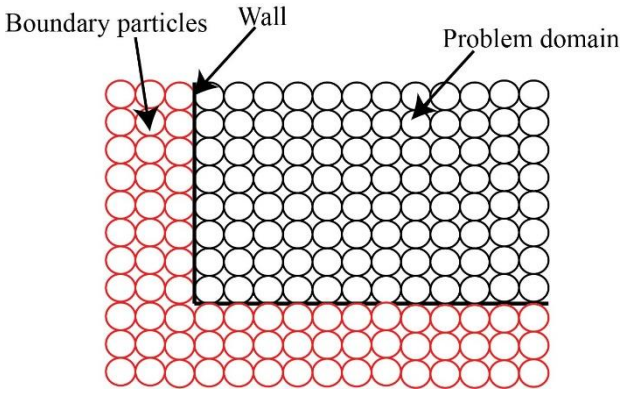

Fig 3.4 No-slip boundary condition

3.7.4 Selection of boundary condition

Fixed layer of boundary particles with Lennard-Jones type repulsive force has been employed in many 2D SPH applications as reported earlier. Yet, parameters of this type

of repulsive force equation are too sensitive and sometimes lead to instability of particles along the boundaries.

Instead, solid boundary treatment (SBT) with improved repulsive force can smoothly simulate the flow condition. In this type of boundary treatment, a fixed layer of particles is placed along the boundary, and it exhibits a repulsive force in the tangential and normal directions of the boundary (Monaghan et al. 2003; Abdolmaleki 2011). Recently, (Liu et al. 2012; Shao et al. 2012) improved this repulsive force computation, which is based on finite distance-dependent repulsive force on fluid particles approaching solid boundaries. Fig.3.5 depicts the effects of boundary condition in the flow process. Lennard-Jones type repulsive boundary particles clogged the real particles near the boundary region, which seriously disrupt the flow. In addition, some particles penetrate the boundary owing to the inappropriate numerical parameters. These effects are distinctly demarcated in Fig. 3.5 (a). On the other hand, improved repulsive boundary forces (Liu et al. 2012; Shao et al. 2012) fairly simulate the flow process as illustrated in Fig. 3.5 (b). Therefore, seeing the different aspects of different boundary conditions, improved repulsive type boundary treatment was chosen for this research work. Detail expressions are given from Eq. (3.17) to (3.20)

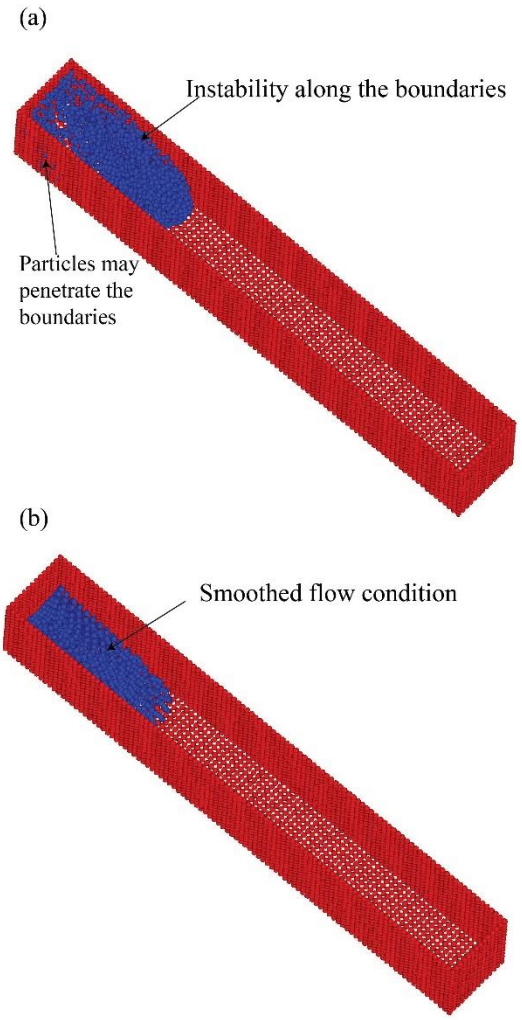

Fig 3.5 Effects of boundary condition in SPH, (a) using Lennard-jones type repulsive boundary particles, (b) using improved repulsive boundary particles

3.8 Use of XSPH variant

A correction term is added to the velocity of each particle in SPH problem domain which makes the particle move in a velocity closer to the average velocity of its neighboring particles (Monaghan 1992; Monaghan and Kocharyan 1995). The following equation gives the detail formulation of XSPH variant.

$$\frac{dx_i}{dt} = v_i - \varepsilon \sum_{j=1}^{N} \frac{m_j}{\rho_j} v_{ij} W_{ij} \tag{3.21}$$

where, m_j mass of particle j, ρ_j is density of particle j, $v_{ij} (= v_i - v_j)$ is the velocity difference between particle i and j, W_{ij} is the smoothing function and ε is a constant value ($0 \leq \varepsilon \leq 1.0$). XSPH techniques mainly includes the contribution from its

neighboring particles and hence avoid extraordinary velocity of any particle in the domain. Most of the applications use ε =0.3 and provide smooth results for incompressible flows (Liu and Liu 2003).

3.9 Validation of SPH

The primary step after the development of any numerical tool is to validate it with some benchmark cases. Two dam break tests with Newtonian fluid model (pure water) and non-Newtonian fluid model (Bingham fluid) was run to validate the developed code. A fluid column was placed initially so that its left side abuts the left boundary of the flume, while the right side is free. The column then collapsed instantaneously and their surge front at different times were tracked and compared with experimental results. Illustration of initial model setup is shown in Fig 3.6, and Table 3.1 portrays the parameters that used in these simulations.

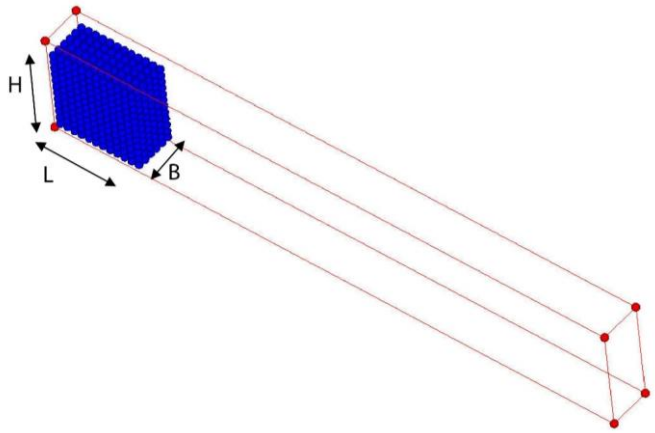

Fig 3.6 Layout of 3D dam break test

Table 3.1 Parameters for SPH simulation of Newtonian (water) & non-Newtonian (water-kaolinite clay mixture) fluid

Parameters	Experiment-1 (Newtonian fluid)		Experiment-2 (Non-Newtonian fluid)	Unit
	(a)	(b)		
Flume dimension	800 x 60 x 150	800 x 60 x150	4500 x 150 x 150	mm
Initial water column	120 x 60 x 120	60 x 60 x 120	2000 x 150 x 100	mm
Density	1000	1000	1200	kg/m^3
Dynamic viscosity	0.001	0.001	0.07	Pa. sec

3.9.1 Dam break test of water particles

A series of dam break test simulations were discussed first. Two different geometrical setups were run and their fronts were tracked moment by moment. Numerical results were compared with experimental results by (Martin and Moyce 1952) and compatible outcomes were seen. Fig 3.7 describes the relation between non-dimensional time and non-dimensional surge front for both experiments and numerical simulations. Time and surge front were normalized as $T = t \times \sqrt{g/H}$ and$X = x/H$, where T, x, H are non-dimensional time, non-dimensional front and initial height of the model. The SPH results agreed well with experiments, hence confirm the accuracy of the developed code.

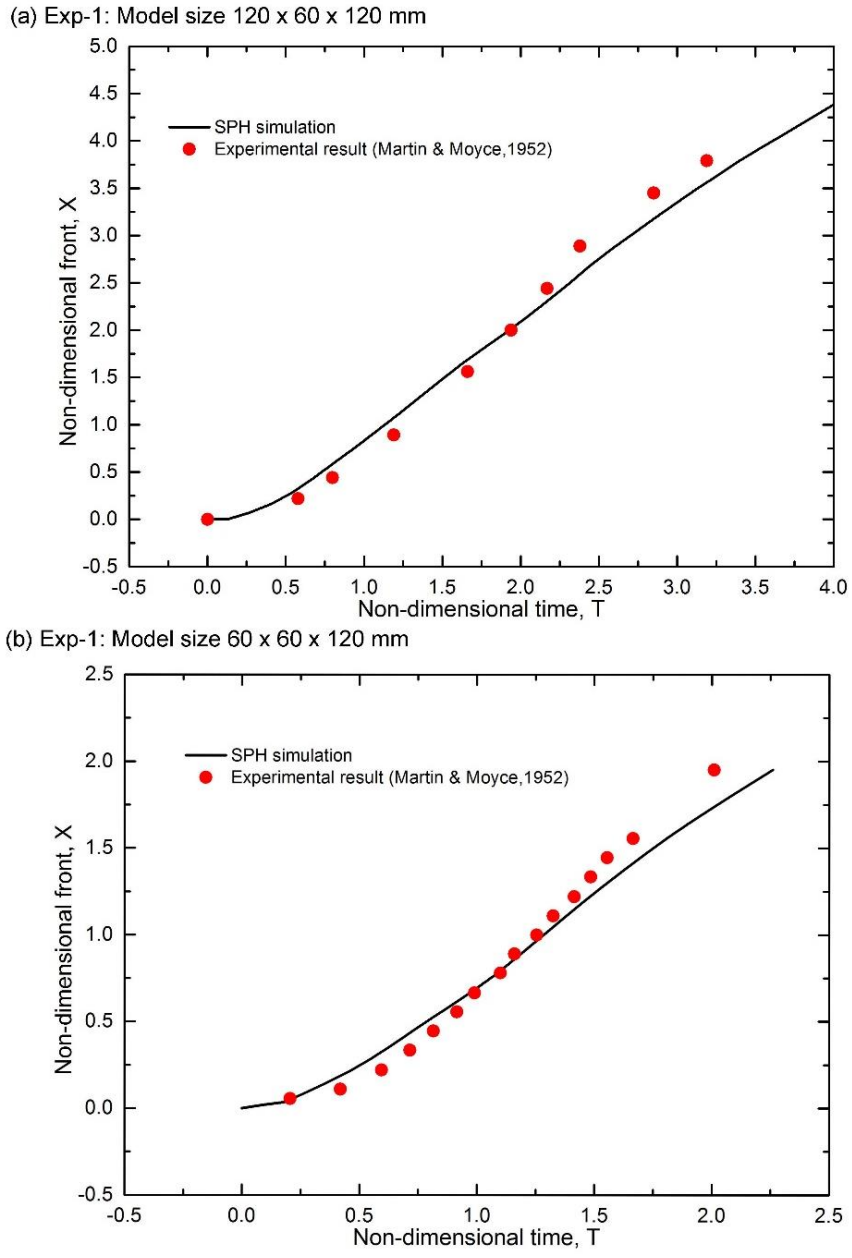

Fig 3.7 Comparison of SPH simulation and experimental results for water flows

Velocity distribution were also plotted, which shows that frontal part exhibits higher velocity compared to the tale and is compatible with the usual dam break behavior. A typical velocity distribution of water particles at different times is shown in Fig 3.8 which contented the above statement with higher frontal velocity.

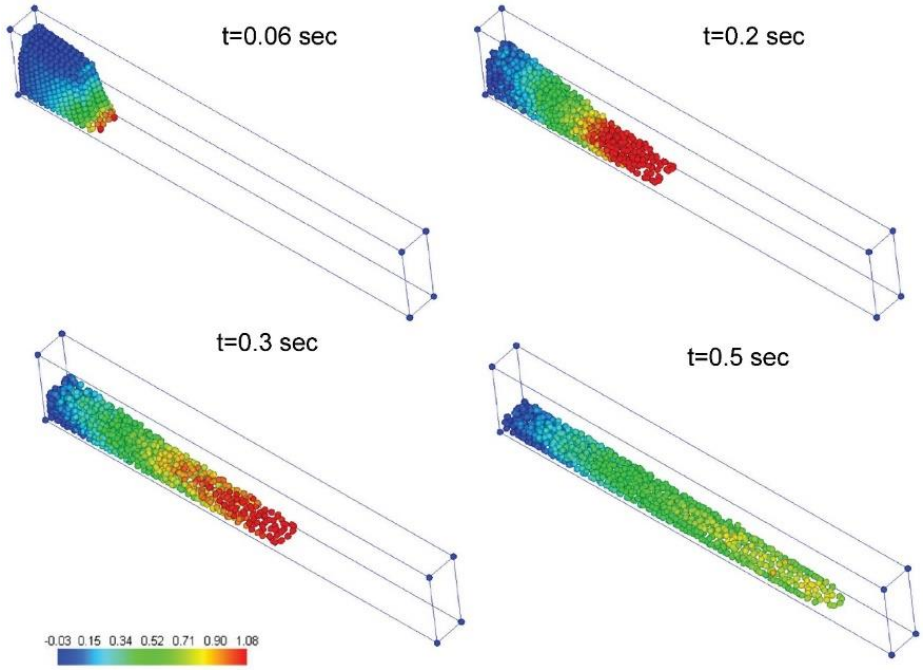

Fig 3.8 Velocity distribution of water particles at different times

3.9.2 Dam break test of non-Newtonian fluid

To further verify the model, especially for viscous flows, a simulation of water-kaolinite clay type mixture considering the Bingham constitutive law were executed and compared with experiments reported in (Komatina and Jovanovic 1997). Simulation was run long enough to check the effectiveness of using SPH for viscous flows. Fig 3.9 shows a good agreement between experiments and numerical simulation for water-kaolinite clay mixture. Parameters (Table 3.1) for SPH simulation of water-kaolinite mixture were extracted from previous numerical simulation conducted by (Shao and Lo 2003).

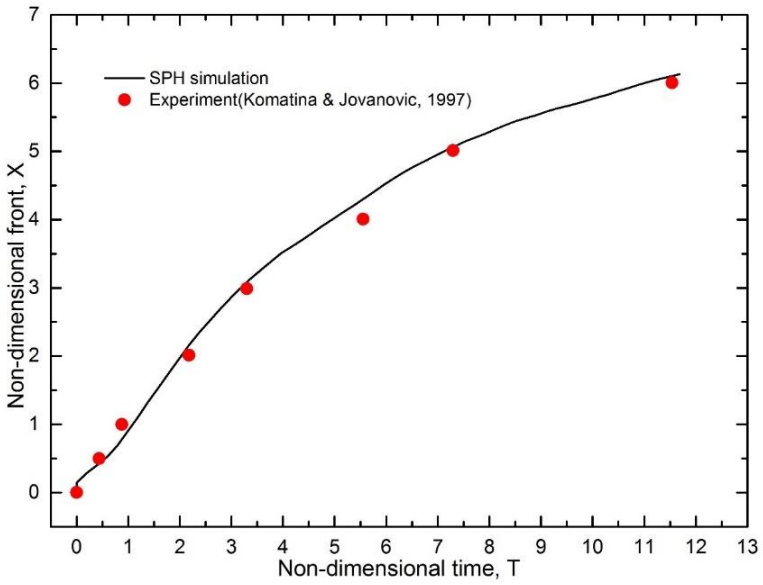

Fig 3.9 Comparison of SPH simulation and experimental results for non-Newtonian fluid

References

Abdolmaleki K (2011) SPH Simulation of Hydrodynamic Forces on Subsea Pipelines. Proceedings of the ASME 30th International Conference on Offshore Mechanics and Arctic Engineering 1–10. doi: 10.1115/OMAE2011-50029

Abe K, Johansson J, Konagai K (2007) A new method for the run-out analysis and motion prediction of rapid long-traveling landslides with MPM. JSCE Journal of Civil Engineering 63:93–109.

Abe K, Soga K, Bandara S (2013) Material Point Method for Coupled Hydromechanical Problems. Journal of Geotechnical and Geoenvironmental Engineering. doi: 10.1061/(ASCE)GT.1943-5606.0001011.

Adami S, Hu XY, Adams NA (2012) A generalized wall boundary condition for smoothed particle hydrodynamics. Journal of Computational Physics 231:7057–7075. doi: 10.1016/j.jcp.2012.05.005

Bui HH, Fukagawa R (2013) An improved SPH method for saturated soils and its application to investigate the mechanisms of embankment failure: Case of hydrostatic pore-water pressure Ha. International Journal for Numerical and Analytical Methods in Geomechanics 37:31–50. doi: 10.1002/nag.1084

Bui HH, Fukagawa R, Sako K, Ohno S (2008) Lagrangian meshfree particles method (SPH) for large deformation and failure flows of geomaterial using elastic–plastic soil constitutive model. International Journal for Numerical and Analytical Methods in Geomechanics 32:1537–1570. doi: 10.1002/nag.688

Bui HH, Fukagawa R, Sako K, Wells J. (2011) Slope stability analysis and discontinuous slope failure simulation by elasto-plastic smoothed particle hydrodynamics (SPH). Géotechnique 61:565–574. doi: 10.1680/geot.9.P.046

Calvo L, Haddad B, Pastor M, Palacios D (2014) Runout and deposit morphology of Bingham fluid as a function of initial volume: implication for debris flow modelling. Natural Hazards 75:489–513. doi: 10.1007/s11069-014-1334-x

Chang T-J, Kao H-M, Chang K-H, Hsu M-H (2011) Numerical simulation of shallow-water dam break flows in open channels using smoothed particle hydrodynamics. Journal of Hydrology 408:78–90. doi: 10.1016/j.jhydrol.2011.07.023

Crespo a. J, Gómez-Gesteira M, Dalrymple R a. (2008) Modeling Dam Break Behavior over a Wet Bed by a SPH Technique. Journal of Waterway, Port, Coastal, and Ocean Engineering 134:313–320. doi: 10.1061/(ASCE)0733-950X(2008)134:6(313)

Dai Z, Huang Y, Cheng H, Xu Q (2014) 3D numerical modeling using smoothed particle hydrodynamics of flow-like landslide propagation triggered by the 2008 Wenchuan earthquake. Engineering Geology 180:21–33. doi: 10.1016/j.enggeo.2014.03.018

Fang J, Owens RG, Tacher L, Parriaux A (2006) A numerical study of the SPH method for simulating transient viscoelastic free surface flows. Journal of Non-Newtonian Fluid Mechanics 139:68–84. doi: 10.1016/j.jnnfm.2006.07.004

Ferrari A (2010) SPH simulation of free surface flow over a sharp-crested weir.

Advances in Water Resources 33:270–276. doi: 10.1016/j.advwatres.2009.12.005

Ferrari A, Dumbser M, Toro EF, Armanini A (2009) A new 3D parallel SPH scheme for free surface flows. Computers and Fluids 38:1203–1217. doi: 10.1016/j.compfluid.2008.11.012

Gomez-Gesteria, M. DRA (2004) Using a Three-Dimensional Smoothed Particle Hydrodynamics Method for Wave Impact on a Tall Structure. Journal of Waterway, Port, Coastal and Ocean Engineering 130:63–69. doi: 10.1061/~ASCE!0733-950X~2004!130:2~63!

Hu M, Liu MB, Xie MW, Liu GR (2014) Three-dimensional run-out analysis and prediction of flow-like landslides using smoothed particle hydrodynamics. Environmental Earth Sciences 73:1629–1640. doi: 10.1007/s12665-014-3513-1

Huang Y, Cheng H, Dai Z, et al (2014) SPH-based numerical simulation of catastrophic debris flows after the 2008 Wenchuan earthquake. Bulletin of Engineering Geology and the Environment 74:1137–1151. doi: 10.1007/s10064-014-0705-6

Huang Y, Dai Z, Zhang W, Chen Z (2011a) Visual simulation of landslide fluidized movement based on smoothed particle hydrodynamics. Natural Hazards 59:1225–1238. doi: 10.1007/s11069-011-9859-8

Huang Y, Zhang W, Mao W, Jin C (2011b) Flow analysis of liquefied soils based on smoothed particle hydrodynamics. Natural Hazards 59:1547–1560. doi: 10.1007/s11069-011-9851-3

Hungr O (1995) A model for the runout analysis of rapid flow slides, debris flows, and avalanches. Canadian Geotechnical Journal 32:610–623.

Jakob M, McDougall S, Weatherly H, Ripley N (2013) Debris-flow simulations on Cheekye River, British Columbia. Landslides 10:685–699. doi: 10.1007/s10346-012-0365-1

Jian W, Liang D, Shao S, et al (2015) SPH study of the evolution of water–water interfaces in dam break flows. Natural Hazards 78:531–553. doi: 10.1007/s11069-015-1726-6

Kazmi ZA, Konagai K, Ikeda T (2014) Field Measurements and Numerical Simulation of Debris Flows from Dolomite Slopes Destabilized during the 2005 Kashmir Earthquake, Pakistan. Journal of Earthquake Engineering 18:364–388. doi: 10.1080/13632469.2013.873372

Khayyer A, Gotoh H, Shao S (2009) Enhanced predictions of wave impact pressure by improved incompressible SPH methods. Applied Ocean Research 31:111–131. doi: 10.1016/j.apor.2009.06.003

Khayyer A, Gotoh H, Shao SD (2008) Corrected Incompressible SPH method for accurate water-surface tracking in breaking waves. Coastal Engineering 55:236–250. doi: 10.1016/j.coastaleng.2007.10.001

Komatina D, Jovanovic M (1997) Experimental study of steady and unsteady free surface flows with water-clay mixtures. Journal of Hydraulic Research 35:579–590. doi: 10.1080/00221689709498395

Liu GR, Liu MB (2003) Smoothed Particle Hydrodynamics a meshfree particle method. World Scientific Publishing Co. Pte. Ltd.

Liu M, Shao J, Chang J (2012) On the treatment of solid boundary in smoothed particle hydrodynamics. Science China Technological Sciences 55:244–254. doi: 10.1007/s11431-011-4663-y

Liu MB, Liu GR (2010) Smoothed particle hydrodynamics (SPH): An overview and recent developments. Archives of Computational Methods in Engineering 17:25–76. doi: 10.1007/s11831-010-9040-7

Lucy LB (1977) A numerical approach to the testing of the fission hypothesis. Astronomical Journal 82:1013–1024.

Maeda K, Sakai H, Sakai M (2006) Development of Seepage Failure Analysis Method of Ground With Smoothed Particle Hydrodynamics. Structural Engineering / Earthquake Engineering 23:307s–319s. doi: 10.2208/jsceseee.23.307s

Manzanal D, Drempetic V, Haddad B, et al (2016) Application of a New Rheological Model to Rock Avalanches : An SPH Approach. Rock Mechanics and Rock Engineering. doi: 10.1007/s00603-015-0909-5

Martin JC, Moyce WJ (1952) An experimental study of the collapse of liquid columns on a rigid horizontal plane. Philosophical Transactions of the Royal Society of London Series 244:312–324.

Minatti L, Pasculli A (2011) SPH numerical approach in modelling 2D muddy debris flow. Italian Journal of Engineering Geology and Environment - Book 467–475. doi: 10.4408/IJEGE.2011-03.B-052

Monaghan JJ (1989) On the Problem of Penetration in Particle Methods. Journal of Computational Physics 82:1–15. doi: 10.1016/0021-9991(89)90032-6

Monaghan JJ (1992) Smoothed Particle Hydrodynamics. Annual Review of Astronomy and Astrophysics 30:543–274. doi: 10.1017/CBO9781107415324.004

Monaghan JJ (1994) Simulating free surface flows with SPH. Journal of Computational Physics 110:399–406.

Monaghan JJ, Gingold RA (1983) Shock simulation by the particle method SPH. Journal of Computational Physics 52:374–389.

Monaghan JJ, Kocharyan A (1995) SPH simulation of multi-phase flow. Computer Physics Communications 87:225–235. doi: 10.1016/0010-4655(94)00174-Z

Monaghan JJ, Kos a, Issa N (2003) Fluid Motion Generated by Impact. Journal of Waterway, Port, Coastal, and Ocean Engineering 129:250–259. doi: 10.1061/(ASCE)0733-950X(2003)129:6(250)

Monaghan JJ, Lattanzio JC (1985) A refined particle method for astrophysical problems. Astronomy and Astrophysics 149:135–143.

Monaghan JJ, Pongracic H (1985) ARTIFICIAL VISCOSITY FOR PARTICLE METHODS. Applied Numerical Mathematics 1:187–194. doi: 10.1016/0168-

9274(85)90015-7

Morris JP, Fox PJ, Zhu Y (1997) Modeling Low Reynolds Number Incompressible Flows Using SPH. Journal of Computational Physics 136:214–226. doi: 10.1006/jcph.1997.5776

Naili M, Matsushima T, Yamada Y (2005) A 2D Smoothed Particle Hydrodynamics method for liquefaction induced.

O'Brien JS, Julien PY, Fullerton WT (1993) Two-dimensional water flood and mudflow simulation. J Hydraul Eng 119:244–261.

Ozbulut M, Yildiz M, Goren O (2014) A numerical investigation into the correction algorithms for SPH method in modeling violent free surface fl ows. International Journal of Mechanical Sciences 79:56–65.

Pastor M, Blanc T, Haddad B, et al (2014) Application of a SPH depth-integrated model to landslide run-out analysis. Landslides 11:793–812. doi: 10.1007/s10346-014-0484-y

Pastor M, Haddad B, Sorbino G, et al (2009) A depth-integrated, coupled SPH model for flow-like landslides and related phenomena. International Journal for Numerical and Analytical Methods in Geomechanics 33:143–172.

Ran Q, Tong J, Shao S, et al (2015) Incompressible SPH scour model for movable bed dam break flows. Advances in Water Resources 82:39–50. doi: 10.1016/j.advwatres.2015.04.009

Shadloo MS, Zainali A, Yildiz M, Suleman A (2012) A robust weakly compressible SPH method and its comparison with an incompressible SPH. International Journal for Numerical Methods in Engineering 89:939–956. doi: 10.1002/nme.3267

Shao JR, Li HQ, Liu GR, Liu MB (2012) An improved SPH method for modeling liquid sloshing dynamics. Computers and Structures 100-101:18–26. doi: 10.1016/j.compstruc.2012.02.005

Shao S, Lo EYM (2003) Incompressible SPH method for simulating Newtonian and non-Newtonian flows with a free surface. Advances in Water Resources 26:787–800. doi: 10.1016/S0309-1708(03)00030-7

Troncone A (2005) Numerical analysis of a landslide in soils with strain-softening behaviour. Géotechnique 55:585–596. doi: 10.1680/geot.2005.55.8.585

Viccione G, Bovolin V (2011) SIMULATING TRIGGERING AND EVOLUTION OF DEBRIS-FLOWS WITH sph. 523–532. doi: 10.4408/IJEGE.2011-03.B-058

Wang W, Chen G, Han Z, et al (2016) 3D numerical simulation of debris-flow motion using SPH method incorporating non-Newtonian fluid behavior. Natural Hazards. doi: 10.1007/s11069-016-2171-x

Zhang W, Maeda K (2015) SPH simulations for slope and levee failure under heavy rainfall considering the effect of air phase. In: Computer Methods and Recent Advances in Geomechanics. pp 1465–1470

Zhang W, Maeda K (2014) Numerical Simulations of Slope and Levee Failure under

Heavy Rainfall Using the Three-phase SPH Model. JSCE Journal of Applied Mechanics 70:483–494.

Zheng X, Duan W yang (2010) Numerical simulation of dam breaking using smoothed particle hydrodynamics and viscosity behavior. Journal of Marine Science and Application 9:34–41. doi: 10.1007/s11804-010-8037-9

Chapter-4

NUMERICAL MODELING OF DEBRIS FLOW

4.1 Introduction to numerical flume modeling

A 3D curved flume is modeled numerically with the developed SPH tool to discuss the practical and rational use of the vortex equation in velocity estimation. In these simulations, constitutive laws for debris masses are to be carefully discussed reflecting the highly complicated natures of mixed-phase debris materials. Since all these numerical 3D flume tests are of reduced scale models, law of similarity is mandatory to deduce behaviors of full-sized debris flows. Details are written in the subsequent sections.

4.2 Constitutive law

Debris flows are the mixture of water and solid particles and concentration of solid particles can vary along the flow trace. Hence, properties of debris materials change in space and time, and depend on many factors such as concentration of solid particles, particle size distribution, frictional behavior of particles , pore water pressure etc. (Wang 2008). Moreover, along the flow path, debris mass can contain uprooted trees, woods and many other substances. Thus, debris materials are in reality, a complex mixture of many things. Computing the intrinsic properties of debris flow materials with the appropriate constitutive model is thus very difficult. Normally, two assumptions have been used in debris flow modeling, namely multi-phase and single-phase material. The behavior of debris material is formulated with different rheological equations in a multi-phase flow model. On the other hand, a single-phase model describes debris flow as a continuous fluid with only one constitutive equation and fluid-particle interactions are implicitly seen in this instance. Truly, Multi-phase model is too intricate to include in SPH numerical computations. On the contrary, single –phase viscous model is relatively easy to use, and also verified by many researchers (Hungr 1995; Takahashi 2009; Calvo et al. 2014; Dai et al. 2014; Pastor et al. 2014) in the debris flow arena. Several viscous single

phase models are available. Brief description and suitability of each model are discussed in the following sub-sections.

4.2.1 Newtonian fluid model

Laminar flow of plain water in which shear stress is linearly vary with shear strain rate is being characterized by the Newtonian fluid (Fig. 4.1). Sediment-water mixtures with low concentration of solid particles can be identified by this theoretical model. Particle interaction and cohesion are not explicitly brought into account in the Newtonian fluid model. The relation between shear stress (τ) and strain rate ($\frac{du}{dz}$) of a Newtonian fluid in 1D condition is given below

$$\tau = \mu \frac{du}{dz} \tag{4.1}$$

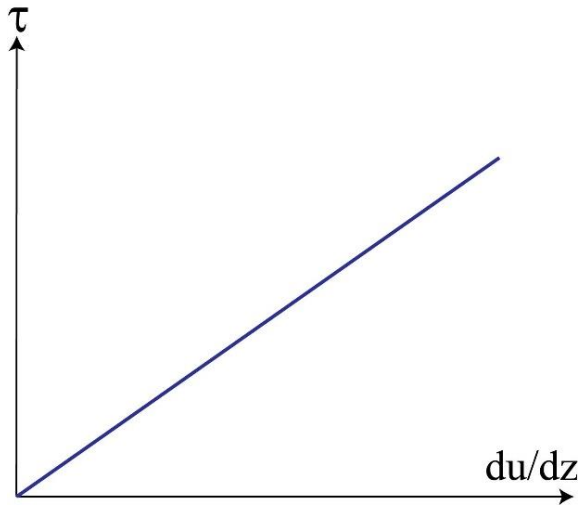

Fig. 4.1 Stress-strain rate relationship of Newtonian model

In 3D formulation, Newtonian model is described as below:

$$\tau^{\alpha\beta} = \mu \varepsilon^{\alpha\beta} \tag{4.2}$$

$$\varepsilon^{\alpha\beta} = \frac{\partial v^{\beta}}{\partial x^{\alpha}} + \frac{\partial v^{\alpha}}{\partial x^{\beta}} \tag{4.3}$$

where, $\tau^{\alpha\beta}$ is the viscous stress tensor, $\varepsilon^{\alpha\beta}$ is the strain rate tensor, μ is the dynamic viscosity, and α and β are Einstein summation index.

4.2.2 Non-Newtonian fluid model

Non-Newtonian fluid model characterizes the change of viscosity with the shear strain rate. A wide variety of non-Newtonian fluid model has been developed. Bingham model

and Hershecl-Bulkley model (Fig. 4.2) are the most frequently used non-Newtonian fluid constitutive relations in debris flow analyses.

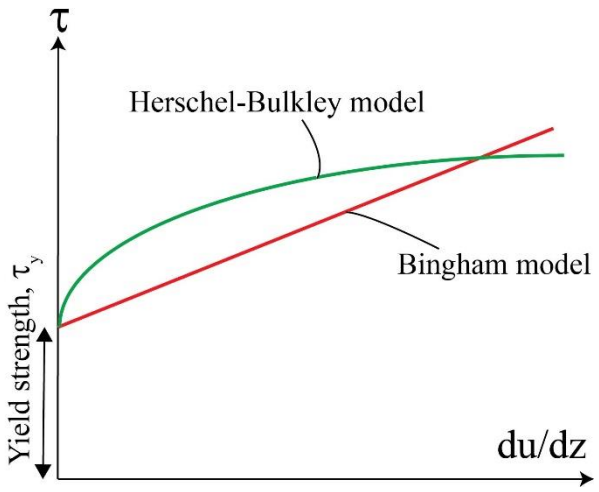

Fig. 4.2 Stress-strain relationship of non-Newtonian model

4.2.2.1 Bingham fluid

Bingham model is the most elementary sort of non-Newtonian fluid, and in this model, an assembly of fluid particles is not deformed till the applied stress is larger than its threshold stress. This threshold stress is defined as yield strength (τ_y) of fluid particles. Once the yield strength has passed, the fluid behaves in a Newtonian fluid manner. 1D formulation of Bingham fluid is given in Eq. 4.4.

$$\begin{aligned} \frac{du}{dz} &= 0 \quad if\ \tau < \tau_y \\ \tau &= \tau_y + \mu \frac{du}{dz} \quad if\ \tau > \tau_y \end{aligned} \tag{4.4}$$

Yield strength of debris mass can be determined through either laboratory experiments or back-calculation schemes. However, in some cases, yield strength can be approximated using the Coulomb's equation, and this model is known as Coulomb viscous model. This yield strength has both cohesion and friction components. 1D Constitutive equation of the Coulomb viscous model is given below:

$$\begin{aligned} \frac{du}{dz} &= 0 \quad if\ \tau < c + \sigma \tan\varphi \\ \tau &= c + \sigma \tan\varphi + \mu \frac{du}{dz} \quad if\ \tau > c + \sigma \tan\varphi \end{aligned} \tag{4.5}$$

where, c is the cohesion, σ is the stress and φ is the angle of internal friction of materials.

Velocity distribution (Fig. 4.3) of Bingham fluid and Coulomb viscous model is alike and commonly referred to as visco-plastic fluid model. Yield strength of a Bingham fluid describes the cohesion of interstitial fluid, while in the Coulomb viscous model, friction has significant effects on the yield strength.

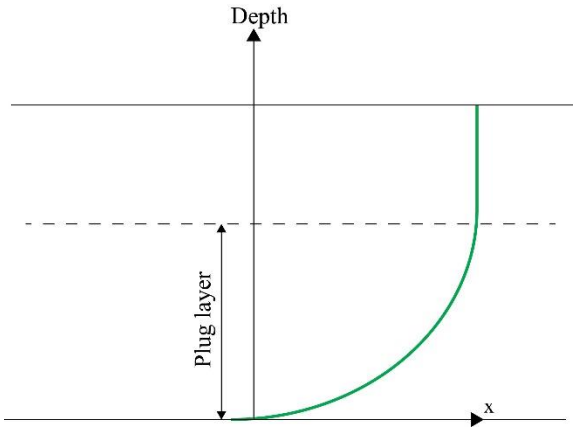

Fig. 4.3 Velocity distribution of Bingham fluid model

3D formulation of Bingham fluid model is given by.

$$\tau^{\alpha\beta} = \begin{cases} \left(\mu + \frac{\tau_y}{\dot{\gamma}}\right)\varepsilon^{\alpha\beta} & if\ \tau > \tau_y \\ 0 & if\ \tau < \tau_y \end{cases} \tag{4.6}$$

where,

$$\dot{\gamma} = \sqrt{\frac{1}{2}\varepsilon^{\alpha\beta}\varepsilon^{\alpha\beta}} \tag{4.7}$$

4.2.2.2 Equivalent Newtonian fluid

Recently, (Uzuoka et al. 1998) introduced an equivalent viscosity, which can be used to model Bingham fluid as Newtonian model and formulation is given below.

$$\tau^{\alpha\beta} = \mu^{/}\varepsilon^{\alpha\beta} \tag{4.8}$$

$$\mu^{/} = \begin{cases} \mu + \frac{\tau_y}{\dot{\gamma}} & if\ \mu^{/} < \mu_{max} \\ \mu_{max} & otherwise \end{cases} \tag{4.9}$$

where, $\mu^{/}$ is the equivalent Newtonian viscosity. The idea of introducing an equivalent viscosity is illustrated in Fig. 4.4. The solid blue line in Fig. 4.4 represents the shear stress and strain rate relationship of a Bingham fluid having a yield strength, while the red solid line portrays the concept of equivalent Newtonian viscosity. The equivalent Newtonian

viscosity is adjusted at every step depending on the induced shear strain rate. Equivalent Newtonian viscosity line moves rightward with increasing shear strain rate, whereas decreasing shear strain rate results in smaller equivalent viscosity and viscosity line moves leftward.

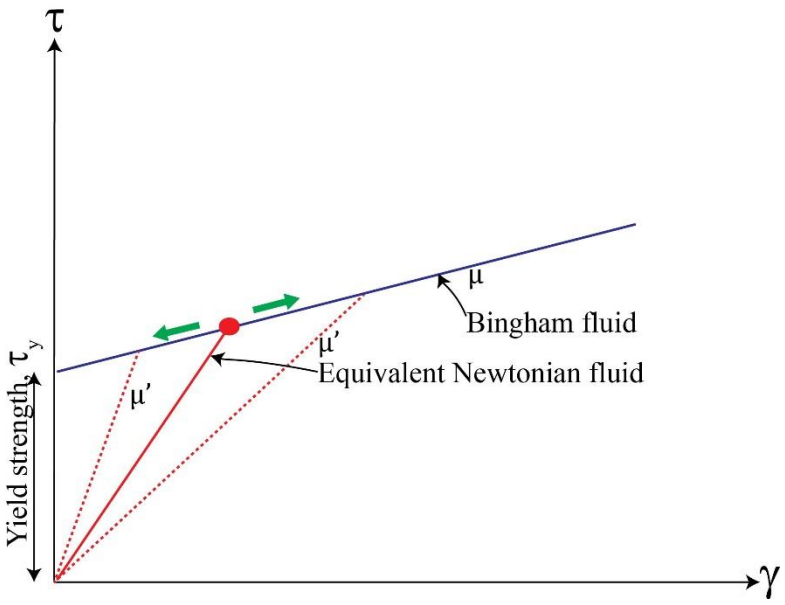

Fig. 4.4 Conceptual illustration of equivalent Newtonian viscosity

4.2.2.3 Herschel-Bulkley fluid

Alongside of the Bingham constitutive model, a Herschel-Bulkley fluid model has been originated to account for shear thinning behavior of water-clay mixture. Linear representation of Herschel-Bulkley fluid is given in Eq. 4.10.

$$\begin{aligned} \frac{du}{dz} &= 0 \quad if\ \tau < \tau_y \\ \tau &= \tau_y + \mu\left(\frac{du}{dz}\right)^n \quad if\ \tau > \tau_y \end{aligned} \tag{4.10}$$

Rheometric tests have been conducted to fit the parameters of Herschel-Bulkley fluid.

4.2.2.4 Quadratic fluid

(Julien and Lan 1991) developed a quadratic rheological model for hydrodynamic problems and relation between shear stress and shear rate in 1D formulation is given below:

$$\frac{du}{dz} = 0 \quad if\ \tau < \tau_y \tag{4.11}$$

$$\tau = \tau_y + \mu\frac{du}{dz} + \zeta\left(\frac{du}{dz}\right)^2 \quad if\ \tau > \tau_y$$

where, ζ is turbulent-dispersive parameter. The physical meaning of this quadratic model comprises yield stress, viscous stress, turbulent and dispersive stress. The first term in Eq. 4.11 describes the yield stress owing to the cohesion between particles. Second term depicts the viscous stress between fluid particles and third term considers turbulent-dispersive stress effects.

4.2.2.5 Dilatant fluid model

A dilatant fluid is a shear thickening fluid whose viscosity increases with increasing shear stress. Highly mobile and destructive debris flows can be modeled using dilatant fluid laws. Dilatant fluid is principally based upon the concepts of dispersive stress given by (Bagnold 1954). Experiments conducted by (Bagnold 1954) demonstrate the linear variation of normal and shear stress to shear rate when the fluid viscosity dominates in the macro-viscous regime and quadratic variation when grain collision dominate in grain-inertial regime. The expression of shear stress and normal stress on the grain-inertia regime are:

$$\tau = a_i\rho_s\lambda^2 d^2\left(\frac{du}{dz}\right)^2 \sin\phi_d \tag{4.12}$$

$$\sigma = a_i\rho_s\lambda^2 d^2\left(\frac{du}{dz}\right)^2 \cos\phi_d \tag{4.13}$$

where, a_i is a numerical constant, ρ_s is the grain density, λ is the linear concentration, d is the grain diameter, ϕ_d is the dynamic angle of internal friction. Linear concentration is calculated using Eq. 4.14.

$$\lambda = \left[\left(\frac{C_b}{C}\right)^{1/3} - 1\right]^{-1} \tag{4.14}$$

where, C and C_b are solid volumetric concentration and maximum possible volume concentration. However, for the macro-viscous regime, the shear and normal stress are formulated as,

$$\tau = a_i\rho_s\lambda^{3/2}\left(\frac{du}{dz}\right)^2 \sin\phi_d \tag{4.15}$$

$$\sigma = a_i\rho_s\lambda^{3/2}\left(\frac{du}{dz}\right)^2 \cos\phi_d \tag{4.16}$$

4.2.3 Difficulties in multi-phase model

Multi-phase material modeling in debris flow studies formulate solid and liquid phase as independent continuums and mass and momentum equations for each phase are solved with proper interaction mechanics. Coupling between solid and fluid elements is a crucial parameter in this kind of model analysis. Importance of coupling depends on types of the events and a characteristic time describing the pore pressure development. Suppose, for rock avalanche problems, air and boulders are the main constitutes and air effects can be neglected in modeling, while in case of mudflows, single viscous phase can govern the flow dynamics. Moreover, debris flow contains large boulder as well as fine particles saturated with water, and viscous nature can prevail in the flow case. Furthermore, mixture theory comprises estimation of several parameters which is difficult for the highly fluctuating debris flow events. Therefore, debris flow dynamics has been extensively studied using single viscous models rather than multi-phase models (Hungr 1995; Dai et al. 2014; Wang et al. 2016) and is taken over in the current research work.

4.2.4 Selection of appropriate constitutive law

Selection of appropriate constitutive relation has been always a challenging task of any numerical simulation. Constitutive model widely used in soil mechanics are not suitable for debris flow analysis as those models are based on small strain theory. All the same, debris material is a mixture of wide varieties of particles and integrating all the properties in an ideal manner is impossible in any case. Therefore, simplification needs in a quantitative way to get the pertinent constitutive equation for debris modeling. In reality, a flowing mass closely resembles a collapsing earth dam with a high percentage of water; whereas, higher solid concentration accrues its interior stress and its failure can occur once the stress exceeds the strength of the soil mass. The large variation of water and sediment concentration as well as channel geometry and geomorphology make it even more difficult to use any single viscous constitutive law.

Mostly, non-Newtonian fluid constitutive equations have been used and seemingly a hands-on approach in computational modeling of debris flow owing to its simplicity. Among various non-Newtonian fluid model, Bingham constitutive law has a long history of being used in many rheological analysis of debris materials (Phillips and Davies 1991; Major and Pierson 1992; Whipple and Dunne 1992; Parsons et al. 2001; Pierson 2005; Boniello et al. 2010) & numerical simulations(Calvo et al. 2014; Dai et al. 2014).

Likewise, Hershel-Bulkley fluid constitutive model has also been employed in many case studies and proven to be compatible with examined examples (Laigle and Coussot 1997; Coussot et al. 1998; Huang et al. 2014). Yet, these non-Newtonian fluid models require appropriate and rational estimation of yield strength and plastic viscosity of the flowing mass. Naturally, debris materials vary noticeably in space and the appraisal of appropriate viscosity and yield strength is also cumbersome. Rheometric tests of collecting samples and field observation can afford an estimation of yield strength, however, the accuracy of the above said procedure is a burning question. Most of the rheometric tests have been conducted on readily sampled, poorly sorted, fine grained slurries and the yield strength vary from 10 to 400 Pa in most cases (Iverson 2003). The above mentioned yield strength range does not reflect the actual viscous nature of the real debris mass. Truly, debris flow exhibits some shear strength; though the magnitude of the strength depends on many factors and there are many glitches to estimate the appropriate values.

Typically, debris flows are viscous flows with a variety of sediment concentration. The flow front of the debris mass consists larger particles, while the tail mainly contains finer particles. In some instances, large boulder at the forefront of the flowing mass resembles the stony type debris flow. This debris flows have large velocities at the upper layer and decreases to zero as we go to the bottom. Therefore, upper particles move faster than average velocity and this velocity distribution can be seen particularly in fast flow debris events, and has been reported in detail in technical writings (Okuda et al. 1977; Takahashi 2009). Fig. 4.5 depicts the debris flow in Kamikamihorizawa area in Japan with large boulders at its front.

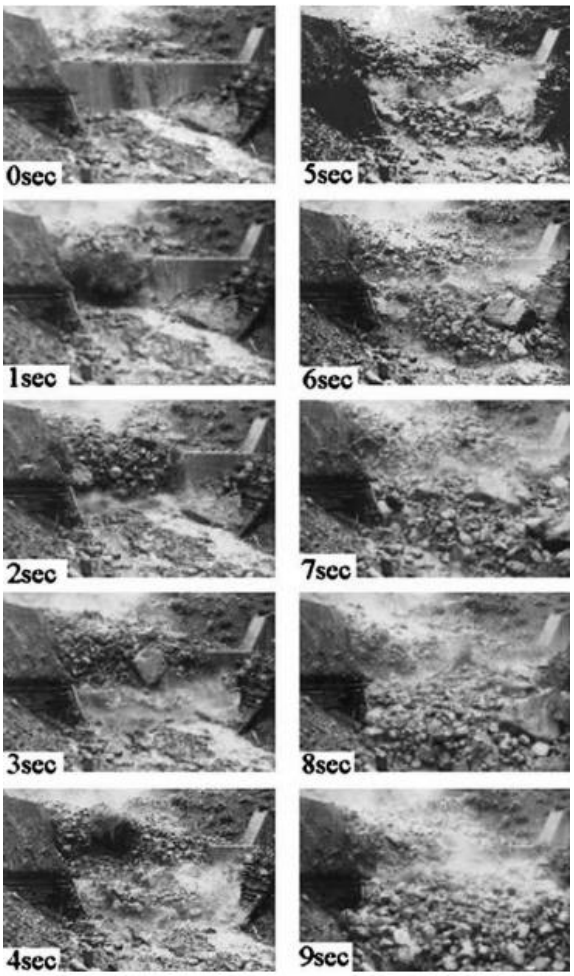

Fig. 4.5 Stony type debris flow at Kamikamihorizawa (Okuda et al. 1977)

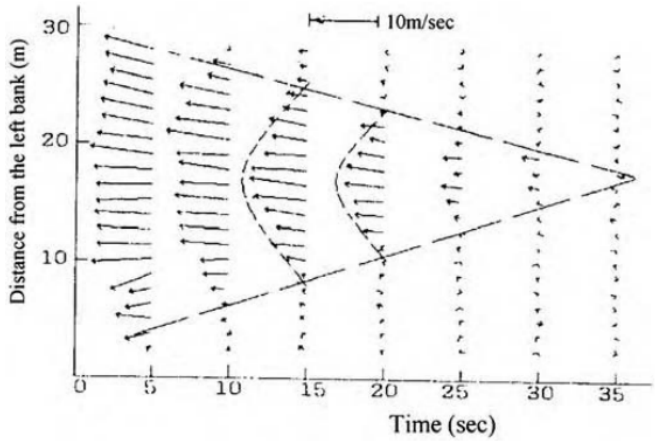

Fig. 4.6 Time history of lateral distribution of surface velocity (Takahashi 2000)

(Takahashi 2000) did a long time monitoring of Jiangjia Gulley debris flows in collaboration with the Chinese Academy of Science and Ministry of Water Conservancy to understand the mechanism of viscous types debris flows. Video cameras were installed

at a particular location and velocities were extracted from the observed video clips. Temporal evolution of surface velocity at a certain section was plotted and the results revealed diminishing nature of flow width time, which eventually decelerate the velocities. Fig. 4.6 shows the time history of surface velocities at the examined section along Jiangjia ravine. The lateral velocities of boulders at the forefront, where the flow is much more turbulent, distribute almost uniformly, whereas as we go rearwards, where the flow is laminar, the velocity distribution is rather parabolic as shown by envelopes (broken lines) in Fig. 4.6.

An analytical model considering Newtonian fluid was developed for coarse viscous debris flows (Takahashi 2000) and afterward an experimental investigation justified the suitability of the Newtonian model for viscous debris flow studies. Velocity distribution of debris flow at particular section of both analytical and experimental observations are plotted in Fig. 4.7 where solid black line represents the analytical calculation result and black dots depict experimental results. It is shown that observed velocities follow Newtonian laminar flow pattern quite well. (Takahashi 2000) also applied his analytical model to Jiangia ravine and observed flow pattern suggested that the Newtonian model can be used for real debris flows along this ravine. It was also confirmed that stress and strain relation exhibits a similar trend of Newtonian fluid model till the volume sediment concentration exceed about 9% (Jan and Shen 1997). Some other experimental and analytical solutions also suggested that it is possible to use the Newtonian flow model for fast debris flood and avalanche problems (Davies 1990; Hunt 1994; Koch 1998; Pritchard et al. 2014). (Rickenmann 1991) conducted an experiments on fine materials and hyper concentrated flows, and stated in his conclusion his support to the use of the Newtonian fluid model in a water-sediment flow cases.

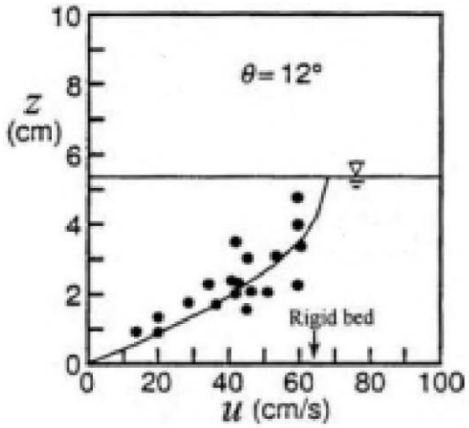

Fig. 4.7 The calculated and experimental velocity distribution (Takahashi 2000)

Long time monitoring of real debris flow event mentioned above tends to favor the use of simplified Newtonian fluid model. Fast moving debris flood can also be plausibly formulated with this simplified constitutive law. Moreover, in some simulations of dam breaks with the particle method assuming "Bingham constitutive law", which will be shown hereafter, it has been seen that flowing slurry forgets its initial height as the collapsed body liquefies and reaches its maximum kinetic energy; hence, the plugging layer of non-Newtonian fluid has less significant effect on the overall behavior of the flowing slurry. Based on the all mentioned above, simplified Newtonian fluid model seems to be a clever approach for debris flow simulations.

However, we cannot completely get over the idea that the clogging nature of debris flow can affect the discussion about super elevations. Therefore, both Newtonian and Bingham fluid models will be used hereafter.

4.3 Scaling consideration

In order to deduce flowing natures of full-scale debris mass , discussion of the law of similarity between a model and its prototype is a pre-requisite (Sohn 2000; Scheidl et al. 2013; Scheidl et al. 2014). In hydrodynamics, any model test results can represent their prototype behaviors, i.e. epitomize the actual scenario using the scaling law.

4.3.1 Complete law of similarity

Neither real scale experiments nor faithful numerical reproduction of a full-size debris flow is possible and critics commonly argue that conventional experiments are minor, brief, idealized, and there is an enormous gap between experiments and complicated reality. The boundary condition is likewise one of the drawbacks for both experimental and numerical analyses. To some extent, these statements are legitimate. However, law of similarity plays an important role to overcome such shortcomings. Scaling can be addressed by using dimensional analysis that describes the evolving dynamics of the system. Simple experimental or numerical model can be compared with the real scale case through this technique.

Complete similarity between model and its real case (prototype) can be reached only when the model satisfies geometric, kinetic and dynamic similarity. Geometric similarity

corresponds to the same pattern of the model and prototype, whereas kinetic similarity confirms the similar time rates of change in motions. Alongside, dynamic similarity refers to the similar forces between two geometrically identical objects. Achieving complete similarity in an experimental study requires different viscous materials for the test which is practically difficult to attain in most of the instances. On the other hand, complete similarity is possible only in numerical simulations and can be comprehended to go through the whole scenario. Seeing these aspects, a series of numerical simulations were carried out based on a scaling analysis considering geometric, kinetic and dynamic similarities.

The ratio of a quantity in the model to that in the prototype is defined by the symbol λ. Geometric (λ_L), velocity (λ_v), time (λ_t) and viscosity (λ_μ) scales are derived based on the law of similarity and outlined in the following equations:

$$\lambda_L = \frac{x_{model}}{x_{prototype}} = \frac{y_{model}}{y_{prototype}} = \frac{z_{model}}{z_{prototype}} \tag{4.17}$$

$$\lambda_v = \lambda_L^{1/2} \tag{4.18}$$

$$\lambda_t = \lambda_L^{1/2} \tag{4.19}$$

$$\lambda_\mu = \lambda_L^{3/2}\lambda_\rho \tag{4.20}$$

where, λ_ρ is density scale.

4.3.2 Justification of current small scale model

Properties of flowing slurry for numerical curved flume simulations are compared with real scale debris properties using the above equations from (4.17) to (4.20) and depicted in Table 4.1. In this comparison, viscosity is one of the key factors for scaled numerical simulations and complete dynamic similarity is pre-requisite for justifying the numerical simulations. Viscosity of real debris slurry can vary noticeably both in space and time depending on the particle size distribution, topography of the terrain and etc. The scaled viscosity range for the numerical simulation (Table 4.1) can cover the substantially wide range of viscosity that can be expected in real debris flow events (Sharp and Nobles 1953; Curry 1966; Cooley et al. 1977; Fink et al. 1981; Li and Luo 1981; Li et al. 1983; Shen and Xie 1985; Zhang et al. 1985). Therefore, the scaled numerical model replicate the actual debris flow scenarios in a quite well manner and outcomes can be applied to update the velocity estimation procedure of real debris disasters.

Table 4.1 Comparison of the model and prototype ($\lambda_L = 1/50$ & $\lambda_\rho = 1$)

Parameters	Model	Prototype	Unit
Initial size of the model	1.125 x 0.270 x 0.375	56.25 x 13.5 x 18.75	m
Initial volume	0.1139	1.4 x 10^4	m^3
Channel slope	15	15	m
Density	1800.0	1800.0	kg/m^3
Viscosity	0.001~10.0	0.35~3535.0	Pa.s
Time	15.0	106.0	sec

4.4 Effects of viscosity

Prior to run scaled flume tests, a sensitivity analysis is conducted herein to check how the change in viscosity affects the overall features of flowing slurry through a simple 3D straight flume shown in Fig. 4.8. A rectangular debris mass is initially placed at the leftmost end of the flume, and suddenly, it starts flowing in a dam break manner. Its surge front and front velocities as well as the velocities at section 1-1 were recorded for discussion. A range of Newtonian viscosities between 0.001 and 10.0 Pa.s was chosen based on the law of similarity, which range is considered to cover a substantially large range of viscosity that can be expected for real debris slurry as shown later. Detail parameters of numerical simulations are given in Table. 4.2.

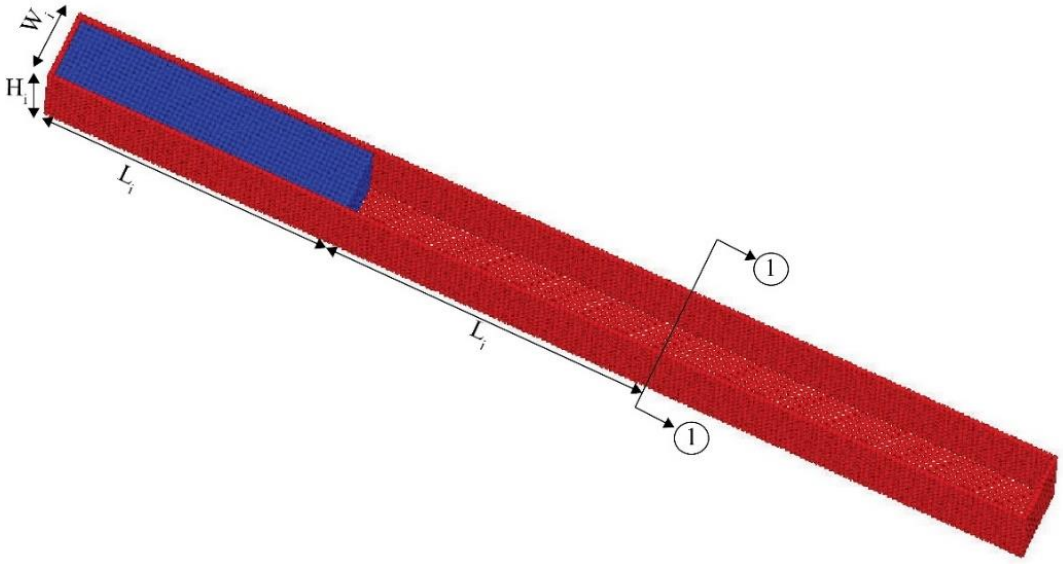

Fig. 4.8 Layout of straight flume test with different viscosities

Table 4.2 Properties of straight flume test

Parameters	Value	Unit
Initial size of the model	1.125 x 0.270 x 0.375	m
Aspect ratio (Initial height/initial length)	0.33	---
No. of fluid particles	14400	---
Density	1800	Kg/m3
Viscosity	0.001~10.0	Pa.s

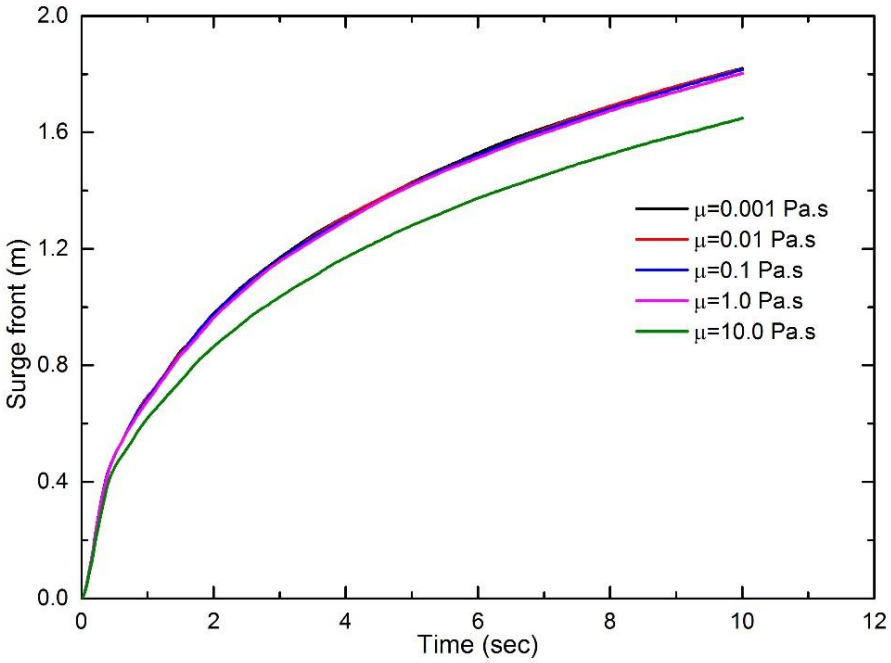

Fig. 4.9 Time-history of surge front for different viscosities

Fig. 4.9 and 4.10 depict respectively the time-histories of surge front and front velocities for different viscosities. Below$\mu = 1.0$ Pa. s, the change of viscosity affects very little both the surge front and the front velocity. However, beyond 1.0 Pa.s, the viscosity slightly decelerates the flow motion. To get more insight, time-histories of velocity at section 1-1 are also plotted for different viscosities in Fig. 4.11. Variations of cross-sectional velocity follow the similar trend and with the increasing time, especially after the maximum kinetic energy is reached, flow trend is about identical to each other for different viscosities. Thus, the above results show the less significant effects of viscosity on the overall behavior of the flowing slurry.

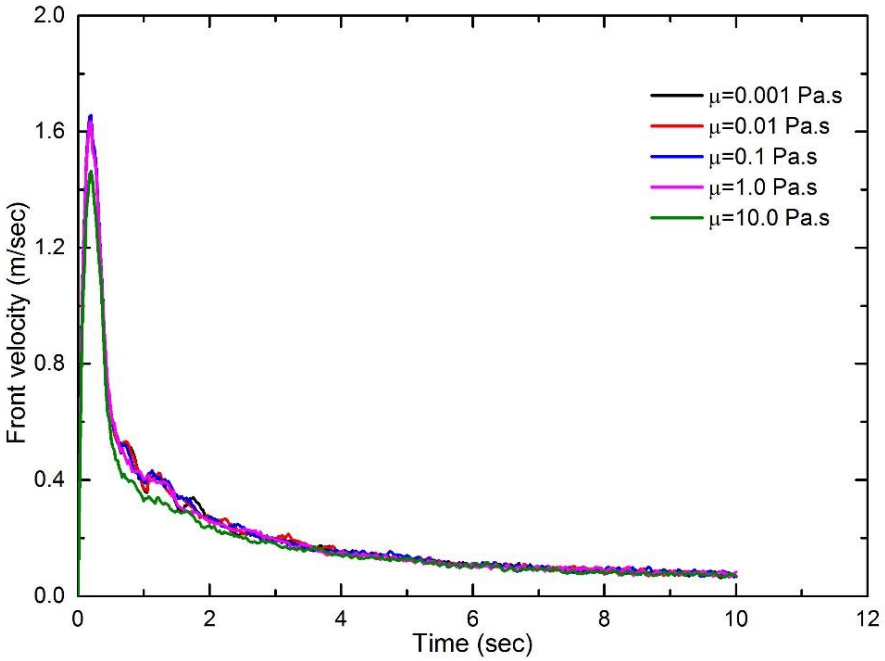

Fig. 4.10 Time-history of front velocities for different viscosities

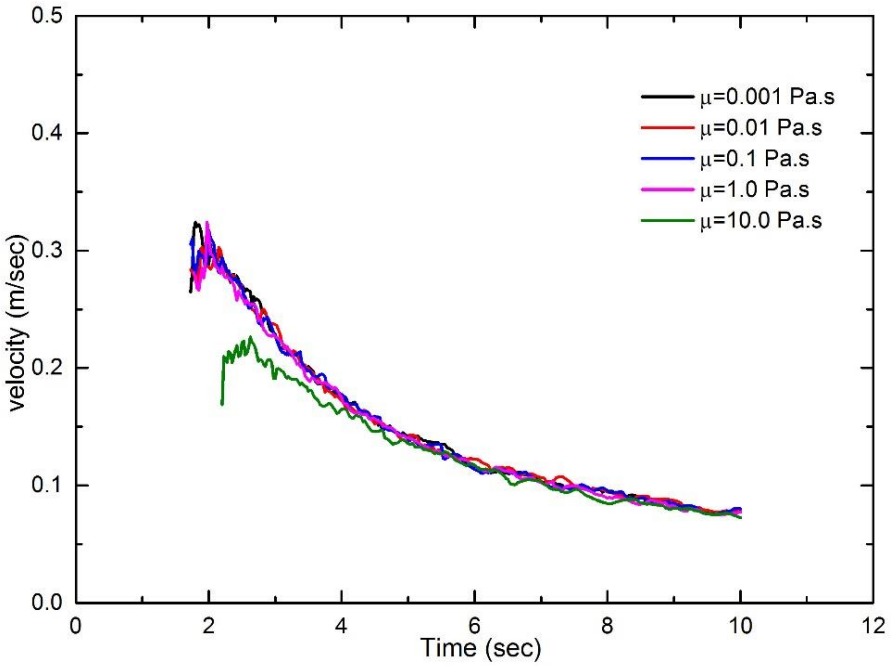

Fig. 4.11 Time-history of velocities at section 1-1

4.5 Numerical flume model

4.5.1 Modeling of 3D curved flume

This and the following sections describe the core part of this dissertation of how the 3D curve flume was modeled and how we can estimate real maximum flow velocities from

super elevations remaining on flume walls. A 3D curved flume was first prepared numerically to examine flow velocities of flowing debris mass. The flume consists of the following parts: a reservoir at the uppermost end, a varying length straight section, followed by the upper curve, a second straight section and a lower curve at the downstream end. Approximately 61000~86000 particles, including debris and boundary particles, were used to draw up the numerical model. The upstream reservoir was outfitted with a gate which instantly opens to initiate debris flow in a dam break fashion. Layout of the numerical flume is shown in Fig. 4.12.

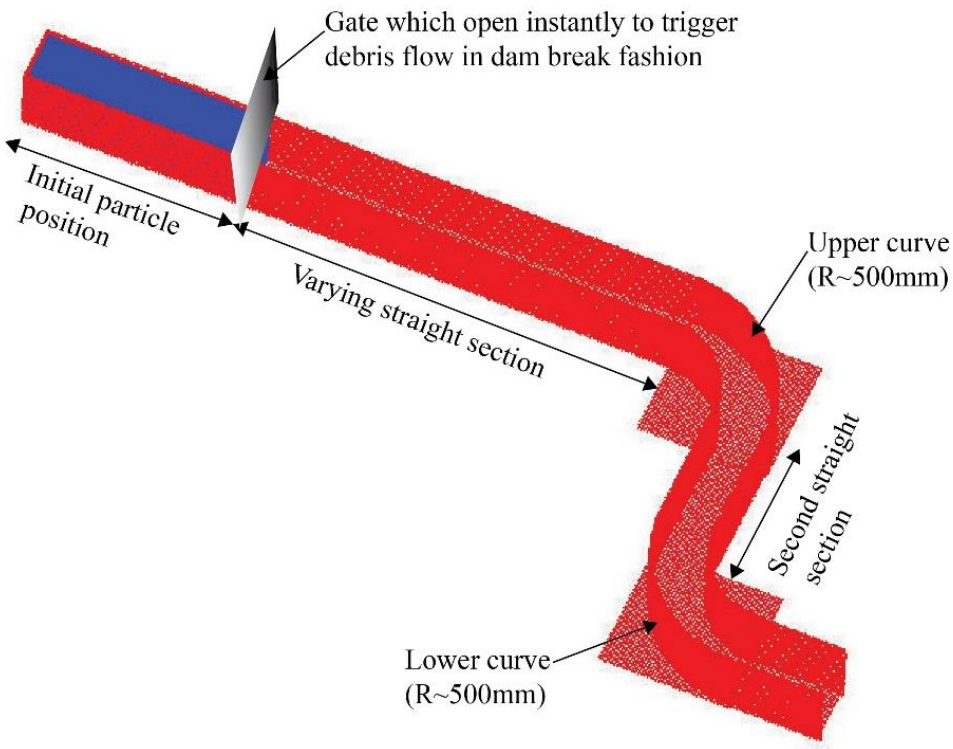

Fig. 4.12 Layout of 3D curved flume

The first straight section of the flume was varied in each simulation so that the effects of super-elevation and velocities could be checked out in a wide range of distance from the origin. At the very first case, the distance from source front to the start of the upper curve was 1125 mm which was increased 500mm by 500mm for the following eleven runs. The other curved and straight portion of the flume shifted accordingly with the first straight section. This subroutine can be more clearly explained with the illustrations in Fig. 4.13. The width of the flume was set at 0.270m and initial length & height were changed depending on the aspect ratios of the source mass. Aspect ratio is defined as the

ratio of initial height to initial source length along the flume. To keep the scenario close to the real event, a small aspect ratio is desirable. However, using very small aspect ratios increase the computational time in a great deal. Thus, considering the computational expense and real scenario, three aspect ratios, 0.33, 0.50 and 0.83 were used for each set of simulations. In addition, flume inclination also plays an important role in the flow dynamics. Usually debris flow occurs between 15~25 degree slope gradients (Pierson 1985) though there are many steep debris flow disasters reported. Three different flume inclinations, 15^0, 20^0, and 25^0 were also considered for current simulations. A total of 6 sets of numerical simulations were run, i.e. total 66 flume tests were run to summarize the findings. Basic properties of the numerical flume model are presented in Table 4.3.

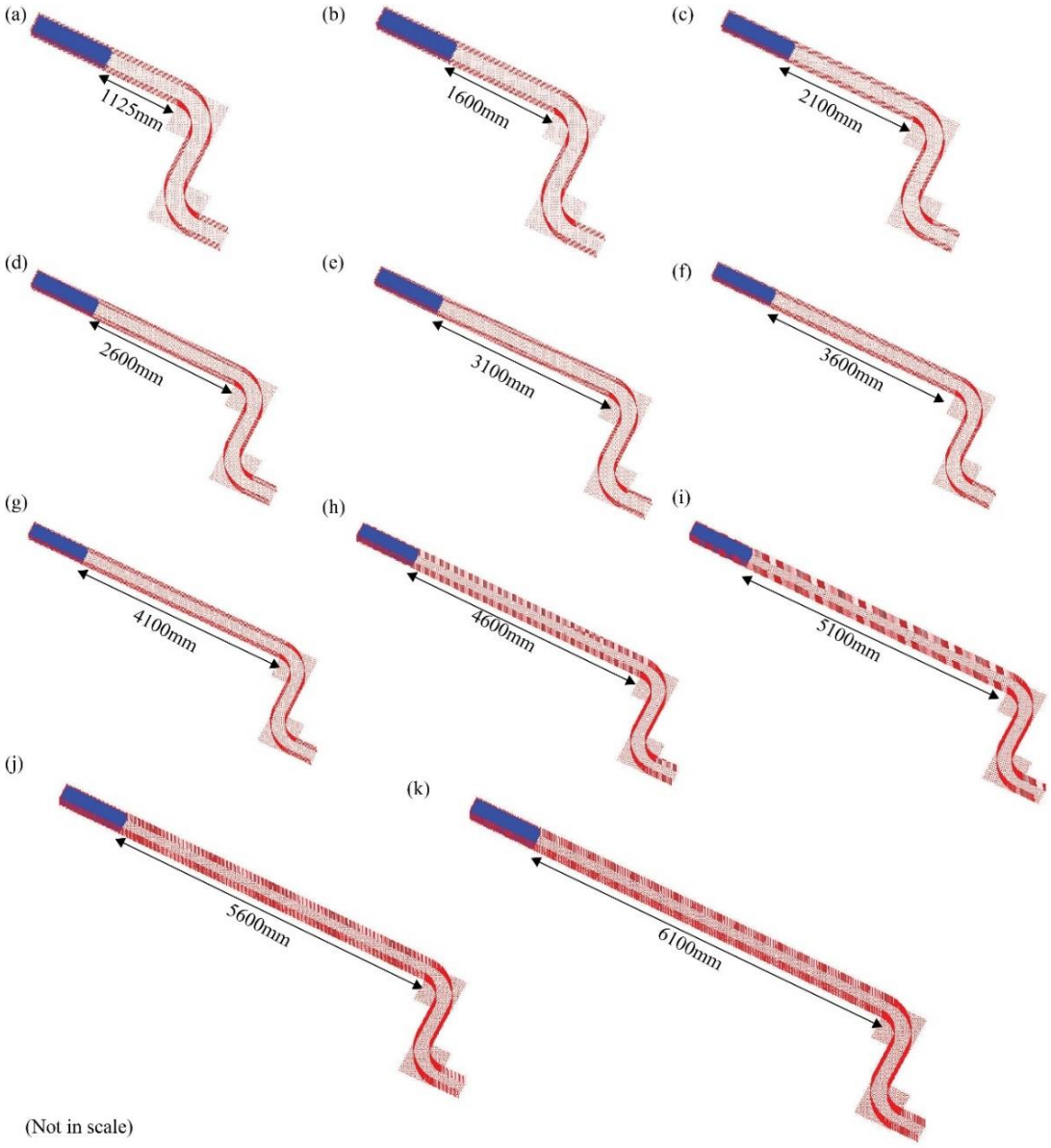

Fig. 4.13 Change of flume configuration for different cases

Table 4.3 Parameters for numerical flume test of debris materials

Parameters	Value	Unit
No. of particles	61000~86000	---
Aspect ratio	0.33~0.83	---
Density	1800	kg/m^3
Dynamic viscosity	0.5	Pa. sec
xSPH coefficient	0.3	---
Channel slope	15~25	degree

4.5.2 Selection of cross-section

In reality, any channel has a natural cross-section and debris mass can flow through this complex natural channel (Fig. 4.14). However, determination of the actual section at any particular location is close to impossible in any case. Rather, a best fit constant arc has been applied in many instances and rationally represent the real situation. It is also desirable to include the circular cross section in the numerical flume test. Nevertheless, modeling of the curved flume with circular cross-section is too intricate and lead to instability of the simulation and therefore, a simplified alternative is required.

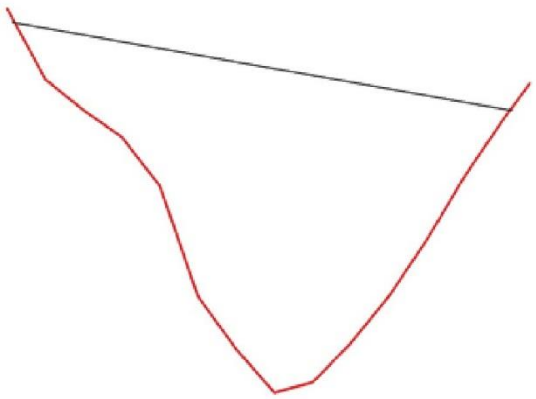

Fig. 4.14 Typical cross-section of a debris flow channel (a cross-section along the Shiraito river debris flow at Nebukawa, Japan)

Regarding the above difficulties, a simplified rectangular channel was employed in numerical modeling. However, aptness of using this simplified cross-section was checked out with 2D simulations. Free sloshing of a simplified rectangular section was simulated and time history of the velocities was recorded. Fig. 4.15 depicts the velocity

distribution of particles at different times. Particles close to the boundary has negligible velocities compare with the inner particles which eventually resembles the semi-circular cross-section. To make it further sure, a small 3D straight flume test was run in a dam break manner and resultant velocity distribution of a particular cross-section at different times were plotted in Fig. 4.16. The result is fairly compatible with the 2D test case with negligible velocities of corner particles. Therefore, rectangular cross-sectional flume was chosen for the following simulations.

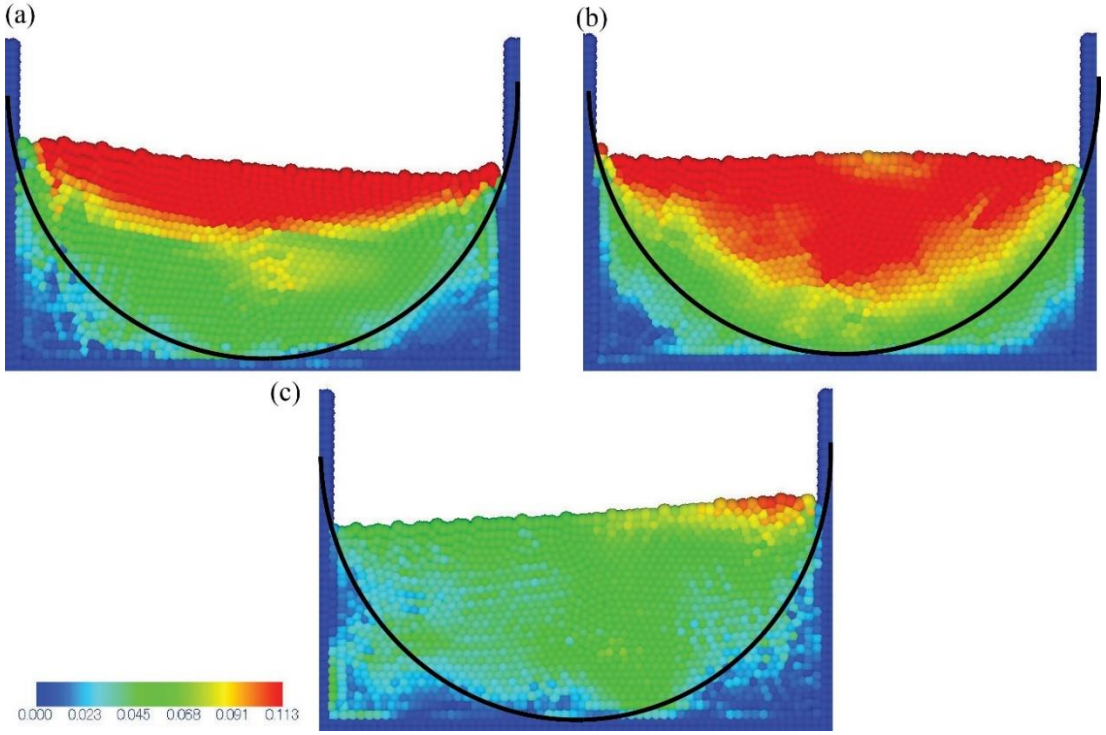

Fig.4.15 Velocity distribution of 2D rectangular tank at different times, (a) at 0.5 sec, (b) at 1.0 sec, (c) at 1.5 sec

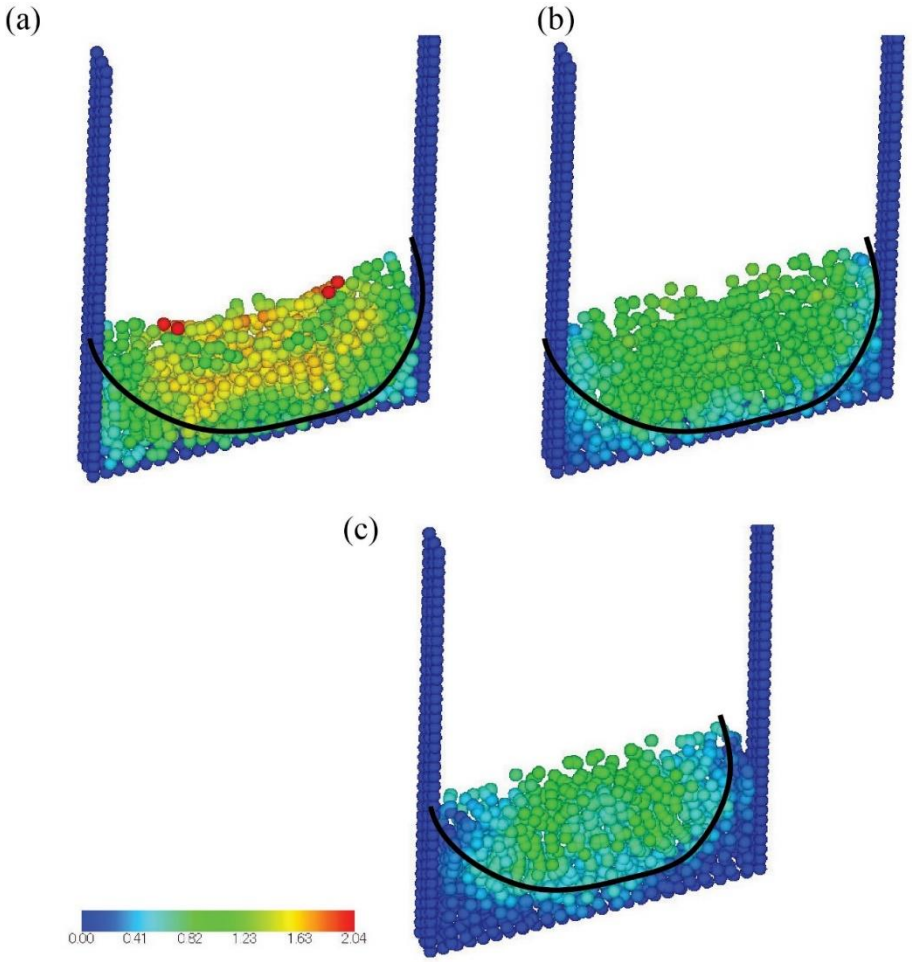

Fig. 4.16 Velocity distribution at a cross-section of 3D flume, (a) at 0.5 sec, (b) at 1.0 sec, (c) at 1.5 sec

4.5.3 Effects of size of particles

In SPH, the problem domain is discretized by the particles, more specific the discrete integration points. Each particle has its own properties and their properties are updated using a smoothing kernel function within the influential domain. Since, this numerical flume test runs on the SPH scheme, determination of size of each particle is important. Apparently, finer particle assemblage would give a better approximation in discrete numerical methods. However, limitation of computational time needs adjustment of particle size so that sufficient numerical analyses can be run within short time. So far, no straight forward approach of selecting the particle size is given in SPH research communities and only few studies have been dealing with mesh convergence (Ferrari et al. 2009). Normally, particle size has been taken based on the problem domain and area of interest in respective research areas. Looking at this issue, a series of dam break test simulation with different particle sizes, from 10 to 20 mm were conducted. Time-history

of the flow front and front velocities were depicted in Fig. 4.17 and Fig. 4.18, respectively. No abrupt change of surge front and front velocities were found among these three configurations. In addition, Fig. 4.19 portrays the flow trace at a particular time for different configurations. Comparing all the cases, simulation with 10 & 15mm seemingly reveals the alike flow dynamics. Thus, to cut down the computational time as well as ensuring the accuracy of the simulation, a spacing of 15mm was chosen for the following debris flow study.

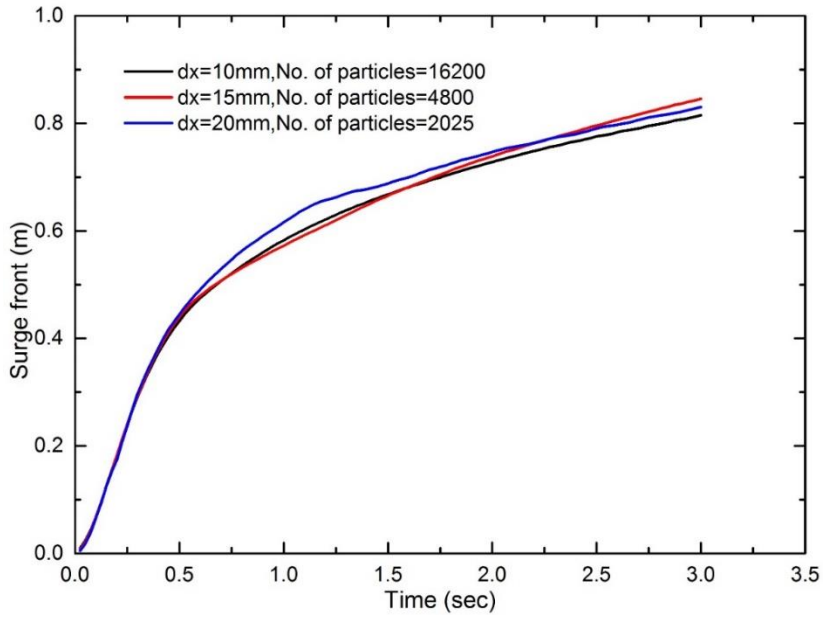

Fig. 4.17 Time-history of surge front for different particle size

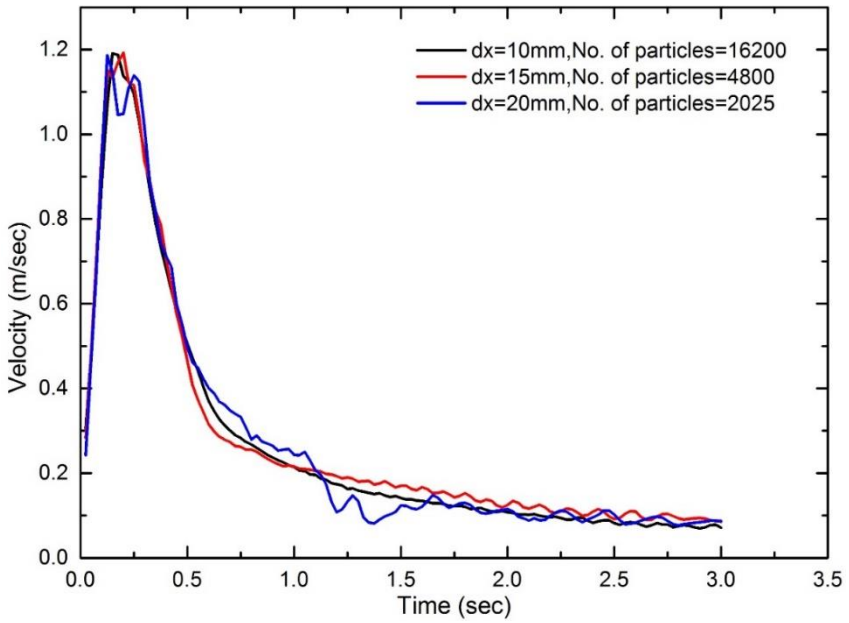

Fig. 4.18 Time-history of front velocity for different particle size

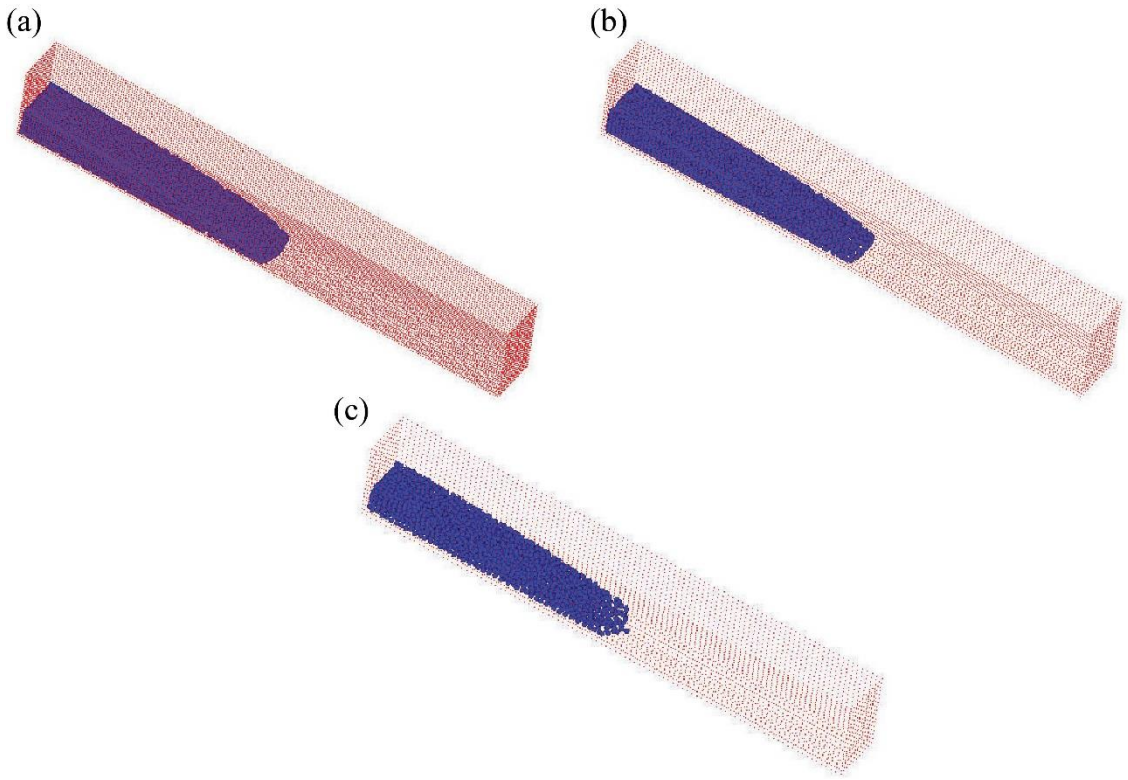

Fig. 4.19 Flow trace at t=2.0 s, (a) dx=10mm, No. of particles=16200, (b) dx=15mm, No. of particles=4800, (c) dx=20mm, No. of particles=2025

4.5.4 Extraction of super-elevation and velocity

Debris flow is highly unsteady and non-uniform in nature and is difficult to analyze both experimentally and numerically. Moreover, extraction of super-elevations and velocities from numerical simulation is more complicated and challenging in this research area as there is no previous literature available. (Proctor 2012; Scheidl et al. 2014) discussed the difficulties associated with estimating mud-marks in their flume experiment's. Besides, the location of maximum super-elevation may vary in each case, depending on the parameters of the materials, flume configuration etc. (Scheidl et al. 2014) run several trial experiments and found that maximum super-elevation appears at the end of the bend section and they measured super-elevation at 20^0 upstream of the end of the curve.

Keeping the experimental obstacles in mind, this study tried to overcome the difficulties and intended to get the insight of the debris flows throughout the curved section. Total eight cross section measurements at a regular 10^0 circumferential angle were taken for each curve and data were recorded at every 0.1s interval of time. A brief idea of the data extraction technique is illustrated in Fig.4.20.

Since SPH is a Lagrangian particle method, estimation of super-elevation of a particular point was not conceivable. Rather, assuming a smaller strip at each section would give a representative cross section and particles within this strip were considered to be the particles on that section (Fig. 4.20c). Afterward, a simple algorithm was used to get the surface particles within the cross-section which eventually provided inner and outer depth. While the flow surface was highly fluctuating, inner and outermost depth of debris slurry was recorded and stored in each section in a frame-by-frame advance manner. The difference between outer and inner depth at a particular time corresponds to the super-elevation. From the time history of inner and outer depth of flow, maximum inner and outer depths were tracked which were the highest mud marks on inner and outer bend, respectively. In reality, only these highest levels of mud marks are visible after any debris events, though actual super-elevation can be quite higher in magnitude at a particular time during the flow. Average velocities of particles within each strip were also recorded frame by frame and used for further conclusion.

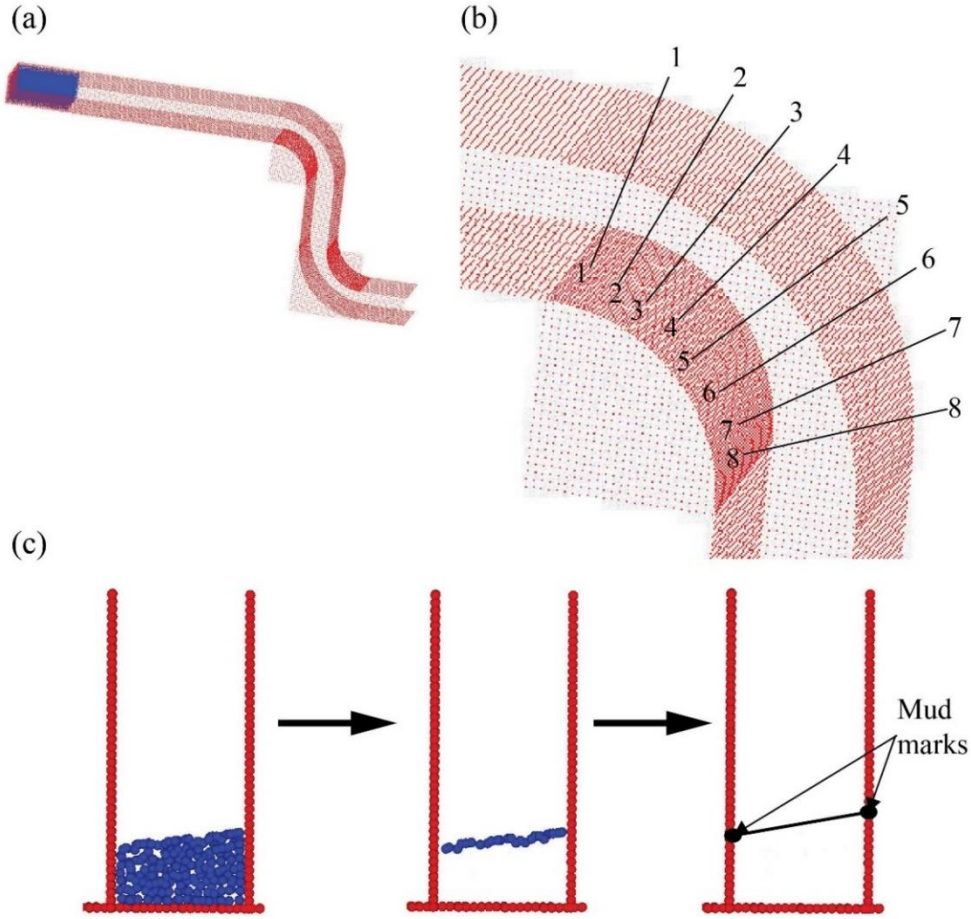

Fig. 4.20 Extraction of super-elevation and velocities, (a) layout of curved flume, (b) zoom in version of curved section, (c) procedure to get mud-marks

4.6 Results and discussions

4.6.1 Discussion on energy contribution in the flow

Energy of the total system was considered in each simulation and recorded at different times. Energy principally comprise of potential and kinetic energy of the system which is given by

$$E_p = \sum_{i=1}^{N} m_i g h_i \tag{4.21}$$

$$E_k = \frac{1}{2}\sum_{i=1}^{N} m_i v_i^2 \tag{4.22}$$

where, E_p and E_k are the potential and kinetic energy respectively, m_i is the mass of particle i, h_i is the height of particle i, v_i is the velocity of particle i, and N is the total number of particles within the system.

At the very beginning, the column of all the particles remained in a static state with its initial potential energy which is formulated as

$$E_0 = \frac{MgH_i}{2} \tag{4.23}$$

$$\mathrm{M} = \sum_{i=1}^{N} m_i \tag{4.24}$$

This initial potential energy is transformed to kinetic energy as the column of particles starts flowing, and the kinetic energy reaches its peak at some time after the collapse. However, a part of potential energy dissipates, mainly due to viscous nature of the fluid. In light of the principle of energy conservation, the energy dissipated in the flow at any given time can be calculated as:

$$E_{dissipated} = E_0 - E_p - E_k \tag{4.25}$$

Where, E_0 is the total energy of the system, which is equal to the initial potential energy. Fig.4.21 depicts the temporal evolution of the energy components of the flow, from the start of the initial column collapse till the end of the motion, where horizontal axis corresponds to the time and vertical axis represent the energy ratios. Particles started to fall downward immediately after the removal of the gate at t=0, with potential energy being progressively transformed into kinetic energy and some thermal energy. When the kinetic energy reaches its peak value, the maximum slope of dissipated energy appears.

Afterward, both potential energy and kinetic energy decrease. This energy distribution is compatible with other numerical analysis of debris flow cases (Gomez-Gesteria, M. 2004; Utili et al. 2015).

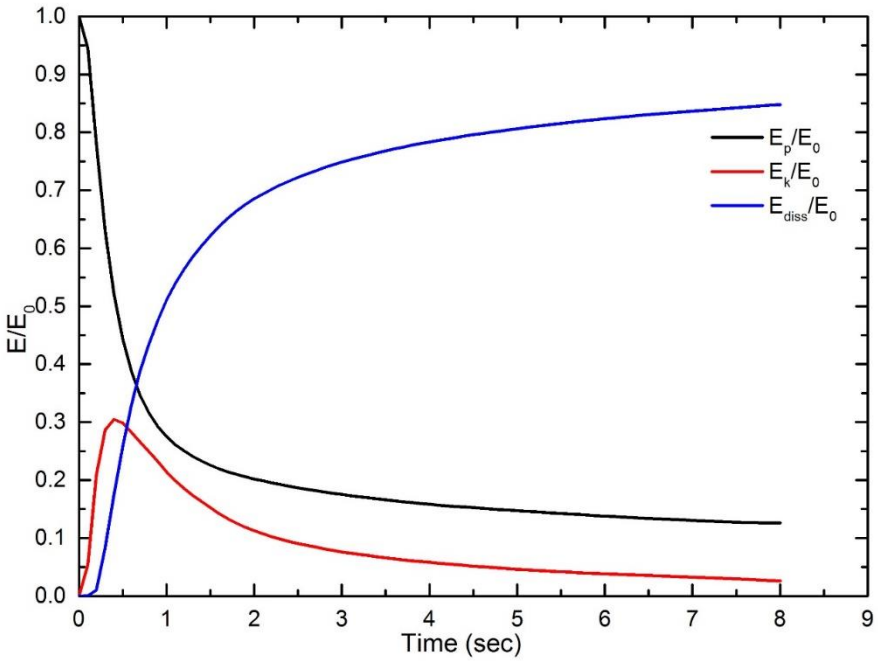

Fig. 4.21 Time-history of energies of the system

The column of debris particles collapses instantaneously, slumps and spreads sideways. This could be seen by plotting the kinetic energy in longitudinal and vertical directions. Time-history of kinetic energy in both longitudinal (E_{kx}) and vertical (E_{kz}) directions are plotted in Fig.4.22. Vertical collapse was described by the rapid peak of E_{kz} and subsequently E_{kx} reached its peak in a short time interval. This short time interval defines the initial unsteady phase of the slumping column, which is then followed by the quasi-steady phase of spreading flow. When the peak value of the kinetic energy is reached, this slumping column spreads over a certain distance.

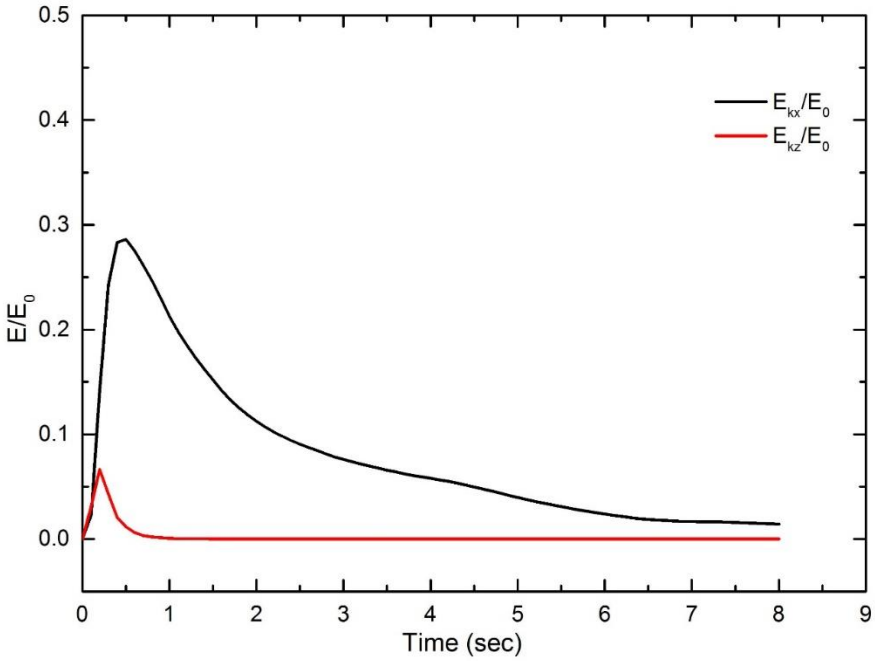

Fig. 4.22 Temporal evolution of kinetic energy of the system

4.6.2 Discussion on normalized distance and velocity

The preceding section described the natural features of the debris flow. However, the primary objective of this research was to check the suitability of using super-elevation in velocity estimation. No eminent guidelines were found in any technical literature describing the details of velocity estimation procedure. Besides, remnant flow marks are widely used to estimate velocities. Therefore, a modification or adjustment is prerequisite for rational estimation of flow velocity. As has been mentioned before, numerical simulation of flume test was chosen as an appropriate tool for checking out the criteria to correlate the super-elevation with remnant mud-marks. Scaling law justified the appropriateness of using numerical simulation and details have been written at the beginning of this chapter.

A series of numerical analyses was run for each set of parameters to get the wide range of velocities and other properties. Maximum average sectional velocities, inner and outer flow depths were recorded at every 0.1s interval for all cross-sections. From the time-history of inner and outer depths, the highest mud-marks on both ends were used to determine the super-elevations at every cross-section. These highest mud-marks resemble the in-situ situation of debris flows and velocities were calculated using those small super-elevation, here denoted by v_{mud}. On the other hand, maximum average velocities at those selected sections were denoted by v_{real}. Distance from the source

region was normalized by the "characteristic length" so that the numerical outcomes can be applied to the real debris event. The explanation of the "characteristic length" follows hereafter.

At the very beginning, flow was unsteady and show erroneous velocities and super-elevations. When the peak kinetic energy is reached, the slumping column spreads over a certain distance. So it is probably rational for the discussion of the transition process of debris flow to normalize the run-out distance of the flowing mass with this particular distance. Velocities as well as mud-marks can be extracted beyond this distance in the simulation. Yet, in reality, determining this distance is almost unimaginable. Simulation with different aspect ratios (initial height to length ratio) suggested that this distance is more or less the same as the initial source length. Fig. 4.23 renders the variation of run-out distance for different aspect ratios at the time of peak kinetic energy. It turned out that the normalized distance is close to 1.0 for different aspect ratios i.e. debris run-out is equal to the initial source length at peak kinetic energy; thus using the initial source length to normalize the run-out distance is considered to be a hands-on approach for further discussion in the subsequent section.

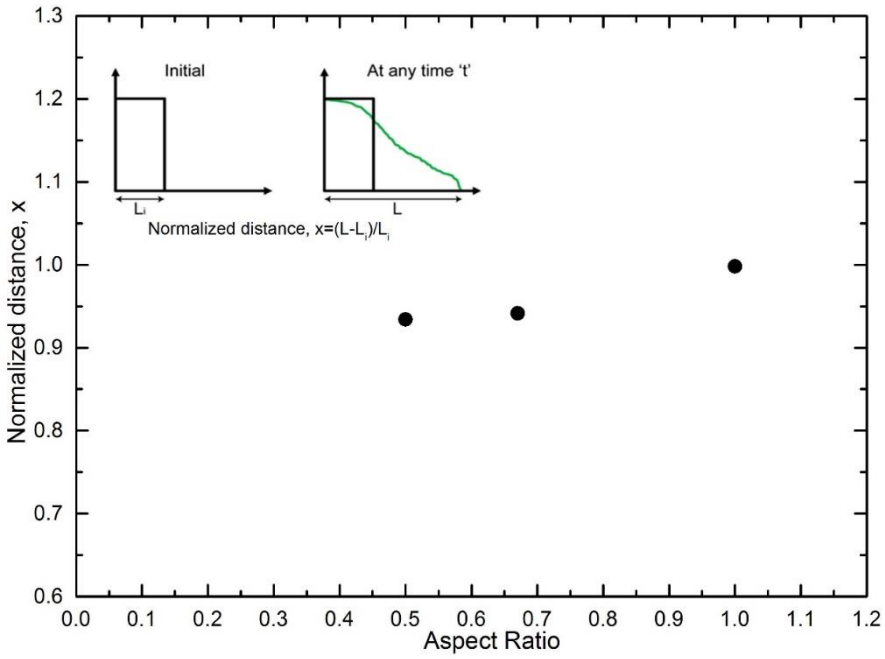

Fig. 4.23 Aptness of using initial source length as characteristic length

Based on the discussion of the preceding passage, distance was normalized using the initial source length of the model and Fig. 4.24 explain the technique of normalizing the run-out distance.

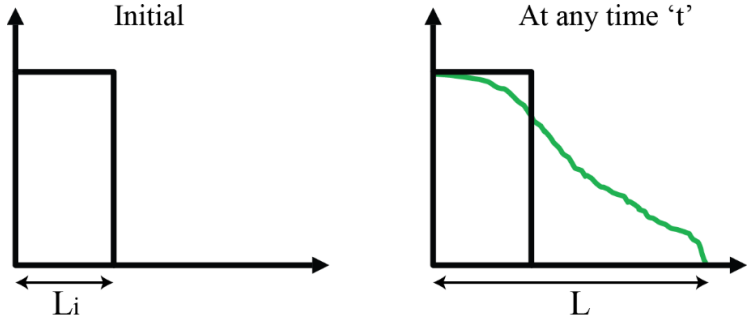

$$\text{Normalized distance , } x = \frac{L - L_i}{L_i}$$

Here, Li is the Characteristics length

Fig. 4.24 Calculation of normalized run-out distance

Velocities calculated using the mud-marks (v_{mud}) were normalized with the real velocities (v_{real}) and plotted against the normalized distance. Variation of flume inclination as well as different aspect ratios was taken into account and normalized distance vs. velocities were plotted for each case. Slope angle was varied from 15~25 degrees, which is comparable to the real events, and aspect ratios were kept below 1.0 from the practical evidence of the past events. Fig. 4.25 depicts the normalized distance and velocity relationship for different aspect ratios. The velocity ratios for different aspect ratios apparently follow the similar trend, though scatter exists because of the unsteady nature of the particle methods. Besides, Fig. 4.26 combines the normalized distance and velocity ratios for different channel gradients and alike features were seen.

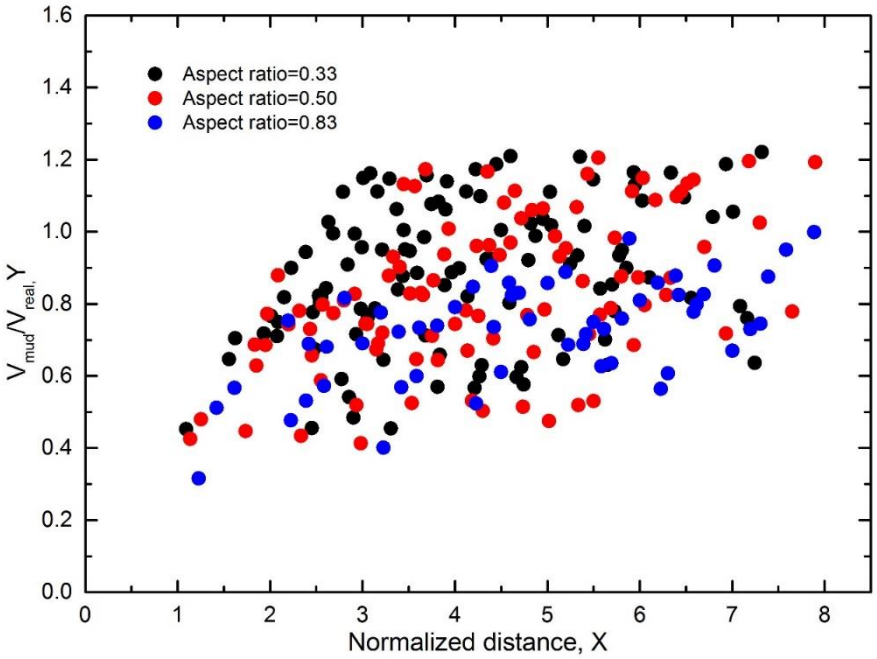

Fig. 4.25 Normalized distance and velocity combining different aspect ratio

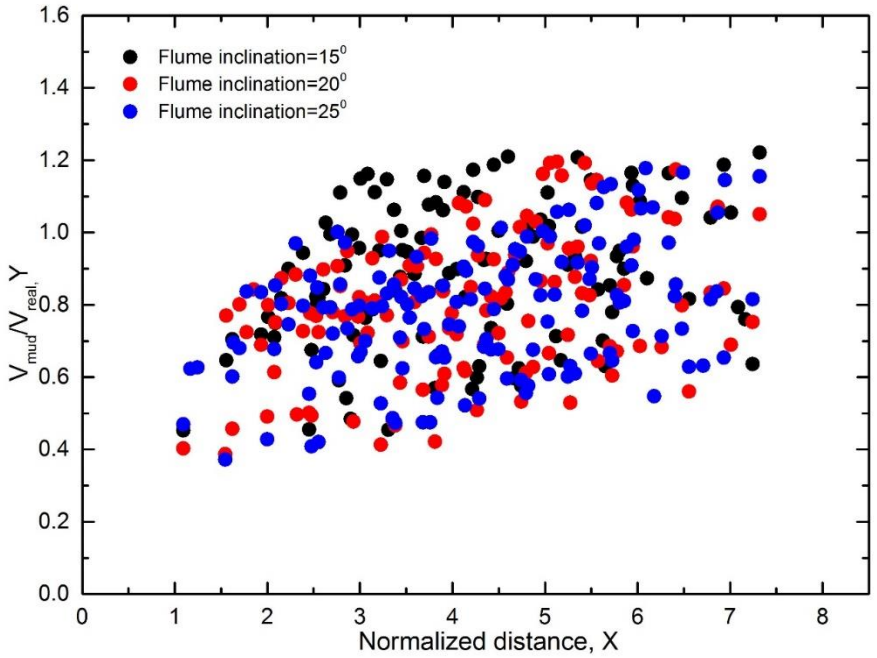

Fig. 4.26 Normalized distance and velocity combining different flume inclination

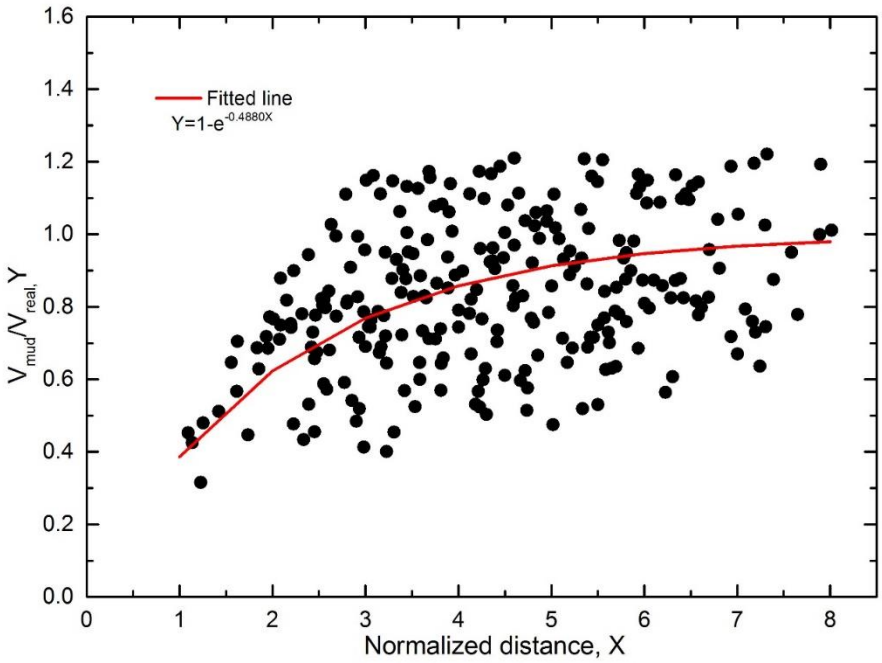

Fig. 4.27 Normalized distance and velocities

Therefore, combining all the scatter plots highlights the overall variation of velocity ratio with the increasing normalized distance. At the beginning stage of the flow, mud-marks does not reflect the actual velocity, mainly because of the highly unsteady flow nature near the source region. Thus the vortex equation with the mud-marks near the source yields underestimation of the actual velocities of the flow, which might correlate the findings of (Iverson et al. 1994). However, as the distance to source increases, mud-marks derived velocities closely approaches to the actual velocities. Assuming that velocities from mud-marks converges on the actual velocities with the increasing normalized distance, a best fit exponential line shown in Fig. 4.27 was fitted on the scatter plot and formulated as

$$Y = 1 - e^{-0.4880X} \tag{4.26}$$

$$\mathrm{Y} = \frac{V_{mud}}{V_{obs}}, X = normalized\ distance$$

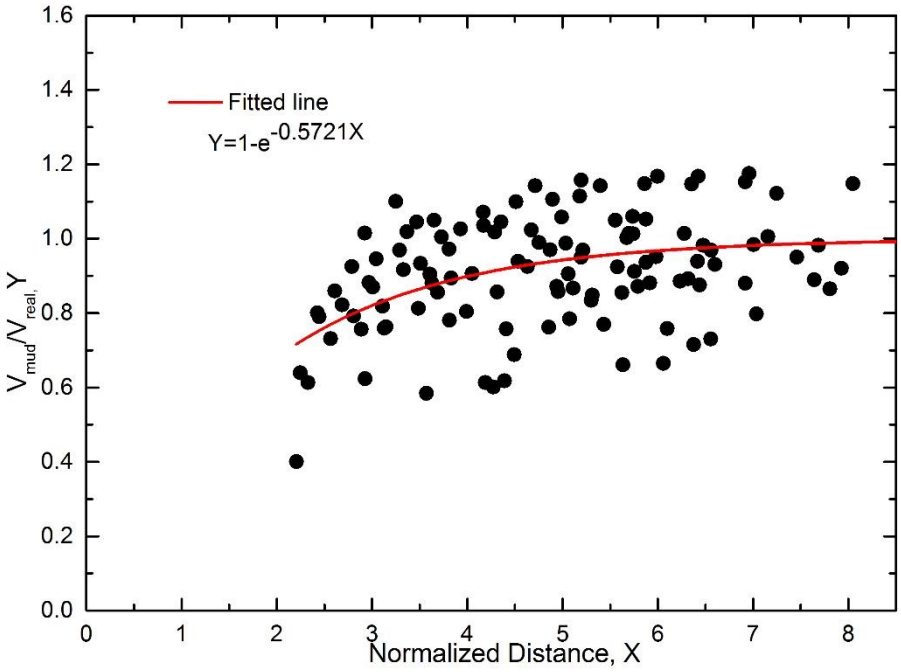

Fig. 4.28 Normalized distance and velocities using Bingham model

4.6.2.1 Discussion of Bingham model

The above discussions are based upon simplified Newtonian fluid model. Alongside with Newtonian fluid, Bingham model was incorporated into the current numerical code (Rahman and Konagai 2016). The only difference between Bingham fluid and Newtonian fluid is the yield strength of material, which causes a rigid plug layer of the flow to form. The existence of the plug layer describes the clogging nature of debris flows which eventually represent the forefront of a flow. Therefore, selection of the appropriate value of the yield strength is important in the modeling. (Iverson 2003) described the difficulties associated with determination of yield strength of debris materials. Despite the shortcomings of appropriate parameters, Bingham fluid is used in many model and prototype debris flow studies and verified with benchmark tests. Therefore, curved flume tests based on Bingham fluid model were run to check if the similar trend shown in Fig. 4.27 can be seen. Based on the reviews of previous numerical simulations of small scale tests (Naili et al. 2005; Huang et al. 2014), a typical value of yield strength of 15 Pas was used. Velocities were estimated from both mud-marks and numerical analyses in the likewise manner as the Newtonian fluid cases, and variation of velocity ratios with normalized distance is plotted in Fig. 4.28. Trend that was seen for the Newtonian fluid case substantiates the Bingham model quite well. A best fit exponential line, assuming the convergence of mud-marks velocities to real velocities

with increasing normalized distance, was also drawn through the scatter plot. These two fitted lines reasonably show the same trend with each other.

Hence, the best fit curve shown above can be used to rationally adjust the flow-mark-based estimate of velocities along a natural debris flume. Validation of the proposed method through some case histories will be given in Chapter-5.

4.6.3 Discussion of arrival time

Mitigation of debris flow hazard is the ultimate goal of this study. Usually, a debris mass detached from a steep slope, flows along its transport channel and is finally deposited on the alluvial fan. Infrastructures built along the flow trace can suffer from serious destruction and people living on those suspicious slopes are always at risk of their lives. An approximation of time for the debris mass to reach the affected area is important for evacuation and early warning systems. Many experimental and analytical works have been done so far to illustrate clearly the run-out feature of debris mass, however, explicit description of arrival time is seldom seen. Feeling the necessity of the real world problems, the current research work makes an attempt to discuss the arrival time of debris mass.

It is expected that the curves shown in Figs. 4.27 and 4.28 can be used to estimate real peak velocity of debris flow from flow marks left on valley walls. Given the variation of the estimated peak velocity along the ravine, arrival time for the debris mass to reach its distal end can also be estimated by adding up piecewise times; each piecewise time can be obtained by dividing each section length by the corresponding peak velocity. However there is no guarantee that the obtained time is identical to the real arrival time. The numerical simulations given above can also provide an answer to this question. In the previous simulations, maximum cross-sectional velocities along the two curve sections were recorded and thus it is possible to estimate the arrival time from these peak velocities. Simultaneously the real arrival times are also recorded in these simulations. To be more precise, the time for the debris mass to travel through the yellow section of the flume shown in Fig 4.29 is examined. A total 20 cross-sections were taken along the yellow section and then the peak velocities were obtained piecewise at all cross-sections. Given the distance between two adjacent cross-sections and the corresponding peak velocity, the time for the debris mass to travel through each flume segment is obtained, and finally summing up all piecewise times, the time t_1 for the debris mass to

travel through the yellow section was obtained. Alongside with the above procedure, debris flow front was recorded frame by frame, and the real time t_2 for the debris mass to travel over the yellow section was obtained as shown in Fig 4.30.

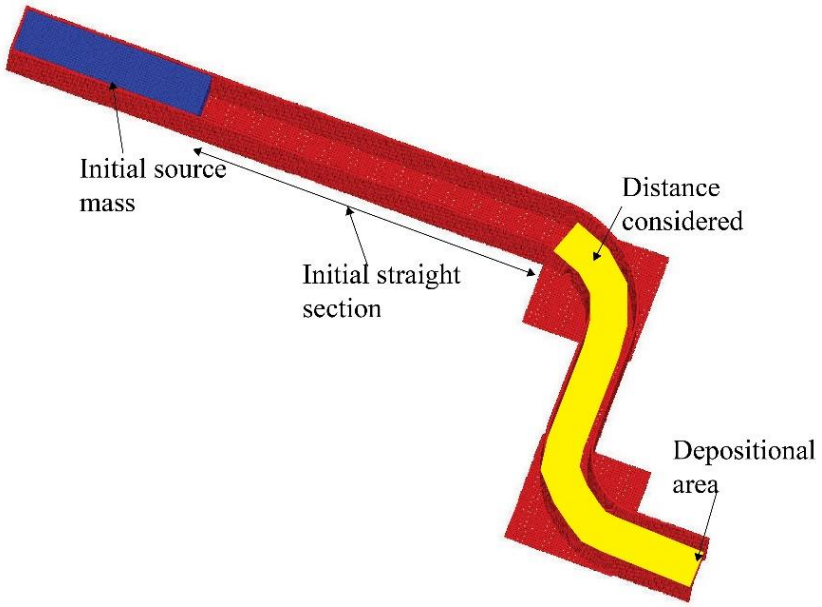

Fig. 4.29 Identification of key factors of time estimation

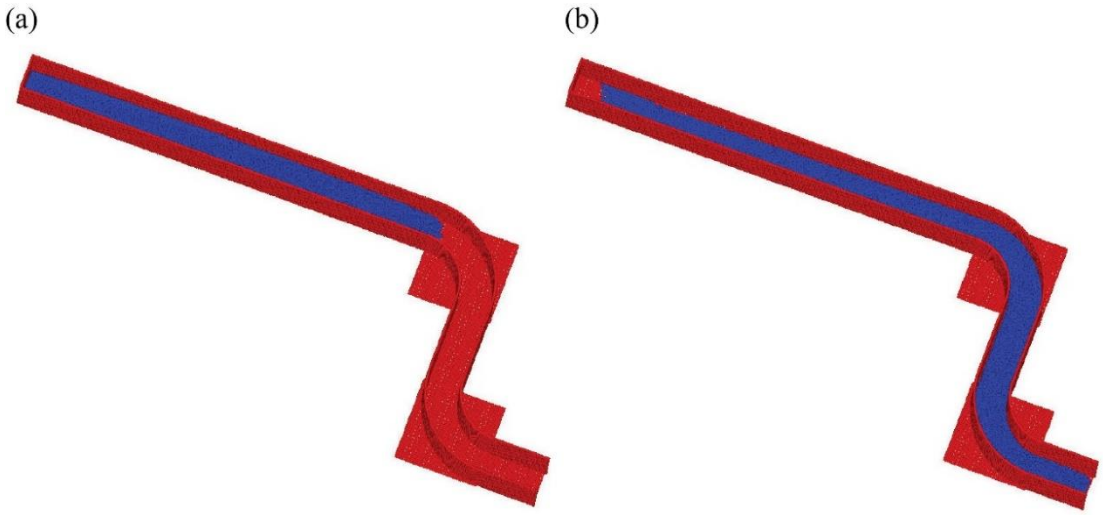

Fig. 4.30 Outline to determine the time from debris front

Changing the length of the first straight section shown in Fig. 4.29 and the aspect ratio of the initial rectangular debris mass, a wide range of depositional distance can be covered. Fig. 4.31 shows the ratios of t_1/t_2 with respect to the locations of deposition zones normalized by the initial source length. It is shown in the figure that the ratio

between two times are in the range of 0.8 to 0.9 though there is a slight increasing trend over the examined normalized depositional distance up to 7.0. This finding is expected to be used in estimating possible arrival times of debris flows.

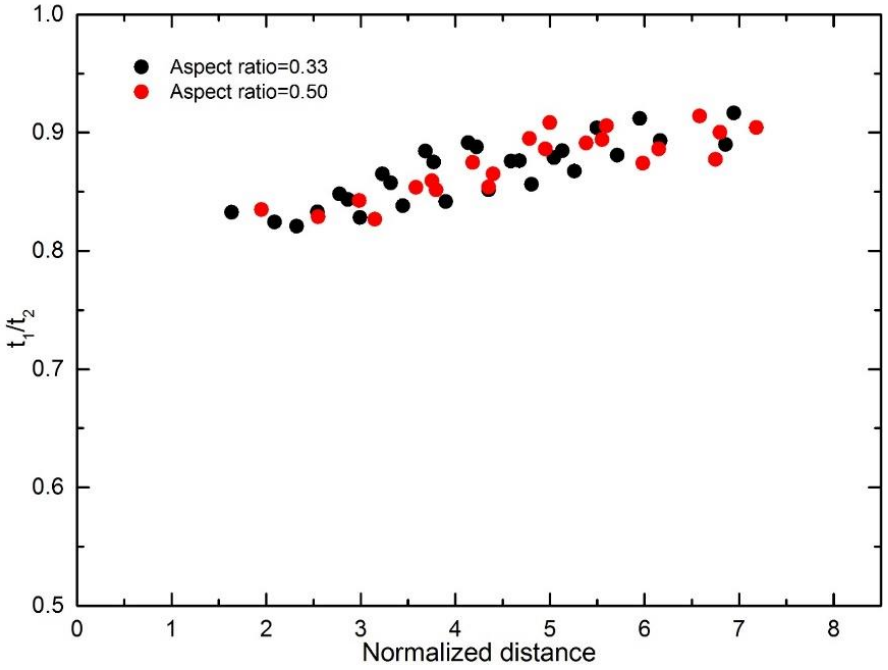

Fig. 4.31 Ratio of estimated times

4.6.4 Discussion on sloshing period and maximum super-elevation

The iterative procedure to determine the radius of curvature of a natural flume described in Chapter-2 is based on the assumption that the time taken to attain the maximum super-elevation of a selected stretch is estimated from the sloshing period of the selected cross-sections. This assumption needs to be checked out quantitatively from the numerical tests. In the preceding sections, several numerical simulations of 3D curved flume were run and in each case, mud-marks on both inner and outer flume walls were recorded. The difference between the maximum outer and inner depth of the mud-marks corresponds to the super-elevation, which is actually seen in the field.

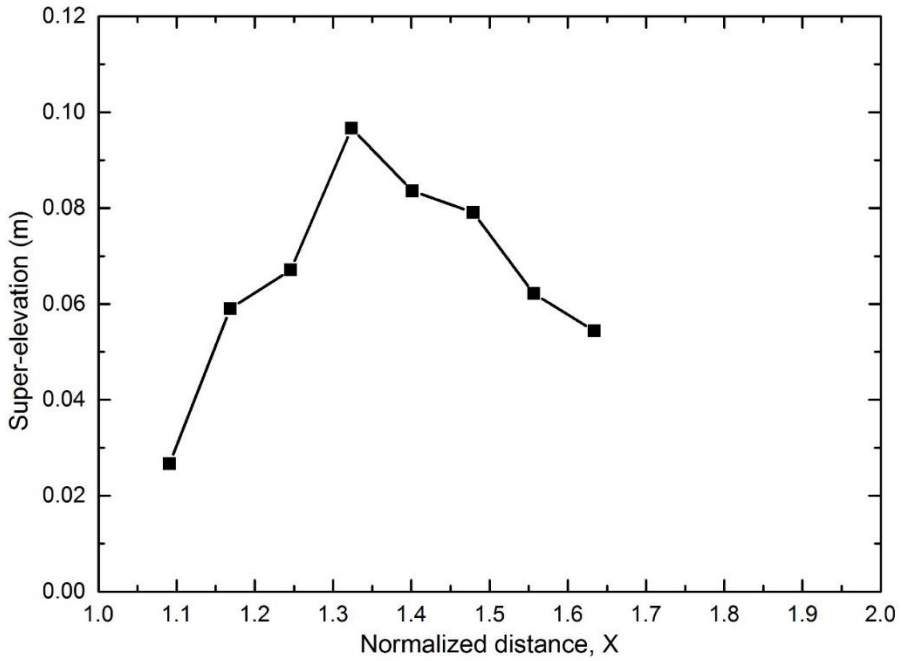

Fig. 4.32 Variation of super-elevation along the curve stretch of the numerical flume

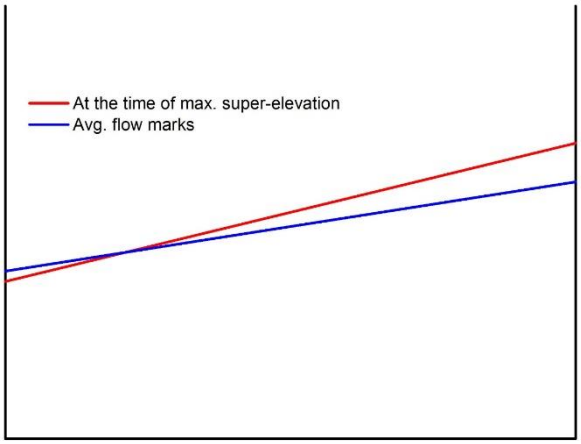

Fig. 4.33 Representative cross-sections

Fig. 4.32 shows the variation of super-elevation along the curved stretch of the numerical flume. Velocities of selected cross-sections were also recorded and using the velocities and known distance, the time taken for the debris mass from the starting point of the curved section to the location of the maximum super-elevation was estimated. Meanwhile, sloshing simulation of a 2D model, which is identical to the representative cross-section of the flume (Fig. 4.33), was carried out and sloshing period was obtained from the numerical analysis. Both the times are depicted in Table 4.4. Comparing the numerically obtained times from both 2D and 3D simulations, it can be said that the time

for the maximum super-elevation is reached is nearly as one-third of the sloshing period. Simulations with different bend radius also justify the use of one-third sloshing period.

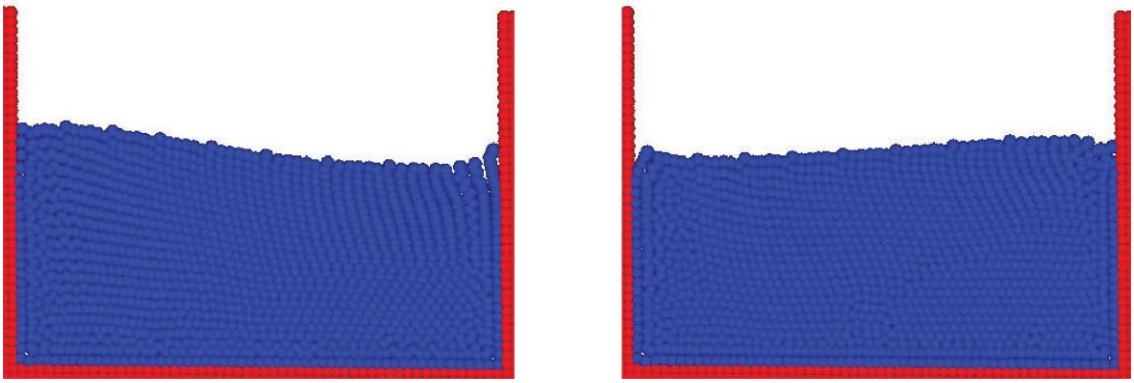

Fig. 4.34 One period of sloshing for a 2D section

Table 4.4 Comparison of time

Description	Time (s)
Sloshing period	0.610
Time estimated from 3D simulation	0.177 (0.30 times the sloshing period

References

Bagnold R a. (1954) Experiments on a Gravity-Free Dispersion of Large Solid Spheres in a Newtonian Fluid under Shear. Proceedings of the Royal Society A: Mathematical, Physical and Engineering Sciences 225:49–63. doi: 10.1098/rspa.1954.0186

Boniello MA, Calligaris C, Lapasin R, Zini L (2010) Rheological investigation and simulation of a debris-flow event in the Fella watershed. Natural Hazards and Earth System Science 10:989–997. doi: 10.5194/nhess-10-989-2010

Calvo L, Haddad B, Pastor M, Palacios D (2014) Runout and deposit morphology of Bingham fluid as a function of initial volume: implication for debris flow modelling. Natural Hazards 75:489–513. doi: 10.1007/s11069-014-1334-x

Cooley ME, Aldridge BN, Euler RC (1977) Effects of the catastrophic flood of December 1966, North Rim Area, Eastern Grand Canyon, Arizona.

Coussot BP, Laigle D, Arattano M, et al (1998) Direct determination of rheological characteristics of debris flow. Journal of hydraulic engineering 865–868.

Curry RR (1966) Observation of apline mudflows in the Tenmile range, Central Colorado. Bulletin of The Geological Society of America 77:771–776.

Dai Z, Huang Y, Cheng H, Xu Q (2014) 3D numerical modeling using smoothed particle hydrodynamics of flow-like landslide propagation triggered by the 2008 Wenchuan earthquake. Engineering Geology 180:21–33. doi: 10.1016/j.enggeo.2014.03.018

Davies TRH (1990) Debris-flow surges-experimental simulation. Journal of Hydrology (NZ) 29:18–46.

Ferrari A, Dumbser M, Toro EF, Armanini A (2009) A new 3D parallel SPH scheme for free surface flows. Computers and Fluids 38:1203–1217. doi: 10.1016/j.compfluid.2008.11.012

Fink JH, Malin MG, D'Alli RE, Greeley R (1981) Rheological properties of mudflows associated with the spring 1980 eruptions of Mount St Helens,Washington. Geophys Res Lett 8:43–46.

Gomez-Gesteria, M. DRA (2004) Using a Three-Dimensional Smoothed Particle Hydrodynamics Method for Wave Impact on a Tall Structure. Journal of Waterway, Port, Coastal and Ocean Engineering 130:63–69. doi: 10.1061/~ASCE!0733-950X~2004!130:2~63!

Huang Y, Cheng H, Dai Z, et al (2014) SPH-based numerical simulation of catastrophic debris flows after the 2008 Wenchuan earthquake. Bulletin of Engineering Geology and the Environment 74:1137–1151. doi: 10.1007/s10064-014-0705-6

Hungr O (1995) A model for the runout analysis of rapid flow slides, debris flows, and avalanches. Canadian Geotechnical Journal 32:610–623.

Hunt B (1994) Newtonian fluid mechanics treatment of debris flows and avalanches. Journal of Hydraulic Engineering 120:1350–1363.

Iverson R (2003) The debris-flow rheology myth. 3rd International Conference on

Debris-Flow Hazards Mitigation: Mechanics, Prediction, and Assessment 303–314.

Iverson RM, LaHusen RG, Major JJ, Zimmerman CL (1994) Debris flow against obstacles and bends; dynamics and deposits. Eos, Transactions, American Geophysical Union 274.

Jan C, Shen H (1997) Review dynamic modeling of debris flows. Recent Developments on Debris Flows 93–117.

Julien PY, Lan Y (1991) Rheology of Hyperconcentrations. Journal of Hydraulic Engineering 117:346–353. doi: 10.1061/(ASCE)0733-9429(1991)117:3(346)

Koch T (1998) Testing various constitutive equations for debris flow modelling. IAHS Publications-Series of Proceedings and Reports-Intern Assoc Hydrological Sciences 248:249–258.

Laigle D, Coussot P (1997) Numerical modeling of mudflows. Journal of Hydraulic Engineering 617–623. doi: 10.1061/(ASCE)0733-9429(1997)123:7(617)

Li J, Luo D (1981) The formation and characteristics of mudflow and flood in the mountain area of Dachao River and its prevention. Z Geo-morph NF 25:470–484.

Li J, Yuan JC, Luo D (1983) The main features of the mudflow in Jiang-Jia Ravine. Z Geo-morph NF 27:325–341.

Major JJ, Pierson TC (1992) Debris flow rheology: experimental analysis of fine-grained slurries. Water Resources Research 28:841–857.

Naili M, Matsushima T, Yamada Y (2005) A 2D Smoothed Particle Hydrodynamics method for liquefaction induced.

Okuda S, Suwa H, Okunishi K, et al (1977) Synthetic observation on debris flow, part 3; observation at valley Kamikamihorizawa Mt. Yakedake in 1976. Annuals, DPRI, Kyoto University 21B-1:277–296.

Parsons JD, Whipple KX, Simoni A (2001) Experimental Study of the Grain- Flow, Fluid- Mud Transition in Debris Flows. The Journal of Geology 109:427–447. doi: 10.1086/320798

Pastor M, Blanc T, Haddad B, et al (2014) Application of a SPH depth-integrated model to landslide run-out analysis. Landslides 11:793–812. doi: 10.1007/s10346-014-0484-y

Phillips CJ, Davies TRH (1991) Determining rheological parameters of debris flow material. Geomorphology 4:101–110. doi: 10.1016/0169-555X(91)90022-3

Pierson T. (2005) Hyperconcentrated flow - transitional process between water flow and debris flow. Debris-flow Hazards and Related Phenomena 159–202. doi: 10.1007/3-540-27129-5

Pierson TC (1985) Initiation and flow behavior of the 1980 Pine Creek and Muddy River lahars, Mount St. Helens, Washington (USA). Geological Society of America Bulletin 96:1056–1069. doi: 10.1130/0016-7606(1985)96<1056:IAFBOT>2.0.CO;2

Pritchard D, Duffy BR, Wilson SK (2014) Shallow flows of generalised Newtonian

fluids on an inclined plane. Journal of Engineering Mathematics 94:115–133. doi: 10.1007/s10665-014-9725-2

Proctor CM (2012) Debris flow dynamics: A flume study of velocity and superelevation. Durham University

Rahman MA, Konagai K (2016) Substantiation of debris flow velocity from super-elevation: a numerical approach. Landslides. doi: 10.1007/s10346-016-0725-3

Rickenmann D (1991) Hyperconcentrated flow and sediment transport at steep slopes. Journal of Hydraulic Engineering 117:1419–1439.

Scheidl C, Chiari M, Kaitna R, et al (2013) Analysing Debris-Flow Impact Models, Based on a Small Scale Modelling Approach. Surveys in Geophysics 34:121–140. doi: 10.1007/s10712-012-9199-6

Scheidl C, Mcardell BW, Rickenmann D (2014) Debris-flow velocities and superelevation in a curved laboratory channel. 20:1–20. doi: 10.1139/cgj-2014-0081

Sharp RL, Nobles LH (1953) Mud flow of 1941 at Wrightwood, Southern California. Bull Geol Soc Am 64:547–560.

Shen S, Xie S (1985) Structure mode and rheologic property of mud debris flow. In: Proceeding of International Symposium on Erosion, Debris flow and Disaster prevention.

Sohn YK (2000) Coarse-grained debris-flow deposits in the Miocene fan deltas, SE Korea: A scaling analysis. Sedimentary Geology 130:45–64. doi: 10.1016/S0037-0738(99)00099-8

Takahashi T (2000) Debris flow Mechanics, Prediction and Countermeasures. Taylor & Francis

Takahashi T (2009) A Review of Japanese Debris Flow Research. International Journal of Erosion Control Engineering 2:1–14. doi: 10.13101/ijece.2.1

Utili S, Zhao T, Houlsby GT (2015) 3D DEM investigation of granular column collapse: Evaluation of debris motion and its destructive power. Engineering Geology 186:3–16. doi: 10.1016/j.enggeo.2014.08.018

Uzuoka R, Yashima A, Kawakami T, Konrad JM (1998) Fluid dynamics based prediction of liquefaction induced lateral spreading. Computers and Geotechnics 22:243–282. doi: 10.1016/S0266-352X(98)00006-8

Wang W, Chen G, Han Z, et al (2016) 3D numerical simulation of debris-flow motion using SPH method incorporating non-Newtonian fluid behavior. Natural Hazards. doi: 10.1007/s11069-016-2171-x

Wang X (2008) Geotechnical analysis of flow slides, debris flows, and related phenomena. University of Alberta

Whipple KX, Dunne T (1992) The influence of debris-flow rheology on fan morphology, Owens valley, California. Geological Society of America Bulletin 104:887–900.

Zhang X, Liu T, Wang Y, Luo J (1985) The mean features of debris flow and control

structures in Hunshui gully, Yuannan Province, China. In: Proceedings of International Symposium on Erosion, Debris flow and Disaster prevention.

Chapter-5

REAL DEBRIS FLOW STUDIES

5.1 Introduction

Preceding chapter described the results of a series of numerical simulations of 3D curved flume tests. A procedure of amending the current practically applied velocity estimation procedure was developed from the findings through the numerical simulations. Moreover, the similarity law for viscous fluids also supported to use the findings in real debris flow events. However, validation is pre-requisite for any numerical tools to be used in real life problems. Therefore, three well known debris flow disasters at three different times are selected as examples for validation and described in the subsequent sections.

5.2 Shiraito River debris flow in 1923

A total of 167 sediment related disasters was reported after The Great Kanto earthquake of 1923. Among them, a massive debris avalanche near the rim of the Hakone crater, Kanagawa prefecture was the most destructive one. The flowing debris mass smashed 64 to 67 houses of Nebukawa town, killing about 300 people of the total 858 of Nebukawa (Nishisaka 1966). A huge amount of soil mass was detached from the mountainous area about 3.5 kilometers upstream of the Shiraito River, and turned into gigantic debris flows. Debris mass swept away the Nebukawa steel deck railway bridge towards the sea, which deck fell down to the valley in the intense shake shortly before the debris surge. It was also reported that locomotive of train no. 116 was buried under the debris surge near the mouth of the Sainome tunnel and shown in Fig. 5.1 (JNR 1927).

Debris mass ran down the Shiraito river which was filled with river water owing to the heavy rain that occurred just the day before the event. Debris flow trail along the Shiraito River is depicted in Fig. 5.2. Furthermore, the Nebukawa region, lying along the foot of Hakone volcano, has long been an important point of traffic through Tokaido route connecting Tokyo with Osaka, and now the high-speed bullet train runs across Shiraito

River at an elevation lower than Nebukawa steel Railway Bridge (Fig. 5.3). Hereafter, necessary measures are to be taken for this region referring to the past events. To verify the preceding numerical results, Shiraito river debris event is considered to be an auspicious option.

Fig. 5.1 Destruction of Shiraito river debris flow: locomotive of train no. 116 buried near the mouth of Sainome tunnel (JNR 1927)

Sliding mass contains andesite, lapilli tuff, and pumice tuff strata of volcanic origin in an inclined manner (Yamasaki and Kamai 2015). This pumice tuff layer is easily sheared and hold a good moisture. Moreover, a heavy rainfall was recorded on August 31, 1923, one day before the earthquake and also intermittent rainfall was reported in the forenoon of that outcome (Kobayashi 1992). This intense rainfall seemingly contributed to increase the saturation, and eventually responsible for the massive slide. On the contrary, no clear descriptions were found regarding the state of debris deposited after this destruction.

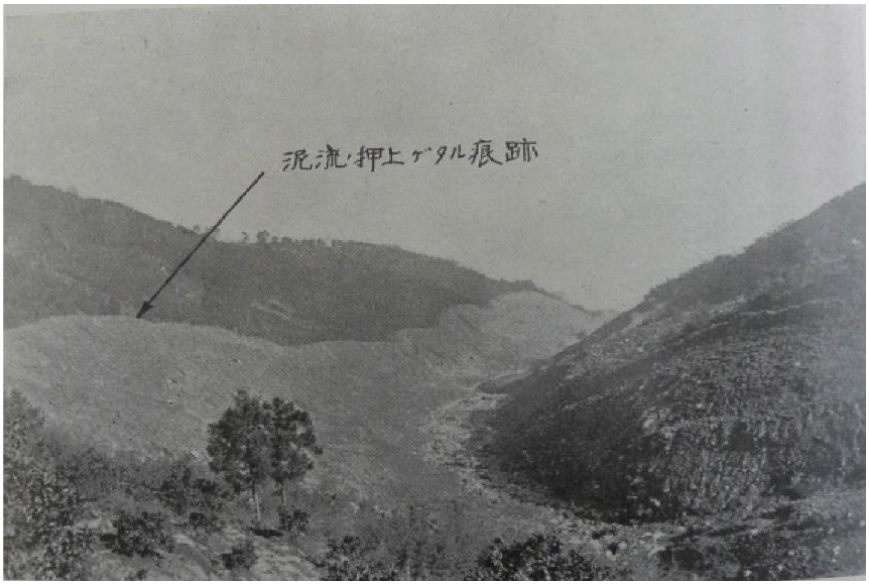

Fig. 5.2 Debris flow trail along the Shiraito River (JNR 1927)

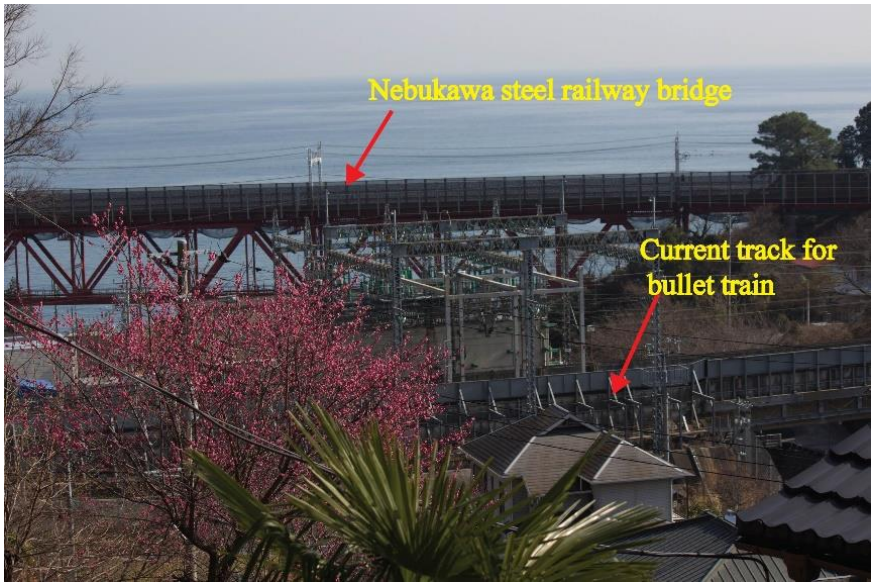

Fig. 5.3 Current track for the high speed train along the Nebukawa region

5.2.1 Source of Shiraito-River debris flow

(Imamura 1925) found some suspicious scars on slopes of the outer rim of Hakone crater at the time of his survey 50 days after the earthquake. These scars may have been the source(s) of this gigantic debris flow that ran down along the Shiraito River. Scars were mostly on (1) the southern slope of Mt. Hijiri, and (2) the northern slope of Mt Hoshi (Shown in Fig. 5.4). In terms of size, those on the southern slope of Mt. Hijiri seem to be more plausible. However local people said that among those on the southern slope of Mt. Hijiri, eastern most Obora scar appeared after the debris flow event. Putting them

together, Imamura (Imamura 1925) concluded that the source of the debris flow was either the south to southwest scars of Mt. Hijiri or east scar of Mt. Shirogane.

Fig. 5.4 Shiraito river debris flow area

(Kobayashi 1979) made an attempt to compare two topographical maps of the source area from different times of 1916 (Taisho 5) and 1970 (Showa 44). Kobayashi assumed that the decrease and increase in elevation are largely due to erosions and depositions respectively, and suggested that the Obora scar (Fig. 5.5), which is the largest in terms of the volume of the detached mass exceeding 10^6 m^3, can be the most plausible as the source among others. This volume conforms to 1 to 3×10^6 m^3 volume estimated by Imamura. Regarding the discrepancy between his opinion and the re-collection of the local people saying that the scar appeared after the debris flow event, Kobayashi explained that the scar at Obora is made up of two major hollows, and one of these two hollows may have appeared after the debris flow event.

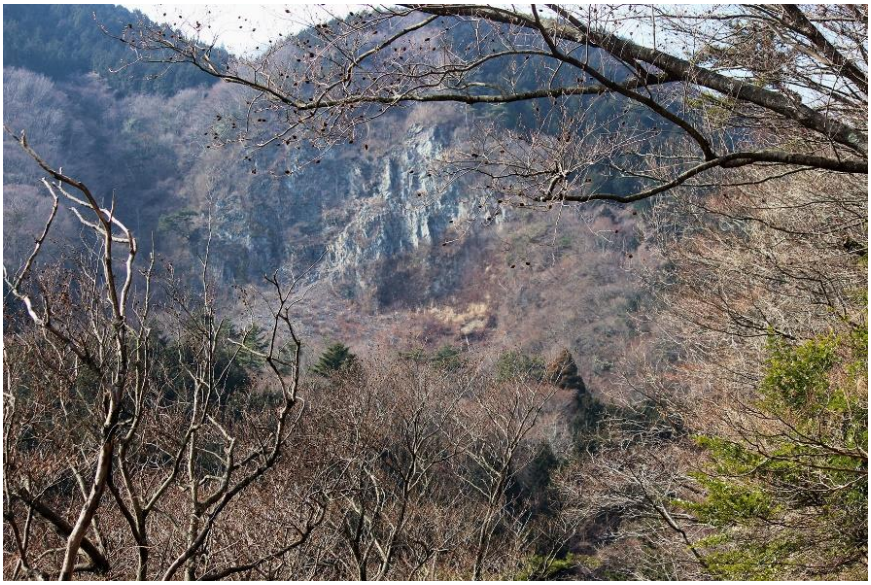

Fig. 5.5 Obora scar

With the help of highly advanced GIS tools, template matching of these two topographical maps was done in a more quantitative manner with reference to locations and elevations of Mt. Hoshi (814.6m a.s.l.), Mt. Hijiri (835.0m a.s.l.) and Mt. Shirogane (993.1m a.s.l.). The 1:50,000 scale map prepared in 1896 (Meiji 29) and the digital elevation model (DEM) of the target terrain prepared by the Geospatial Information Authority of Japan (GSI,Japan) on December 4th, 2008 were used herein as maps to compare. In the older map of 1896, the elevations of these peaks were 814.4m and 838m and 992.6m, respectively, and differ a little from those in the map of 2008. The error was probably attributed to the old way of measuring, called plane table measurement in which a drafting board on a tripod, an alidad, a pole and a tape line were used. However, the distances among these peaks in the old map matched very well in the new map, and the error in elevation is much less significant that in the drastic change in contour lines. Therefore, geo-referencing of the scanned and digitized older map was done for the longitudes and latitudes of these reference (control) points.

Fig. 5.6 shows the obtained change in elevation in the source area of the Shiraito River debris flow. Though the accuracy is yet debatable, the change in volume was estimated to be -3.8×10^6 m^3 for the rectangular area shown in Fig. 5.6 with Obora scar in its middle, which volume conforms to 1 to 3×10^6 m^3 estimated by Imamura. However, at the same time, Fig. 5.6 shows that there are some suspicious dents remaining on mountain slopes and along river channels, indicating that there is a possibility that several debris

masses from different sources joined together to be a large debris mass. Summarizing the above discussion, it can be concluded that Obora scar was the major source of the Shiraito River debris flow.

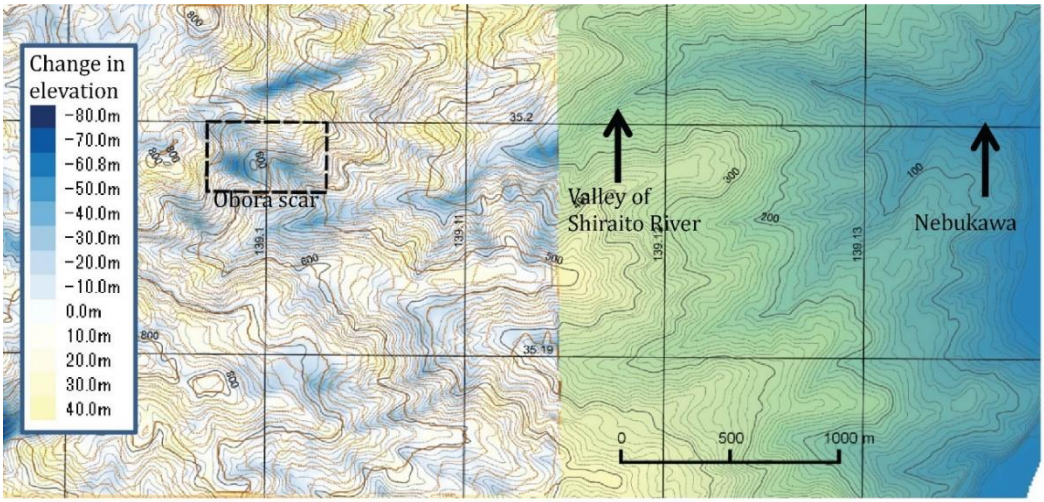

Fig. 5.6 Change in elevation in the source area of the 1923 Shiraito River debris flow: brown and black contour lines are for 1896 and 2008 terrains, respectively. The change in volume was estimated to be – 3.8 x 10^6 m^3 for the rectangular area in this figure.

5.2.2 Estimation of flow velocities

Given a number of precedent field surveys and studies, Shiraito river debris flow is competent in examining the proposed hypothesis. Kazumasa Uchida, a 10 year old boy at the time of disaster whose house was buried under the debris deposit, illustrated longitudinal and transverse profiles of the flowing slurry along the Shiraito River. His illustrations on scrolls of wrinkled Japanese paper are in storage at Kanagawa Prefectural Archives (Fig. 5.7 and Fig. 5.8).

Fig. 5.7 Illustration of mud-marks along Shiraito River by Mr. Kazumasa Uchida (Kanagawa Prefectural Archives)

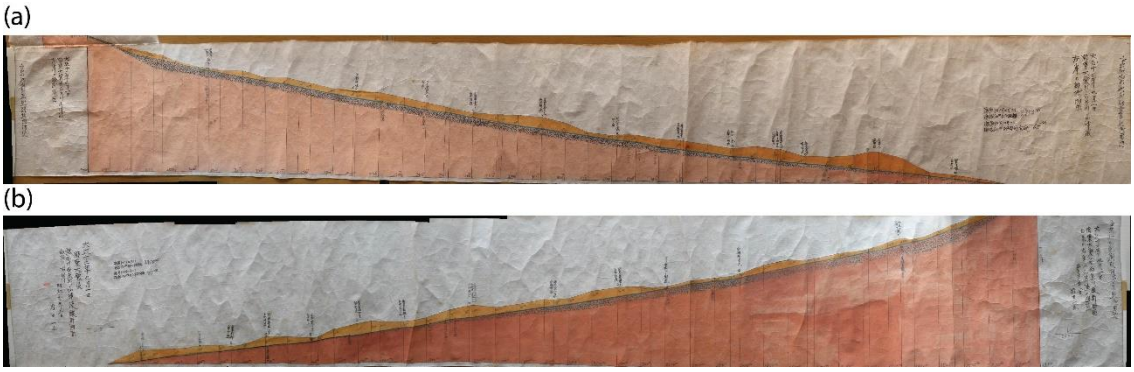

Fig. 5.8 Elevations of bank of Shiraito River illustrated by Mr. Kazumasa Uchida , (a) left bank elevations, (b) right bank elevations (Kanagawa Prefectural Archives)

With the aid of advanced GIS tools, Mr. Uchida's illustration was digitized and geo-referenced to be overlaid on current topographic map to extract the necessary pieces of information (Fig.5.9). Afterward, debris flow boundaries on left and right bank of Shiraito River were determined and marked on the current map to cover the entire flow trace, which is depicted in Fig. 5.10. Elevation of left and right bank of the Shiraito River at every 100-meter interval, found in Mr. Uchida's illustration (Fig. 5.8) were used to determine the variation of super-elevations along the river stream.

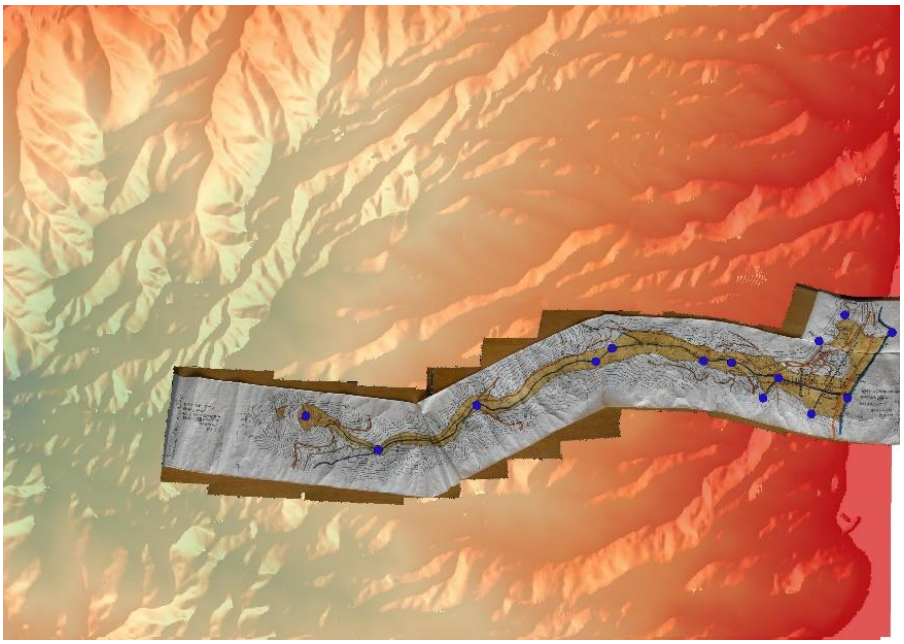

Fig. 5.9 DEM of current topography at Nebukawa area and overlaid of Mr. Uchida's illustration

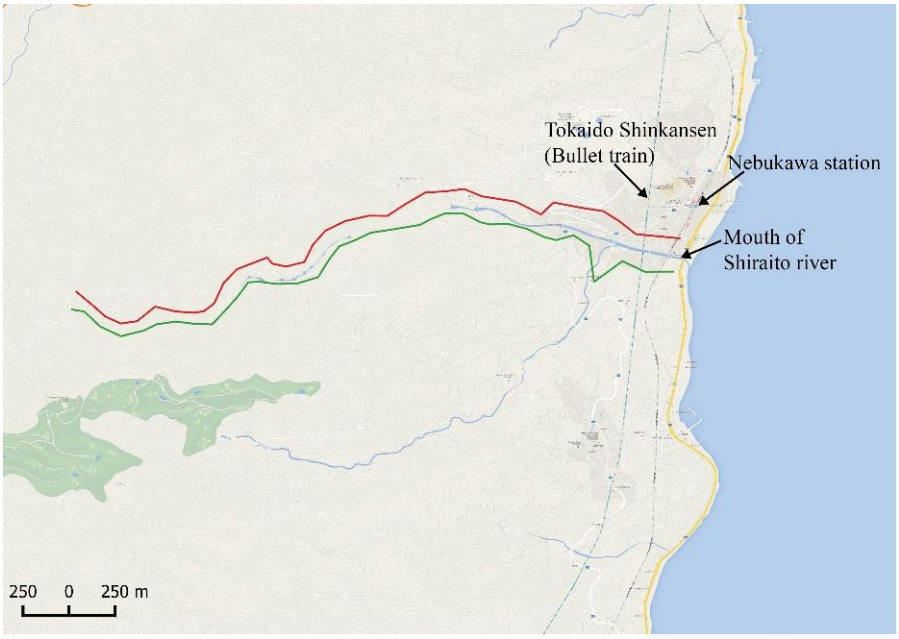

Fig. 5.10 Digitization of debris flow boundary and overlaid on current map

Fig.5.11 shows the left and right bank elevations along Shiraito River, which depict the change of the curvature of flow path from concave to convex nature and vice versa. So, Careful observation was needed to determine the bend radius as erroneous radius could mislead the total results. An iterative approach described in the Literature Review chapter was used to avoid the direct determination of radius of curvature of bend (Rahman Md. et al. 2015). The locations of the point of highest super-elevations were considered for selecting the stretch. For each stretch, initially a best-fit circle using the least square method was determined longitudinally. Several transverse cross-sections were also taken along the selected stretch and finally the average cross-section was determined. Length of the selected stretch was then updated from the sloshing period and the procedure was repeated till the convergence. Necessary information's were gathered using the current topographic map prepared by the GSI, Japan.

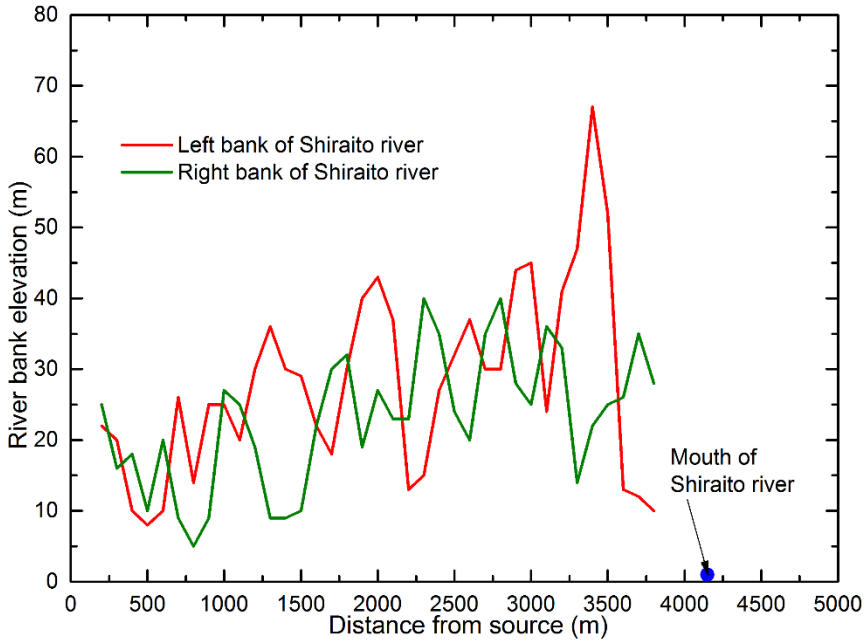

Fig. 5.11 Elevation of left and right bank of Shiraito River based on Mr. Uchida's illustration

5.2.3 Discussion on velocity variation

Mud-marks given in Mr. Uchida's illustration was used to estimate the flow velocities and plotted against normalized distance in Fig. 5.12. Template matching of two topographic maps gives the possible source dimension which was used to normalize the run-out length. Obtained velocities were compared with Kobayashi's result (Kobayashi 1985) which is based on Saint-Venant hypothesis for a one dimensional non-Newtonian flow with the inclusion of an additional friction slope term.

$$\frac{dv}{dt} = g\left(a - \frac{v^2}{\xi D_f}\right) \tag{5.1}$$

where, $a = \sin\beta - \mu\cos\beta$, with β= river-bed slope, μ= basal frictional coefficient, ξ= turbulence coefficient after Voellmy, and D_f= depth of flow.

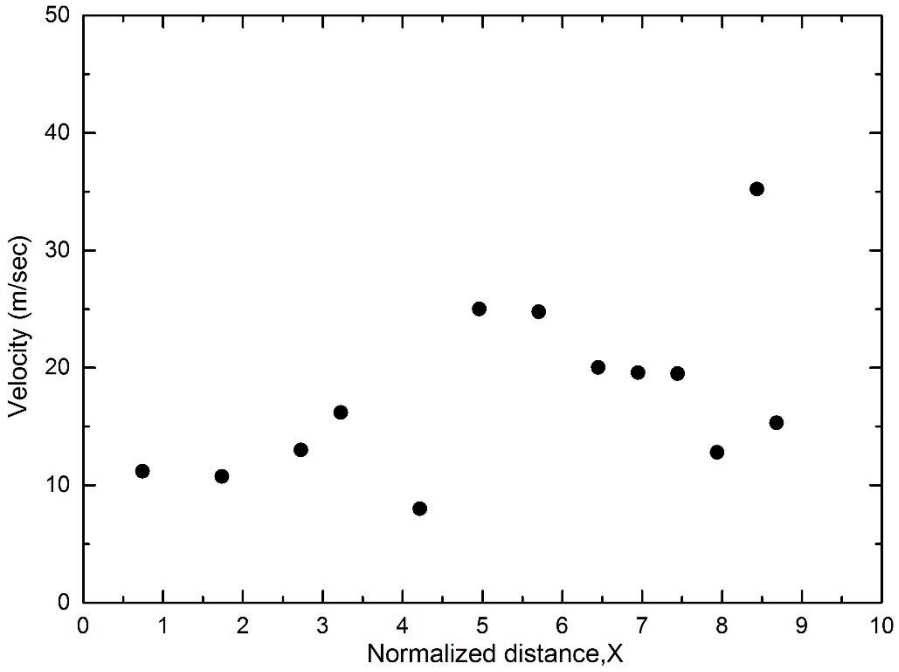

Fig. 5.12 Debris flow velocities along the Shiraito River

Adjusted velocities using the numerical upshot along the Shiraito River are depicted in Fig. 5.13. In Fig. 5.13, black circles represent the velocities estimated directly from mud-marks, while red circles give the adjusted velocities calculated using Eq. 4.26. Broken lines in Fig. 5.13 renders the velocity distribution from Kobayashi's numerical simulation. It is seen that adjusted velocities exhibit good agreement with the Kobayashi's results even in the proximity of the source region. (Matsuzawa 1925) described the super-elevation and possible radius at about 1.5 km from the mouth of Shiraito River and estimated velocity was 25.4 m/s which is close to the adjusted velocity corresponds to the normalized distance in between 6 and 7 in Fig. 5.13. However, Kobayashi's estimation is also based upon simplified numerical techniques and hence, it can't directly justify the accuracy of the numerical outcomes.

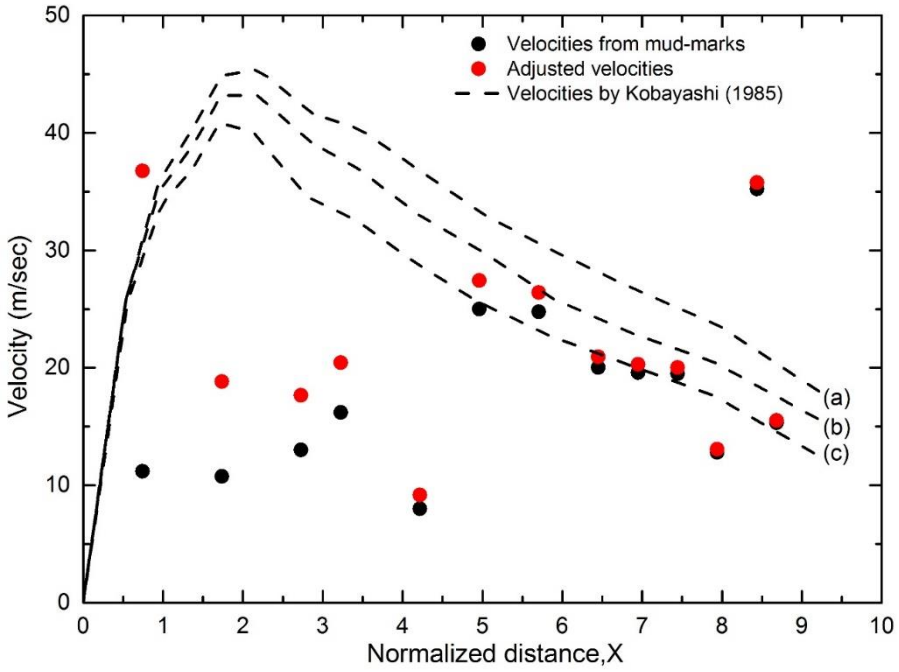

Fig. 5.13 Adjusted debris flow velocity from numerical results: (a) $\mu = 0.08, \xi D_f = 12000\ m^2/s^2$, (b) $\mu = 0.08, \xi D_f = 10000\ m^2/s^2$, (c) $\mu = 0.08, \xi D_f = 8000\ m^2/s^2$

5.2.4 Discussion on time

To mark out the aptness, estimated time is an important standard. There were several views about the time for the debris mass to travel from source to Nebukawa town. Imamura said (Imamura 1925) it was about five minutes, whereas the history of Odawara city said it was about 10 minutes.

However, Mr. Kazumasa Uchida stated that he came back to his house after the first shock settled, and met his grandfather. Suddenly, they felt the second shake, it was so vivid that the door case was detached from his house. They heard a shout of someone saying "A debris flow!" after the second shake ceased down. They looked back and saw a thick cloud of dust rising from the mountain side. Besides, major shocks measured at Hongo, The University of Tokyo (Yasuda 1925) were as follows:

1. Time: 11:58′44″, λ=139°21.8′, φ=34°58.6′, d_{max}=88.6mm, Δt=0.0s
2. Time: 12:01′49″, λ=139°28.0′, φ=35°10.0′, d_{max}=60.0mm, Δt=3m05s
3. Time: 12:15′36″, d_{max}=4.0mm, Δt=16m52s
4. Time: 12:16′49″, d_{max}=4.0mm, Δt=18m05s

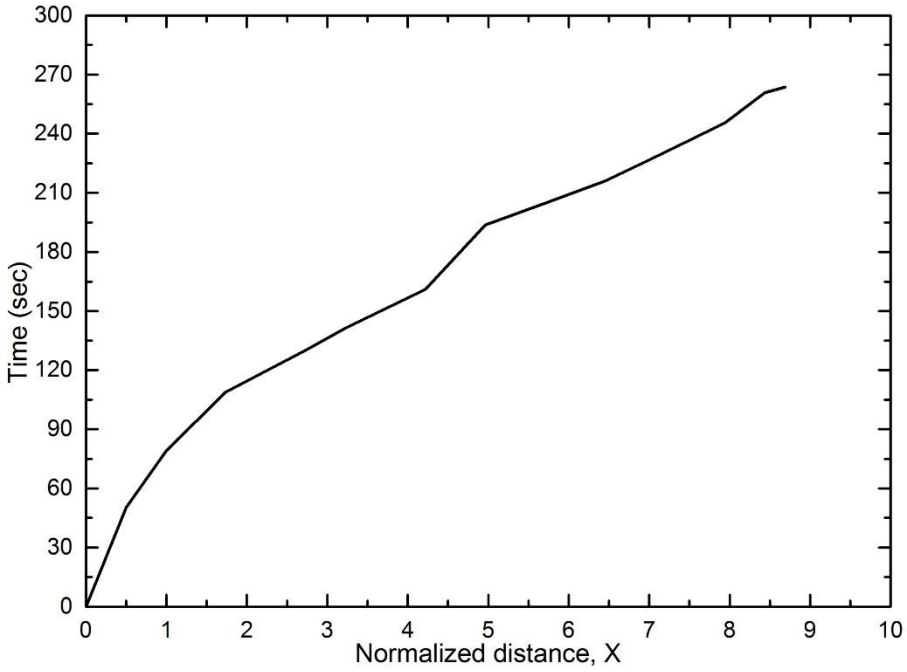

Fig. 5.14 Estimation of time from adjusted velocities

Considering the interval and the intensity of the shock that collapsed the door case, the second major shock was presumably No.2. Assuming that the shock of this scale can last a few minutes and the debris mass detached immediately after the main shock, the time for the debris mass to reach Nebukawa town could be about 5 minutes (Kobayashi 1979). The estimated time from the adjusted velocities were calculated and shown in Fig. 5.14. This figure revealed that debris mass reached the Nebukawa town (at normalized distance 9) in about 5 minutes, which is close to the statement from the eyewitness reported in (Kobayashi 1979). Therefore, piecing the scatter information's from different aspects, it can be implicitly said that the adjusted velocities yielded to the real velocities.

5.3 Komano-yu Debris flow in 2008

A big earthquake triggered along the boundary between Iwate and Miyagi Prefecture, Japan on 14th June, 2008 at 8:43 AM in the morning. The energy was estimated as magnitude of 7.2 (Japan Meteorological Agency). 23 people were lost their lives owing to this devastating earthquake (Kazama et al. 2012). One of the significant aspects of this earthquake was that a number of landslides were triggered in the affected areas (Nomura et al. 2010). Among many, a long travelling debris flow occurred after the main shake. Debris flow was initiated around the eastern peak of Mount Higashi-kurikoma facing

Dozou-sawa. A total of 1.5 million cubic meters of debris mass slid down from the source region and went over the ridge of the opposite bank, and the lower side of the snow gorge in the lower left part was covered with mud splashes. The detached masses contained a considerable amount of water at the time of collapse and eventually became a mud flow. The slurry flowed along the river channel to the "Komano-Yu" hot spring inn, where seven people were reportedly killed in soil and rubble. GSI surveyed the entire area and possible source dimensions were estimated and available in GSI website. Topography of the affected region is shown in Fig. 5.15.

Fig. 5.15 Komano-yu debris affected areas

5.3.1 Estimation of debris flow velocity

High resolution satellite imageries (Fig. 5.16) of the damaged area are available on the GSI website and used to determine the debris flow trace. The satellite image was geo-referenced and overlaid on the current terrain map to determine the boundary and flow trace of the flowing mass. Fig. 5.17 depicts the boundaries of the debris flow mark along the river channel. Necessary pieces of information's were then extracted from the current map to estimate the flow velocities at several sections. Bend radii at selected stretches were determined following the procedure described in Shiraito River event. Moreover, GSI measured super-elevations and radius at certain points of the flow trace which are also described in the following sub-section.

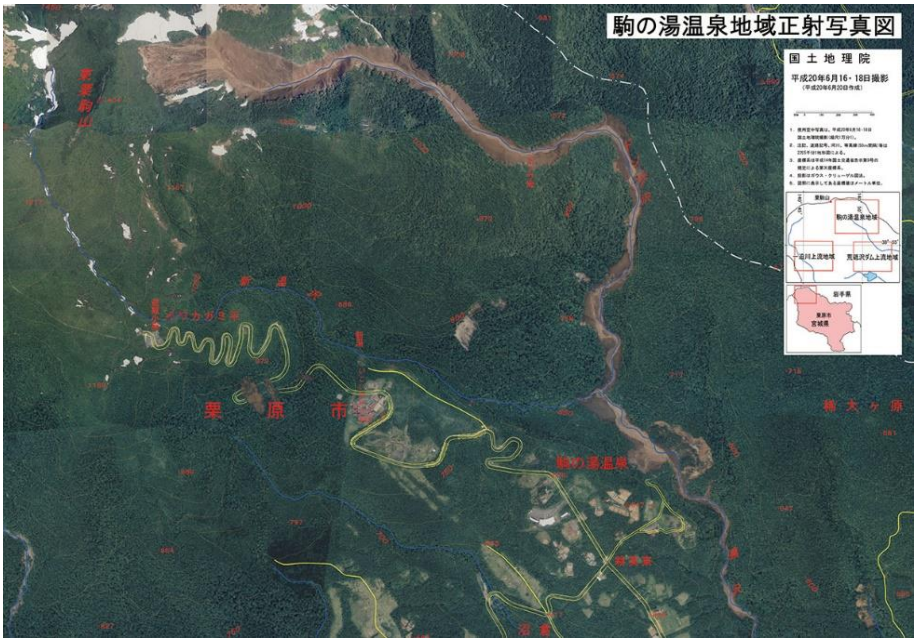

Fig. 5.16 Satellite imagery of Komano-yu debris flow (GSI, Japan)

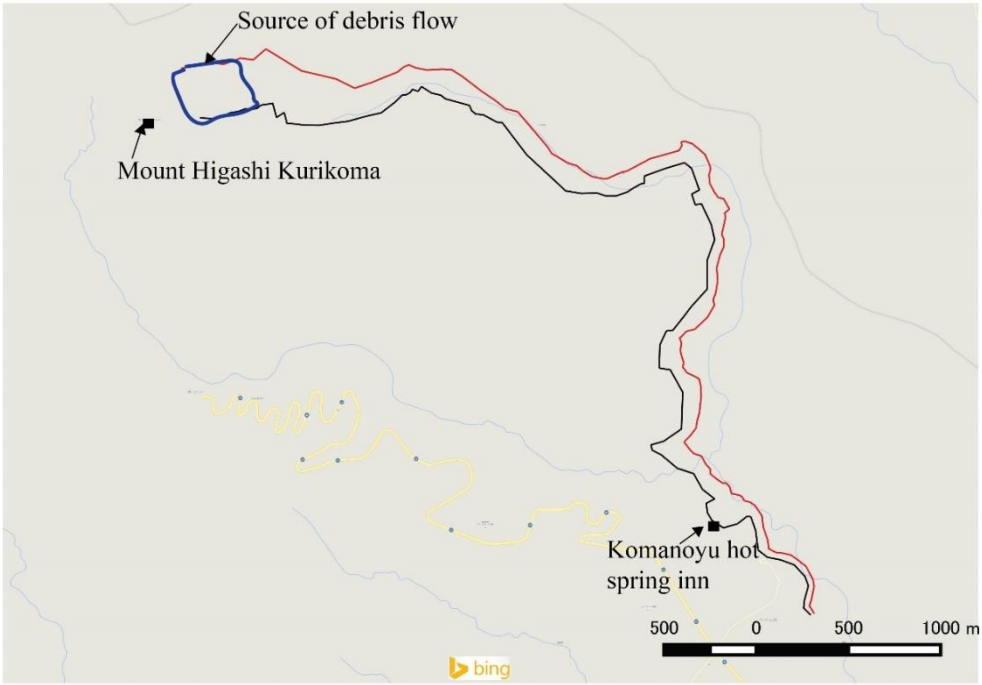

Fig. 5.17 Komano-yu debris flow boundary

5.3.2 Discussion on debris flow velocity

Estimated velocities at different normalized distances are plotted in Fig. 5.18 for Komano-yu debris disaster. Solid circles are the velocities calculated from mud-marks, while blue pyramids show the velocities estimated by GSI, Japan. Afterward, these mud-marks-derived velocities were adjusted using the curve and shown in Fig. 5.19. These

updated velocities were found compatible with the results from previous research (Nomura et al. 2010) who ran MPM numerical simulations on the described areas.

Estimated arrival time was also calculated using the adjusted velocities and shown in Fig. 5.20. Eye-witness statement revealed that the approximate time for the debris mass to reach the hot spring inn was about 10minutes. Time calculated from adjusted velocities is seemingly close to the statement of the survivors.

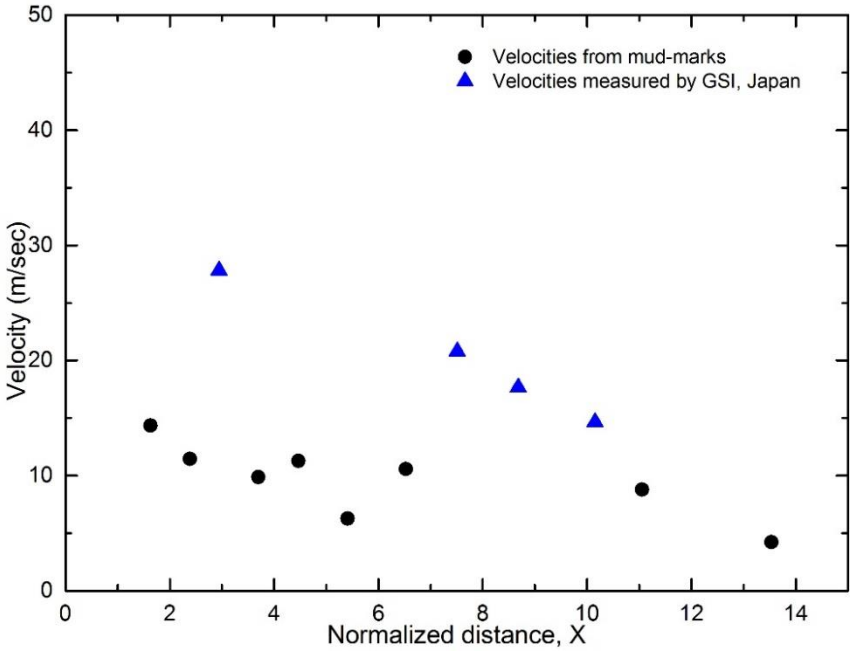

Fig. 5.18 Debris flow velocity from mud-marks

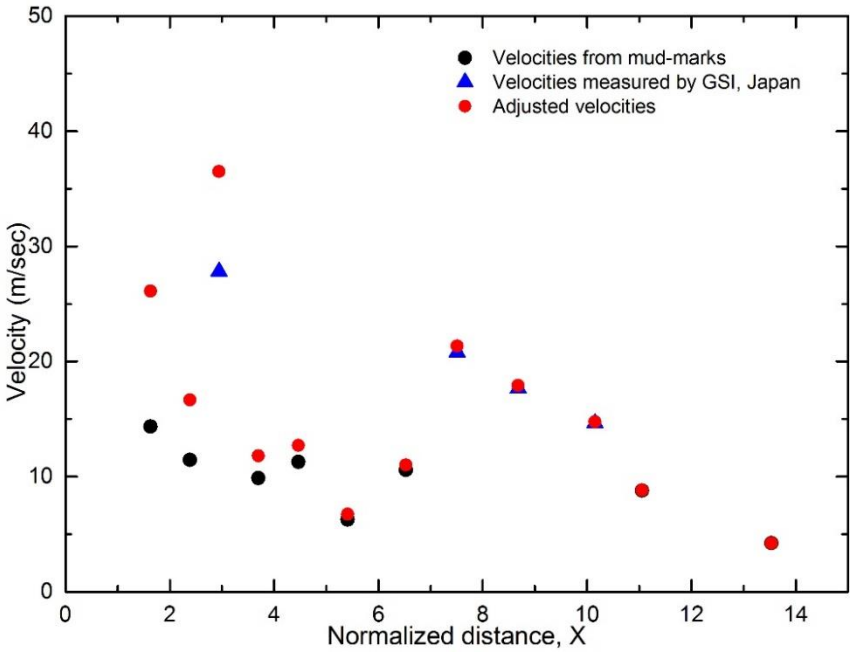

Fig. 5.19 Adjusted flow velocity for Komano-yu debris flow

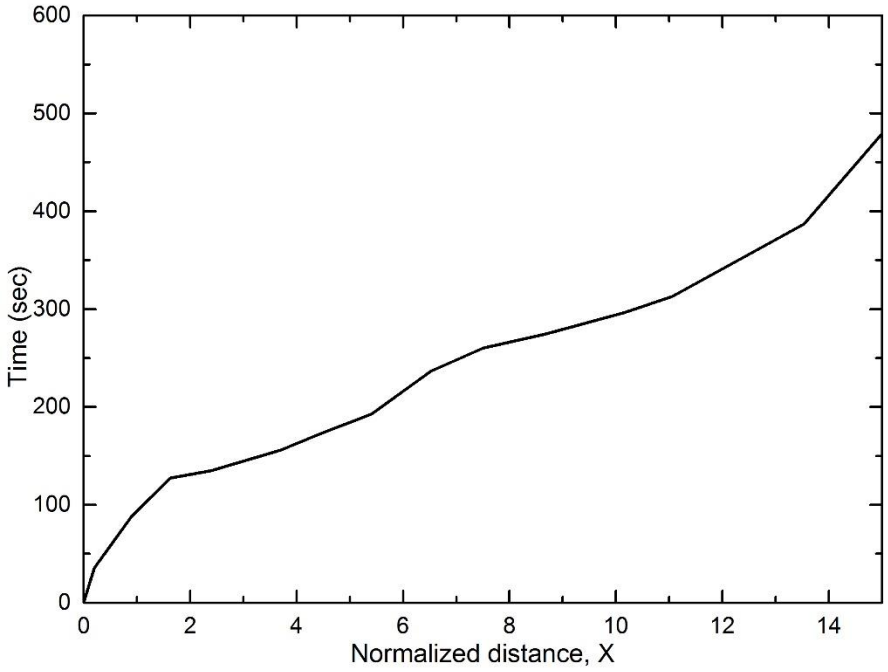

Fig. 5.20 Estimation of time for Komano-yu debris flow

5.4 Ontake avalanche in the 1984 West Nagano Prefecture Earthquake

An earthquake induced mass failure on mountain slope can evolve run-out of a huge volume of debris mass to several kilometers. A shallow slope failure can also lead to a destructive, long run-out debris flow in some instances. One good example to describe such a type of debris flow is the Ontake avalanche, which is locally known as 'Ontake Kuzure' (Hara and Yazawa 1987a). A M6.8 earthquake jolted the Nagano prefecture on September 14, 1984 at 8:48 AM (known as West Nagano Prefecture- earthquake), which triggered a massive debris flow on the southern flank of Mount Ontake. The detached soil mass started to slide straight off after the main tremor. Its initial volume of the rock mass of around 34 million cubic meters failed and developed into a gigantic debris flow, traveled over total 12 kilometers distance and descended 1600 meters before its halt at Ohtaki. 29 lives were lost (Ashida and Egashira 1986) in this catastrophic event.

The collapse was initiated from one of the southern ridges of Mount Ontake. Altitude of the top of the scar was about 2500m, situated on a ridge adjacent to the head of the Denjo River. Oval shaped collapsed area were visible after the debris event, measuring 1300 x 450 meters, and total volume was estimated to be around 3.4 x 10^6 m^3. The failed mass ran down the ravines of Denjo and Nigori Rivers and finally made a halt within a reach

of the mainstream of Ohtaki River. At the starting time, detached mass flowed along the Denjo River, and the ravine of Denjo River was nearly filled with debris slurries and then the slurry overtopped both sides of Mount Komikasa, leading to the Mizoguchi and Suzukasawa Rivers. Debris mass, then splits into two parts and flowed into both the Nigorisawa creek and Denjo River on the first turn of the river which is about 2 km from Mount Komikasa. Debris mass again merged and surged into the Nigori River. Mass flow had continued along the Nigori River and reached the confluence point of Nigori and Ohtaki Rivers. They partly overflowed one bank at the confluence point owing to the nearly-90-degrees sharp turn of the river course. Afterward, debris mass continued flowing and stopped near the Ohtaki village about 3.7km from downstream the confluence point. Fig. 5.21 describes the topography of the Ontake avalanche area.

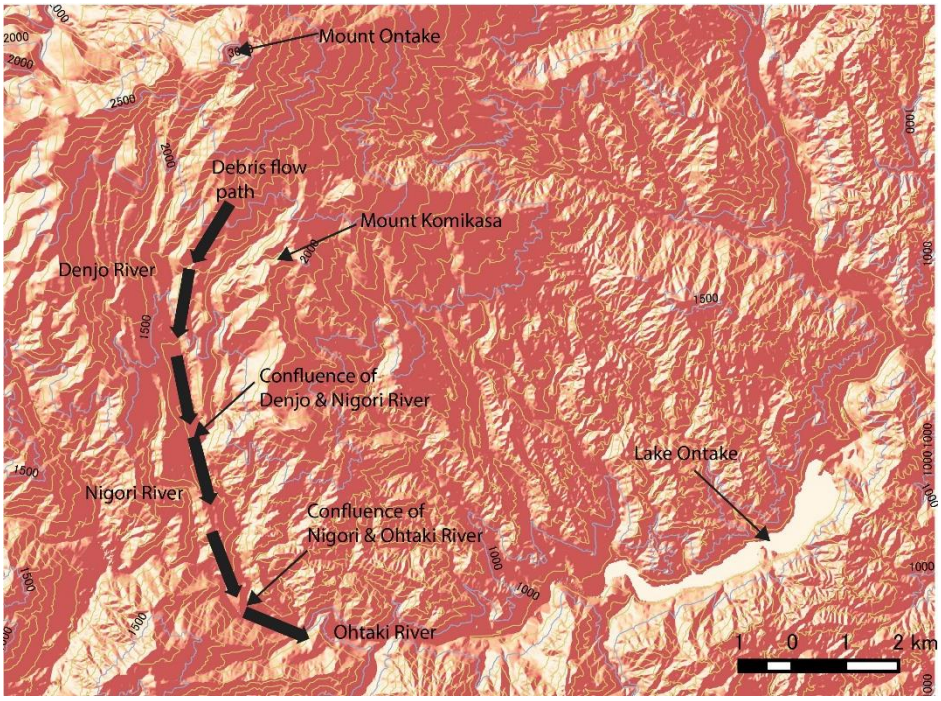

Fig. 5.21 Topography of Ontake area

Debris avalanche scoured the side walls of the U - shaped Valley of Denjo River up to the depth of 20m; hence exposing the bedrock. About 70% of the debris materials deposited in the Ohtaki river bed, and the remainder was deposited in the upstream reach of the confluence point of Ohtaki and Nigori Rivers. Numerous field surveys were conducted after this destructive disaster. These field studies revealed that liquefaction may have occurred at the basal soil layer which is responsible for the accelerated massive debris flow movement.

5.4.1 Source area of Ontake avalanche

Old topographic maps can be used to extract the necessary pieces of information which can be used to detect the dimension of the source region. Determination of the dimensions of the source from old maps was described in detail for Nebukawa case in the earlier section of this chapter. However, old contour maps of Ontake area are not available in the GSI website. To get the source dimensions, an indirect approach was then taken. Several satellite imageries which have been taken shortly after the event, were available on the GSI database, and their spatial resolution was satisfactory. However, the biggest challenge was to overlay those images on the current topographic map. Initially, images were geo-referenced with only few known points. Yet, those images didn't portray good fit and needed further adjustment. After this casual fit, many known points were taken using the current Google map and images were overlaid and compared to get the comprehensive adjustment of the debris flow trace. Geo-referenced image on the topographic map is illustrated in Fig. 5.22. Initial scratch zone was identified from geo-referenced image and the dimensions of the source region were extracted in a quantitative way, which can agree well with the previously obtained dimensions from field survey (Ashida and Egashira 1986).

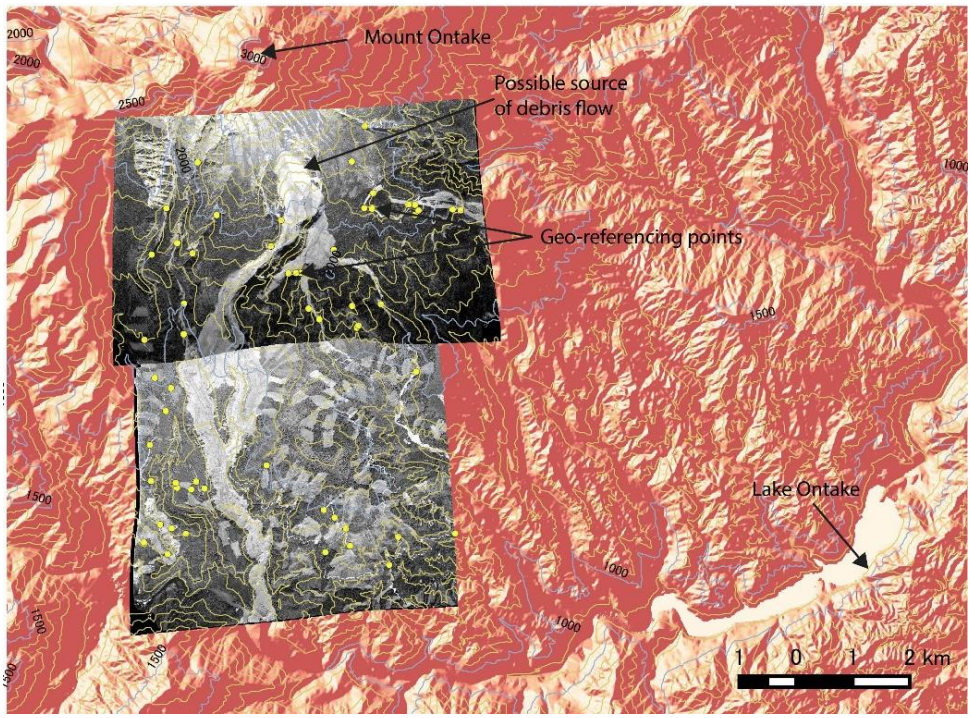

Fig. 5.22 Geo-referencing of satellite imagery

5.4.2 Estimation of debris flow velocity

Geo-referenced images were used to define the boundary of the entire flow trace. Initial source, flow trace and overtopped areas were identified and laid over on current map (Fig. 5.23). Afterward, left and right bank elevation of the flume were extracted and used to estimate the flow velocities at several locations along the trail.

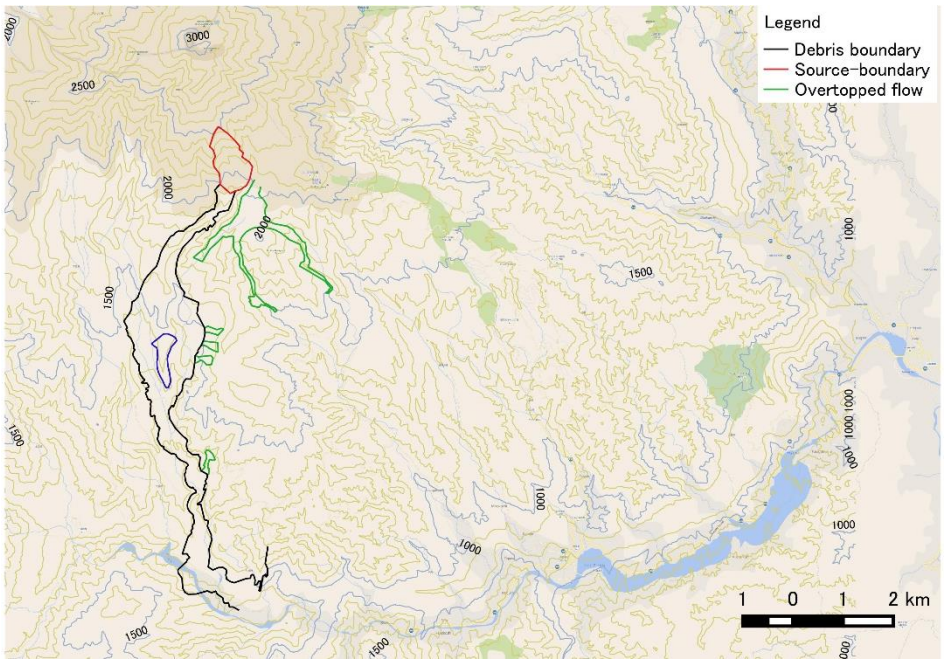

Fig. 5.23 Debris flow boundary

5.4.3 Discussion on flow velocity

Lack of topographic maps of that time makes it difficult to calculate the flow velocities. However, advancement of GIS tools allows to extract necessary information's which were used to determine the flowing velocities of the Ontake avalanche at different points of the flow trail. Satellite imageries were used to determine the source dimension which normalized the run-out length. Normalized distance and velocities are shown in Fig. 5.24. Mud-marks-derived velocities were then corrected using the curve in Fig. 4.27 and plotted in Fig. 5.25. There are many technical papers (Endo et al. 1986; Anma and Maikuma 1987; Okunishi et al. 1987; Hara and Yazawa 1987b; Voight and Sousa 1994) available describing the detail features of the Ontake disaster, however velocity is seldom described in a quantitative manner. Only, (Ashida and Egashira 1986) developed a two-phase model to identify the mechanism of Ontake avalanche and estimated velocities using the following equations from 5.2 to 5.5.

$$\frac{u}{\sqrt{gh}} = \left\{\frac{u_0^2}{gh}e^{2ax/h} - \frac{a}{b}\left(1 - e^{2ax/h}\right)\right\}^{1/2} \tag{5.2}$$

$$a = -2\left(\rho_{fs}/\rho_b\right)f \tag{5.3}$$

$$b = \cos\theta\left\{\tan\theta - \mu_{ka}(1-\lambda_s)\left(\rho_s - \rho_{fs}\right)/\rho_b\right\} \tag{5.4}$$

$$\mu_{ka} = 0.7\tan\phi \tag{5.5}$$

where, u is the velocity, u_0 is the initial velocity, ρ_{fs} is fluid density in static state, ρ_s is the density of solid particles, ρ_b is the bulk density, μ_{ka} is the apparent friction, f is the friction coefficient. Their results are consistent with the proposed numerical outcomes over the entire reach of the flow.

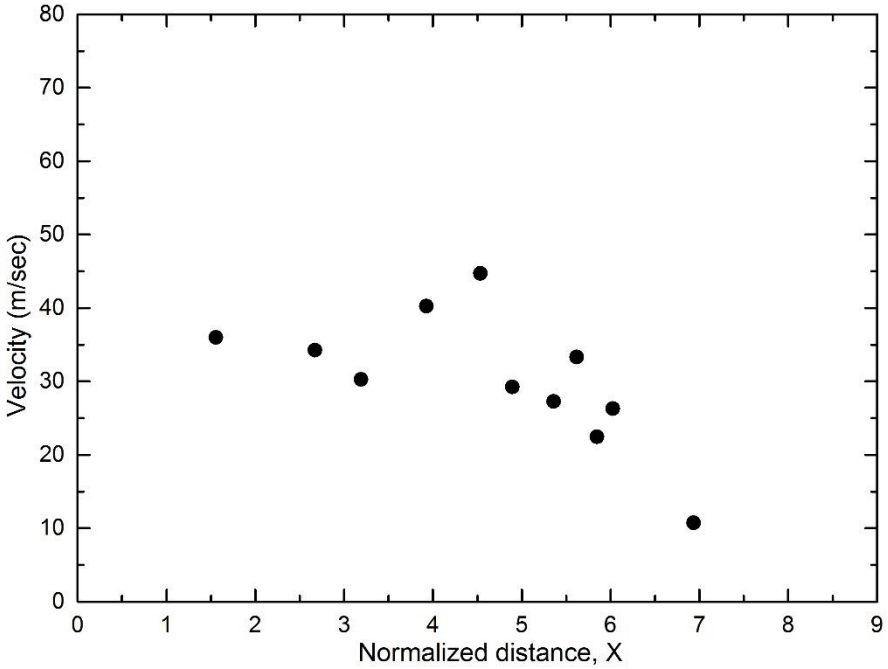

Fig 5.24 Velocities of Ontake avalanche

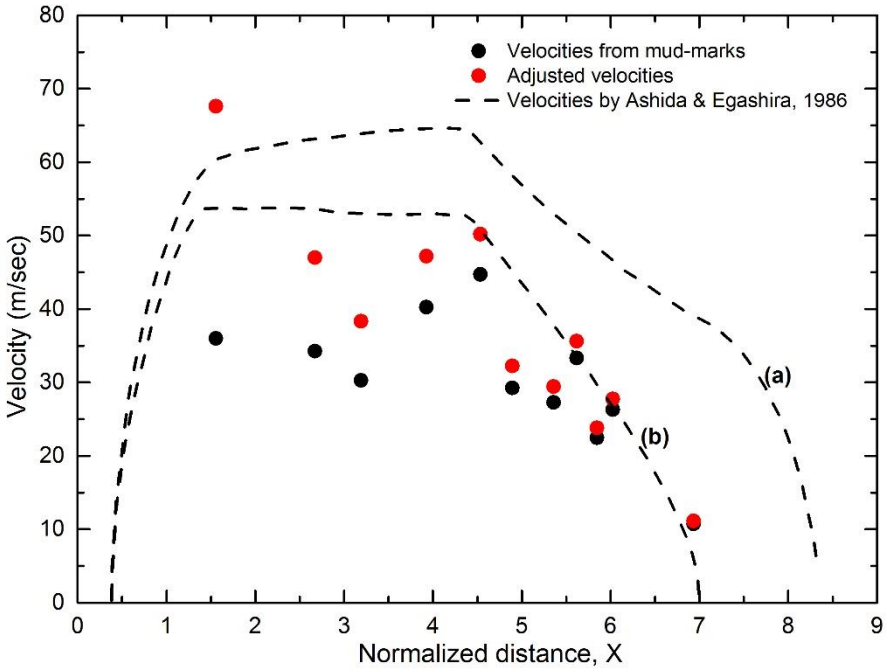

Fig. 5.25 Adjusted velocities of Ontake avalanche, (a) $\phi = 10^0$, (b) $\phi = 14^0$

However, the good agreement between the sets of velocities by two different estimation methods does not assure that the estimation is correct. Among very few evidences, verbal evidences from eyewitnesses who have actually experienced this event are very important. Mr. Tsutomu Minato heard a thunderous sound at 8:49 AM, about 1 km east of the source area (Okuda et al.). This statement brought out that the initiation was almost instantaneous with the main impact. Another eyewitness, Mr. Yoshihiro Ome, who was passing Gakiganodo tunnel, heard a thunderous sound at 8:56 AM and left his car. Summing up the statements from eyewitnesses, the debris mass can reach the Gakiganodo tunnel in about 7-8 minutes. This tunnel was located at 7 to 7.5 of the normalized distance from the source, and the estimated time for the debris mass to reach this tunnel was about 6.5 minutes using the proposed method, which time is in the proximity of the verbal evidence.

References

Anma S, Maikuma H (1987) Earthquake-induced debris-flow features in neovolcanic mountains. In: Proceedings of the Corvallis Symposium. pp 147–148

Ashida K, Egashira S (1986) Running-out processes of the debris associated with the Ontake land slide. Natural Disaster Science 8:63–79.

Endo K, Sumita M, Machida M, Furuichi M (1986) The 1984 collapse and debris avalanche deposits of Ontake volcano, central Japan. In: Proceedings of the International Volcanological Congress.

Hara Y, Yazawa A (1987a) Ontake landslide of September 14,1984, in Japan. In: Proceedings of the Corvallis Symposium. pp 137–138

Hara Y, Yazawa A (1987b) Ontake landslide of September 14,1984, in Japan. In: Proceedings of the Corvallis Symposium.

Imamura A (1925) Mud flow in Nebukawa, Report of the Imperial Earthquake Investigation Committee.

JNR (1927) JNR report of the damage to railway facilities, The Ministry of Railways, 1927.

Kazama M, Kataoka S, Uzuoka R (2012) Volcanic mountain area disaster caused by the Iwate-Miyagi Nairiku Earthquake of 2008, Japan. Soils and Foundations 52:168–184. doi: 10.1016/j.sandf.2012.01.003

Kobayashi Y (1992) Travel dynamics of large debris avalanche. In: International Symposion. pp 275–284

Kobayashi Y (1979) A catastrophic debris flow at Nebukawa in The Great Kanto earthquakeof 1923. Earthquake Ser2 32:57–73.

Kobayashi Y (1985) A catastrophic debris avalanche induced by the 1923 Great Kanto Earhtquake. Natural Disaster Science 7:1–9.

Matsuzawa T (1925) Mud-flow in Nebukawa. ibid 100B:81–83.

Nishisaka K (1966) The great earthquake fire and activities of police in Kanagawa prefecture, History of Odawara city (in Japanese).

Nomura F, Konagai K, Tajima Y (2010) EXTRACTION OF GEOTECHNICAL PARAMETERS FROM TRACES LEFT IN THE JUNE 14 th 2008 , IWATE-MIYAGI INLAND EARTHQUAKE. Bulletin of ERS, University of Tokyo 43:13–24.

Okuda S, Okunishi K, Suwa H, et al Restoration of motion of debris avalanche at Mt. Ontake in 1984 and some discussions on its moving state.

Okunishi K, Okuda S, Suwa H (1987) A large-scale debris avalanche as an episode in slope-channel processes. Proceedings of the Corvallis Symposium 225–232.

Rahman Md. A, Hashimoto T, Konagai K (2015) An attempt for velocity estimation of Nebukawa debris flow triggered by the Great Kanto Earthquake, 1923. Journal of Japan Society of Civil Engineers, Ser A1 (SE/EE) 71:I_387–I_394. doi:

doi.org/10.2208/jscejseee.71.I_387

Voight B, Sousa J (1994) Lessons from Ontake-san: A comparative analysis of debris avalanche dynamics. Engineering Geology 38:261–297. doi: 10.1016/0013-7952(94)90042-6

Yamasaki S, Kamai T (2015) A novel method of surveying submerged landslide ruins: Case study of the Nebukawa landslide in Japan. Engineering Geology 186:28–33. doi: 10.1016/j.enggeo.2014.11.010

Yasuda T (1925) Tokyo observations of the aftershocks. ibid 100A:261–310.

Chapter-6

CONCLUSION AND FUTURE SCOPE

6.1 Conclusion

Flow velocity is one of the key factors of the dynamic features of debris flow. The hazard mitigation strategy also requires the knowledge about how fast the velocity can be. Rational estimation of flow velocity is thus a pre-requisite for any research arena of debris flows. No clear guideline is available in any technical writings and code provisions regarding the velocity estimation procedure. Velocities are often back-calculated from the flow marks observed in post-flow field investigations. Super-elevations, radii of curvature and channel widths are the necessary parameters that are used in the vortex equation to back-calculate flow velocities. However, a field survey only provides remnant flow marks which do not portray the actual peak super-elevations. Approximation of bend radius is also a hard undertaking. Yet, this back-calculation approach is widely used by the authorities concerned for debris flow impacts because of its simplicity. Therefore, based on the above glitches of the current method of velocity estimation, this research study has been devoted solely to improve the existing velocity estimation procedure. This dissertation may also contribute to the hazard mitigation policy of debris flow disaster by improving the velocity estimation procedure.

6.1.1 Major findings regarding flowing slurry velocities

A simple numerical scheme based on SPH was developed to estimate debris flow velocities through a series of numerical flume tests. The flume has a reservoir of debris slurry at its uppermost end and a varying straight section, which is followed by the curved part. Different flume inclinations as well as different aspect ratios of the initially rectangular slurry mass were taken into consideration to estimate the flow velocity. The Newtonian fluid model was chosen for describing flowing nature of the debris slurry. Temporal evolution of velocities as well as flow marks on both sides of the curved section of the flume were recorded at every 10^0 bend angle interval to cover up the whole curved section. Highest mud-marks on both sides were used to calculate

velocities along the stretch and compared with the actual maximum velocities averaged over SPH particles that existed upon a particular cross-section at a particular time. Numerical results revealed that velocities using the mud-marks underestimated the actual velocity in the vicinity of the source region. Meanwhile, velocities estimated from flow marks converge on the actual velocities as the distance to source increases. Non-Newtonian Bingham fluid model was also examined with the current numerical code. The findings of the Bingham model (Rahman and Konagai, 2016)show the similar responses as those from Newtonian fluids movements, thus, justified the above upshots. Based on the numerical flume tests, finally, a curve having the shape of exponential cumulative distribution function was fit to the ratios of flow-mark-based estimation of velocity and the actual peak velocities reached at cross-sections of curved flume. This curve is thus used to adjust the flow-mark-based estimation of velocity to the actual slurry velocities. These velocities adjusted at regular intervals along the flume were used to estimate the time t_1 for the debris mass to reach to its distal end. Numerical simulation revealed that this time t_1 is 80 to 90 % of the actual arrival time t_2, and this ratio t_1/t_2 is given as a function of the normalized distance. This finding is of potential to be used in estimating the actual arrival time from flow-marks in a rational manner.

To avoid the subjective manner of measuring radii of curvature along irregularly curved natural flume, an iterative procedure was formulated earlier by the author (Rahman Md. et al., 2015) based on the assumption that the time for the flowing slurry to reach its maximum super-elevation is a quarter of the sloshing period at that particular cross-section. Both 2D and 3D numerical simulations were carried out to examine the above assumption, and it was found that the time is rather closer to one third of sloshing period than a quarter of it.

All above findings were examined through discussions about three documented debris flow events that occurred in Japan, namely, Shiraito River debris flow in 1923, Komano-yu debris flow in 2008, and Ontake avalanche in 1984, which were triggered respectively by the Great Kanto earthquake of 1923, the 2008 Iwate–Miyagi Nairiku earthquake and the West Nagano Prefecture earthquake of 1984. After the Shiraito River debris flow event, mud-marks on both banks of Shiraito River were recorded by one of the survivors of that event and these mud-marks were used to estimate the flow

velocities at different sections. Afterward, velocities were adjusted using the above-mentioned findings and adjusted velocities portrayed good agreement with the previously estimated velocities by Kobayashi (Kobayashi, 1985). Moreover, the adjusted velocities were found consistent with verbal evidence. Two other debris flow disasters were also analyzed and adjusted mud-marks-based estimations of velocities in those cases exhibit good match with the verbal evidences.

6.2 Future scope

The validity of the findings obtained through this numerical study have been examined carefully in the range of idealized channel geometry and simplified models for flowing slurries. Discussion on the actual debris flow events have also proven the validity of these findings, and showed the potential of these findings to be applied to disaster mitigation measures. However, these findings are to be further refined taking into consideration more realistic geometries of natural flumes, ravine wall roughness which is often a reflection of vegetation covering the ravine walls, more complicated nature of mixed-phase debris material.

The proposed procedure to rationally estimate flowing slurry velocities, arrival times and appropriate radii of natural flume curvature is basically for the event that has already happened. The next important step is surely to extract remaining unstable rock/soil masses that can exist near the examined debris flow location, having the similar properties as those of the examined debris mass. Physical countermeasures such as check domes and feasible evacuation plans are to be carefully designed taking into account the clarified nature of possible debris flows. Further extensive studies are expected in the future.

References

Kobayashi, Y., 1985. A catastrophic debris avalanche induced by the 1923 Great Kanto Earhtquake. Natural Disaster Science 7, 1–9.

Rahman Md., A., Hashimoto, T., Konagai, K., 2015. An attempt for velocity estimation of Nebukawa debris flow triggered by the Great Kanto Earthquake, 1923. Journal of Japan Society of Civil Engineers, Ser. A1 (SE/EE) 71, I_387–I_394. doi:doi.org/10.2208/jscejseee.71.I_387

Rahman, M.A., Konagai, K., 2016. Substantiation of debris flow velocity from super-elevation: a numerical approach. Landslides. doi:10.1007/s10346-016-0725-3